PhD dissertation

Single-molecule imaging reveals rapid estradiol action on the surface movement of AMPA receptors in live neurons

Godó Soma

Phd supervisors:

Prof. Dr. István Ábrahám

Dr. Klaudia Barabás

Phd Program Leader: Prof. Dr. Dóra Reglődi

University of Pécs

Medical School

Department of Physiology

Pécs

2022

Table of contents

1. List of abbreviation

ADF	actin-depolymerization factor
AMPAR	α-amino-3-hydroxy-5-methyl-4-isoxazolepropionic acid receptor
ATD	amino-terminal domain
cAMP	cyclic adenosine monophosphate
CHO	chinese hamster ovary cell
CLSM	confocal laser scanning microscope
cLTP	chemical long-term potentiation
CNS	central nervous system
cRPMI	complete RPMI
CTD	carboxyl-terminal domain
D	diffusion coefficient
DMSO	dimethyl sulfoxide
dPC12	differentiated PC12 cell
DPN	diarylpropionitrile
E2	17β-estradiol
EPSC	excitatory postsynaptic current
ERα or β	estrogen receptor α or β
ERE	estrogen responsive elements
FBS	foetal bovine serum
FSH	follicle-stimulating hormone
GnRH	gonadotropin-releasing hormone
GPER1	G-protein coupled estrogen receptor
HILO	highly inclined laminated optical sheet microscopy
JNK	c-Jun terminal kinase
latA	latrunculin A
LBD	ligand-binding domain
LH	luteinizing hormone
LTD	long-term depression
LTP	long-term potentiation
MAP2	microtubule-associated protein 2
MAPK	mitogen-associated protein kinase
mGluR1	metabotropic glutamate receptor 1
MSD	mean square displacement
NGF	nerve growth factor
NMDA	N-methyl-D-aspartate
PBS	phosphate buffer saline
PC12	pheochromocytoma cell
PFA	paraformaldehyde
PKA	protein kinase A
PSD	post-synaptic density
ROCK	Rho-associated protein kinase

ROI	region of interest
SEM	standard error of mean
STED	stimulated emission depletion microscopy
STORM	stohastical optical reconstruction microscopy
TIRF	total internal reflection fluorescence

2. Introduction

2.1. 17β-estradiol

Estrogens are gonadal steroid hormons playing major role in the reproductive system but they are also crucial for osteogeneis, cardiovascular health, lipid metabolism and nervous system functions. (Ábrahám et al., 2009) Human body produces three types of estrogen: estrone, estriol and 17β-estradiol (E2). Estrone is the least potent type mostly acts as an inert precursor of E2 in the body. Estriol is only produced in the placenta during pregnancy and has an important role in preparing the mother for delivery. E2 has the highest biological activity and the most diverse effect in both sexes. (Katzenellenbogen et al., 2000)

E2 is mainly produced by the ovaries in premenopausal woman. The theca interna cells of the ovaries convert cholesterol into androstenedione, which is taken up by the surrounding granulosa cells, which produce estrone or testosterone, that both act as precursors for E2. The final step of E2 synthesis is catalized by an aromatase enzyme: during this step a methyl group is removed that transforms the carbon ring aromatized. The synthesized E2 diffuses into the circulatory system where it binds to sex hormone binding globulins and transported to target tissues. E2 production is under the strict control of hypothalamic-pituitary-gonadal axis. Gonadotropin-releasing hormone (GnRH) expressing neurons secrete GnRH, which increases the production of luteinizing hormone (LH) and follicle-stimulating hormone (FSH). FSH and LH stimulates 17β-estradiol secretion from the ovaries. In turn, E2 has a negative feedback – during most of the cycle - on neurons expressing GnRH or producing LH or FSH. (Gruber et al., 2002)

E2 is also produced by extragonadal tissues. For instance, the brain can synthetize E2 locally as aromatase enzyme is also expressed by neurons in different parts of the brain such as hippocampus, medial preoptic area, medialis amygdala and cortex. The regulation and the function of the so-called neurosteroids is not fully explored yet. Aromatase enzyme activity and neurosteroid E2 have been linked to several physiological functions such as neurogenesis, synaptic plasticity, neuroprotection and cognitive behaviour. It has also been shown that aromatase activity is disturbed in the pathophysiology of Alzheimer's disease or autism spectrum disorder. (Ubuka and Tsutsui, 2014)

2.2. Estradiol receptors

The first estrogen receptor (ER), the estrogen receptor α (ERα) was described in 1958 and was classified as a ligand-activated nuclear receptor. ERα consist of an N-terminal domain, a DNA-binding domain, a hinge region, a ligand-binding domain and a C-terminal domain. There are three more isoforms that have been described since then, two of them lack the N-terminal domain, which hinders the autoactivation of the receptor.

The second ER was cloned and named to estrogen receptor β (ERβ) in 1996. This receptor is also the member of the ligand-activated nuclear receptor superfamily and contains the same domains as ERα. Five shorter isoforms have also been identified. These isoforms are unable to bind ligands and have no transcriptional activity but are able to form dimers with ERα to reduce its effectivity. (N et al., 2007)

In 1997, a G-protein-coupled receptor was identified in cell lines responsive to E2. (Carmeci et al., 1997; Thomas et al., 2005) G-protein-coupled estrogen receptor-1 (GPER1) is a seven transmembrane receptor and localizes in the cell membrane and the endoplasmatic reticulum. E2 has a lower affinity to GPER1 than to ERα or ERβ, but the ligand binding and release occur more rapidly. (Filardo and Thomas, 2012)

The expression of ERs is tissue and cell type specific. Most reproductive organs and tissues express ERs in different ratios. The ratio of ERs vary between different brain regions resulting in various effects of E2 in the central nervous system (CNS) and cognitive functions. (Filardo et al., 2002; Olde and Leeb-Lundberg, 2009; Nilsson et al., 2011)

2.3. Classical estradiol pathway

According to the classic paradigm, the ”free hormone hypothesis” E2 as a lipohpilic molecule enters cells by diffusing through the cell membrane and binds to the cytoplasmic classical genomic receptors. However, several papers suggested that the cellular uptake of E2 is mediated and controlled by specific carrier proteins. (Hammond and Bocchinfuso, 1995; Hammes et al., 2005) During the classical or genomic effect of E2, ERα and ERβ act as ligand activated transcriptional factors. (Marino et al., 2006) Upon E2 binding, ERs dimerize and translocate into the nucleus from the cytoplasm. (Le Dily and Beato, 2018) In the nucleus the ERα and ERβ dimers bind to the promoter region of their target sequences, the so called Estrogen Responsive Elements (ERE). ERE is found throughout the genom as

part of a complex regulatory system for hundreds of proteins involved in reproduction, cardiovascular system, neuronal development or cognitive system. (Bourdeau et al., 2004)

In addition, the ER-E2 complex is able to influence gene expression through other transcription factors such as AP1. Several factors form a transcriptional complex, which recruits RNA polymerase II and initiates gene transcription. (Klinge, 2001) The classical effect of E2 develops slowly and lasts for hours or days.

2.4. Non-classical estradiol pathway

E2 affects several cellular processes in seconds or minutes that cannot be explained by the action of the slow classical pathway. This suggests the presence of a non-classical pathway for E2 effects where E2 modulates gene expression without directly interacting with DNA. (Vrtačnik et al., 2014)

The first evidence of non-classical E2 effect was described by Szego and Davis in 1967. The level of cAMP was increased double-fold after E2 treatment in rat uterus in less than a minute. (Szego and Davis, 1967) Since then several studies reported non-classical effects of different steroid hormones. (Fujimoto and Kitamura, 2004; Glidewell-Kenney et al., 2007; McDevitt et al., 2008; Rudolph et al., 2016) The non-classical effect of E2 is mostly initiated by GPER1 and membrane associated ERα and ERβ. E2 can change the function of ion channels (Kelly and Rønnekleiv, 2009), modulate membrane fluidity (Kumar et al., 2011) or induce activation of signaling pathways and second messengers such as phospholipase C (Marino et al., 1998), adenyl cyclase, protein kinase A (PKA) (Gu and Moss, 1996), protein kinase C (PKC) (Marino et al., 1998), the phophatidyl inosytol 3 kinase A cascade, the extracellular signal-related kinase pathway (Dos Santos et al., 2002), the intracellular Ca^{2+} and cAMP levels. (Björnström and Sjöberg, 2005) These mechanisms finally also lead to gene expression changes: gene silencing or enhancing.

ERs are also able to act without ligand binding: ER activation occurs through phosphorylation by regulatory proteins such as PKA, PKC or mitogen-associated protein kinase (MAPK). (Fuentes and Silveyra, 2019)

E2 also has epigenetic effects. E2 may alter transcriptional activity and gene expression through posttranslational modifications, microRNA regulation and DNA methylation steps. Therefore, E2 may alter gene expression even in a heritable form. (Gibney and Nolan, 2010; Portela and Esteller, 2010)

It is now clear that the classical pathways are involved in only a small portions of E2 effects. It is also proved that the convergence of classical and non-classical pathways can alter the expression of the same gene in multiple ways. (Björnström and Sjöberg, 2005)

2.5. Glutamaterg neurotransmission

Glutamate is a neurotransmitter that plays a pivotal role in most excitatory synapses in the CNS. (Izquierdo, 1994) Glutamaterg neurotransmission is essential for almost every sensory and motor function, neuronal development, memory formation and cognitive functions. (Niciu et al., 2012) In the CNS the extra- and intracellular levels of glutamate are tightly regulated by a vast number of molecular mechanisms. These mechanisms control the expression and release of glutamate at the synaptic site as well as their clearance and recycling. Disturbance in these systems may cause serious neuropshychiatric disorders such as Huntington's disease. (Storey et al., 1992) The excessive release of extracellular glutamate leads to hiperexcitability in target neurons called excitotoxicity, followed by neuronal damage and apoptosis that may impair learning and cause neurodegenerative diseases. (Choi, 1994; Doble, 1999) Reduced glutamate recycling from synapses lowers the sensitivity of neurons to glutamate that weakens the synapse. (Bechtholt-Gompf et al., 2010)

Glutamate is not able to cross the blood-brain barrier, thus it is generated from glucose in the brain. It is produced in the tricarboxylic acid cycle: glucose is converted into α-ketoglutarate which is transaminated into glutamate. (Pellerin and Magistretti, 2004) The synthesized glutamate is transported via vesicular glutamate transporters into the presynaptic site of synapses and released into the synaptic cleft. When glutamate release is triggered by an action potential, the glutamate loaded membrane vesicles fuse with the presynaptic membrane of the synapse. (Pang and Südhof, 2010) Glutamate molecules then diffuse through the synaptic cleft and bind the receptors located in the postsynaptic membrane, where action potential is provoked if treshold value is reached. To avoid excitotoxicity, glutamate synapses are enclosed by astrocytes, microglia and oligodendrocytes. (Olive, 2009) Glial cells actively remove excess glutamate from the synaptic cleft under milliseconds with their excitatory amino acid transporters. (Danbolt, 2001; O'Shea, 2002) The removed glutamate enters the glutamate-glutamine cycle in the glial cells. Glutamine synthetase turns glutamate into glutamine, which is transported back to the presynaptic nerve terminal to help regenerate the presynaptic glutamate pool. (Palmada and Centelles, 1998)

2.6. Glutamate receptors

The composition of glutamate receptor pool in the postsynaptic density (PSD) determines the behaviour of the synapse. PSD is a specific membrane compartment at the size of 50 nm in the active site of the synapse. It is densely packed with a plethora of membrane and structural proteins. (van Zundert et al., 2004) In these membrane-associated protein clusters two main glutamate receptor types are found: metabotropic and ionotropic receptors.

2.6.1 Metabotropic glutamate receptors

Metabotropic glutamate receptors (mGluRs) are the members of the seven transmembrane domain-spanning receptor family. Most metabotropic glutamate receptors are located outside the active site of synapses, but also presented in glia cells. (Kim et al., 2008) Eight type of mGluRs have been identified in the CNS (mGluR1-8) classified into three groups based on their function. Metabotropic glutamate receptors are slow acting receptors and induce activation of membrane bound G-proteins. Group I mGluRs mediate gene expression through phospholipase C and inositol-1,4,5-triphosphate induced intracellular Ca^{2+} release, or diacylglycerol activated protein kinase C phosporylation. (Niciu et al., 2012) Group II and III mGluRs are linked to inhibitory G-proteins. The activated G-proteins inhibit adenyl cyclase and protein kinase A pathways resulting in reduced cAMP levels. (Conn and Pin, 1997) These events precisely control the sensitivity of cells to neurotransmitters, fine tune excitatory and inhibitory neurotransmission and enhance synapse development. (Lesage and Steckler, 2010) G-protein activated second messengers can also directly open or close ion channels to influence synaptic activity. (Kuzmiski and Bains, 2010)

2.6.2 Ionotropic glutamate receptors

Ionotropic glutamate receptors are ligand-gated ion channels that are activated by the neurotransmitter glutamate. They are the fast acting component of the synapse and responsible for most of the excitatory synaptic transmission. Ionotropic glutamate receptors are homotetrameric or heterotetrameric transmembrane proteins composed of four subunits assembled into a dimer of a dimer structure. Each subunit has four domains: extracellular

amino-terminal domain (ATD), extracellular ligand-binding domain (LBD), transmembrane domain and intracellular carboxyl-terminal domain (CTD). ATD and LBD are responsible for binding ligands, agonists or antagonists. (Sobolevsky et al., 2009) Ionotropic glutamate receptors are subdivided into three categories based on their selective agonists: N-methyl-D-aspartate (NMDA), α-amino-3-hydroxy-5-methyl-4-isoxazole proprionic acid (AMPA) and kainate.

NMDA receptors are heterotetramer ion channels formed from dimers of two subunits: GluN1, 4 isoforms of GluN2 (A-D) and two isoforms of GluN3 (A-B). GluN1 is ubiquitous, obligatory and presented as homodimer in each NMDA receptor. Knocking out of GluN1 in mice is lethal and causes respiratory failure of the newborn pups. (Tsien et al., 1996) GluN2 isoform expression changes during neurogenesis and differs between regions of the developed brain. (Monyer et al., 1994) GluN2A is dominant in the neocortex and hippocampus, GluN2B is expressed mostly in the forebrain. GluN2C and GluN2D are abundant in the cerebellum and diencephalon. (Nakanishi, 1992) GluN3A plays important role during neurogenesis and expressed in the neocortex in the adult brain (Henson et al., 2008), while GluN3B is found in the brainstem, hippocampus and cerebellum. (Chatterton et al., 2002; Bendel et al., 2005) The subunit determines the properties and functions of NMDA receptors in the synapse.

NMDA receptors are glutamate-gated ion channels with high Ca^{2+} permeability. Activation of NMDA receptor is initiated by binding of glutamate to GluN2 subunit and requires membrane depolarization to remove Mg^{2+}, which blocks the ion channel. In response to the binding of necessary co-agonists to GluN1, the ion channel opens with a relatively slow gating kinetics. As a non-selective ion channel, glutamate-gated NMDA receptors allow the efflux of K^+ and influx of Na^+ and Ca^{2+}. (Kumar, 2015) Six ligand binding sites are characterized on NMDA receptors that influence channel opening. Two of these binding sites are specific for glutamine and glycine, while the others for polyamines, Mg^{2+}, which blocks the ion flux and Zn^{2+}, which is an allosteric modulator released from glutamate vesicles. (Nowak et al., 1984) H^+ is also an important modulator ligand, its binding to GluN2B decreases the chance of ion channel opening. Polyamines (spermine and spermidine) counterbalance this effect of H^+ and increase the gate opening frequency. (Traynelis et al., 1995)

AMPA receptors are heterotetrameric ion channels located in the post and perisynaptic areas and responsible for the rapid postsynaptic response to the presynaptic glutamate release. (Diering and Huganir, 2018) Four AMPA subunits (GluA1-4) assemble a functional AMPA ion channel. The subunits are split into two groups based on their cytoplasmic carboxyl terminal: GluA1 and GluA4 are long-tailed, while GluA2 and GluA3 are short-tailed. AMPA receptors with long-tailed subunits are more frequent in the active site of synapse, while short-tailed subunits are perisynaptic. (Shi et al., 2001) The most abundant AMPA receptor subunit in neurons is GluA2 paired with GluA1 or GluA3. (Wenthold et al., 1996) GluA4 subunit is expressed during CNS development and in some interneurons of the adult brain. (Zhu et al., 2000; Schwenk et al., 2014) Subunit composition of AMPA receptors, but mostly the presence or absence of GluA2 subunit determines the main properties of the ion channel. GluA2 containing receptors are Ca^{2+} impermeable and show a slow decay kinetics. Lack of GluA2 subunit turns AMPA receptors into Ca^{2+} permeable channels with high conductance and rapid decay kinetics. Ca^{2+} permeable AMPA receptors are presented in the early postnatal development and sparsely detected in the adult brain. (Burnashev et al., 1992)

Binding of glutamate to AMPA receptor quickly opens the ion channel, Na^{+}, K^{+} and Ca^{2+} flow in for a brief period of time (Collingridge et al., 2004; Traynelis et al., 2010) that results in membrane depolarization and subsequent excitatory postsynaptic potential if threshold is reached. Deactivation and desenzitization of the AMPA receptors terminate the ion influx.

The number, type and localization of glutamate receptors in and around the PSD are dynamic. Rapid redistribution of glutamate receptors contributes to synaptogenesis, synapse maturation, normal synaptic function and one of the key steps in the process of synaptic plasticity. (Diering and Huganir, 2018)

2.7. Synaptic plasticity

One of the most complex properties of the adult brain is the synaptic plasticity, its capacity to adapt to external factors and effects. It was first described by Eric Kandel, who demonstrated in sea slug that the learning is accompanied with the strengthening of preexisting synapses. (Castellucci et al., 1970) Synaptic plasticity cannot be described as a single event, but a series of actions at molecular and cellular levels. The most dominant

change during synaptic plasticity is the stimulus-dependent strengthening or weakening of the already existing synapses. (Fig. 1). This change can be transient (milliseconds) only or persistent (days or longer) and subsequently influence future behaviour, learning and other cognitive functions. Synaptic plasticity is also crucial for development of CNS and its disturbance could lead to serious neurological disorders.

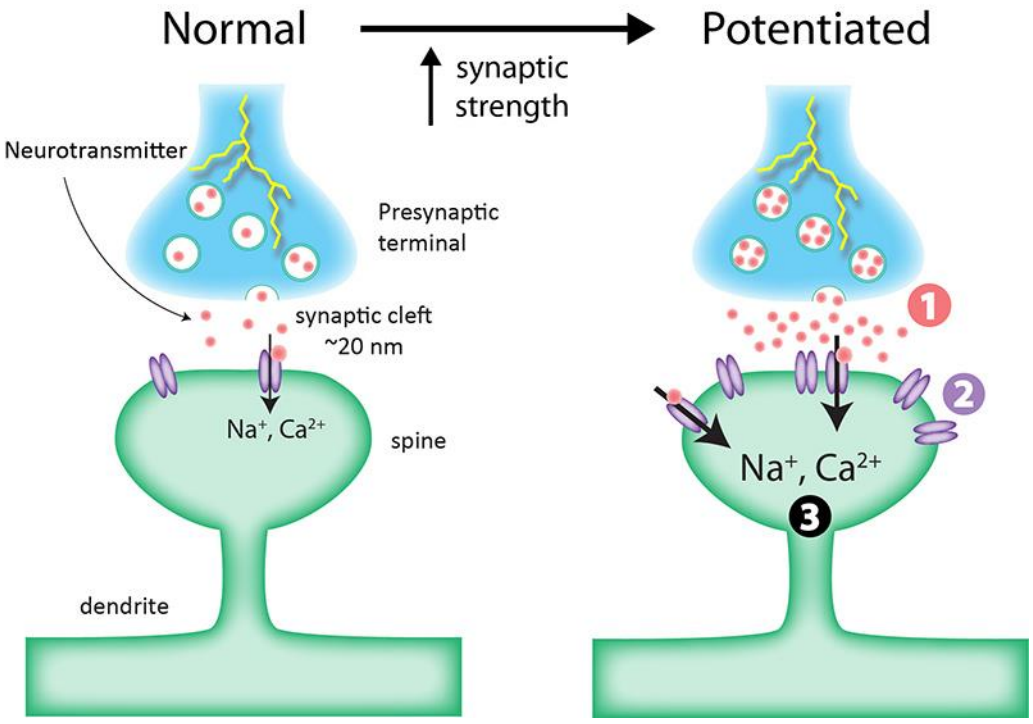

Figure 1. Potentiation of a synapse involves several pre- and postsynaptic functional (1-2) and morphological (3) changes. Synaptogenesis and synapse strengthening is the base of memory formation. (Figure is made by Alan Woodruff, The University of Queensland, Australia)

2.7.1. Short-term synaptic plasticity

Change in synaptic strength that lasts only for milliseconds to minutes is termed short-term synaptic plasticity. It plays an important role in adaptation to sensory inputs or short-term memory formation. This process is mostly provoked by short repeats of stimuli, which cause either the facilitation or the depression of the synapse. Two types of stimuli have been connected to short-term synaptic plasticity: paired-pulse impulses and tetanic stimuli.

During paired-pulse impulses, two stimuli reach the synapse within a short period of time. Paired-pulse facilitation and depression have been described in several neuronal systems: the reaction to a second stimulus quickly after the first can be potentiated or depressed relatively to the first stimulus. (Zucker and Regehr, 2002) Depression of a synapse occurs if the interval between two stimuli is less than 20 ms, potentiation is observed if the stimulus interval is larger than 20 ms up to even 500 ms. Short-time depression of a synapse may be the result of desensitization of voltage-dependent Ca^{2+} ion channels or total depletion of neurotransmitter containing vesicles after the first action potential. During potentiation, residual Ca^{2+} of the first stimulus is added to the Ca^{2+} that flows in after the second stimulus resulting in an increased release of neurotransmitters. (Fisher et al., 1997) The other type of stimulus is the tetanic stimulation in which a longer period (more than 200 ms) of high frequency repetitive stimuli (10-200 Hz) reaches the synapse. This may result in a continous accumulation of residual Ca^{2+} in the presynaptic button causing a higher probability of neurotransmitter release. (Zucker and Regehr, 2002) High frequency repetitive stimuli can also cause synaptic depression in synapses with a high probability of glutamate release, because the stored vesicle pool is quickly depleted. It is believed that the essential function of short-term synaptic plasticity is to act as a filter to external stimuli and fine-tune the response. For instance, synapses with high initial release probability will be weakened while synapses with low initial release probability will be strengthened by high frequency burst stimuli.

2.7.2. Long term synaptic plasticity

Long-term synaptic plasticity refers to the long-lasting answer to external or internal stimuli at the level of neuronal circuits and is believed to be the very basis of learning and memory formation. (Bliss and Gardner-Medwin, 1973; Fusi et al., 2005) This activity-dependent reaction either enhances or weakens the synaptic efficacy and results in changes of presynaptic neurotransmitter release and the modulation of the number and characteristics of postsynaptic receptors. The most studied brain area in terms of synaptic plasticity is the CA1 region of the hippocampus, which is proved to be involved in long-term memory formation. Two main forms of long-term synaptic plasticity have been described: long-term depression (LTD) and long-term potentiation (LTP). These mechanism involve the two most abundant glutamate receptors: AMPA and NMDA receptors.

LTD is initiated when the synapse is triggered by minutes-long low-frequency stimulation. Formation of LTD involves NMDA-dependent postsynaptical Ca^{2+} level increase (Mulkey and Malenka, 1992) following the activation of a series of phosphatases such as calcium-dependent protein phosphatase or calcium/calmodulin dependent phosphatase. (Lisman, 1989) The activation of these signal transduction mechanisms cause the removal of AMPA receptors from the active site of the synapse. (Bredt and Nicoll, 2003; Malenka and Bear, 2004) The exact mechanism is not yet fully understood but it is associated with the release and mobilization of AMPA receptors from the PSD by dephosphorylation of stargazin, the main anchoring protein that binds AMPA receptors to the actin filaments in the PSD. AMPA receptors move to perisynaptical areas where they are endocytosed in a process mediated by clathrin and dynamin. (Ashby et al., 2004; Groc et al., 2004)

LTP is one of the most studied neuronal phenomenon, which can be developed in every synapse counterbalancing LTD. Similar to LTD the receptors responsible for LTP are the NMDA and AMPA receptors. LTP can be induced by high-frequency tetanic stimulation, which depolarizes the postsynaptic membrane and activates NMDA receptors. (Malenka, 1991) If the elevated postsynaptic Ca^{2+} levels reach the treshold value, it activates the molecular machinery that develop LTP. Many proteins have been described as mediators for LTP such as calcium/calmodulin dependent protein kinase II (Pettit et al., 1994), cyclin adenosine monophosphate-dependent PKA (Makhinson et al., 1999) or MAPK. (Lisman, 1989) The major mechanism of LTP is the enrichment of AMPA receptors in the PSD. This is achieved by incorporation of AMPA receptors from endosomes and the perisynaptic area into the PSD in a process mediated by the submembrane actin structure. It has been demonstrated that actin network and its dynamic remodeling is essential for the rearrangement of AMPA receptors. (Hanley, 2014b; Baglietto-Vargas et al., 2018) The major protein during actin remodeling is actin-depolymerization factor (ADF)/cofilin, which is activated after dephosphorylation and increase the speed of actin filament depolymerization. (Pavlov et al., 2006) The result of ADF/cofilin activation is a loosened submembrane actin network, which allows the exocytosis and trafficking of AMPA receptors into the PSD. (Ben Zablah et al., 2020) The subsequent inactivation of ADF/cofilin during LTP consolidation results in a more dense actin network, which traps AMPA receptors inside the PSD. (Gu et al., 2010; Rust, 2015) The increased number of AMPA receptors enhance the probability of depolarization of the postsynaptic membrane. The synaptic strength is maintained for hours to days or even longer by upregulation of the synthesis of synaptic proteins. (Citri and Malenka, 2008)

2.8. Surface movement of transmembrane proteins

Since the trafficking of NMDA and AMPA receptors is crucial for LTP, many studies focus on the membrane movement of these proteins. The fluid mosaic model established by Singer and Nicholson in 1972 describes the structure of the cell membrane as a mixture of phospholipids, cholesterol, proteins and carbohydrates arranged into a bilayer. It also states that integral membrane proteins are diffusing freely. Recent studies, however, have disproved this hypothesis. According to latter findings membrane proteins are not moving freely in the plasma membrane, their movements are restricted by many factors such as the submembrane actin network, the surrounding lipid composition, extracellular matrix or other interacting proteins (Fig. 2). The development of single molecule techniques enabled researchers to study the movement of single membrane receptors in live cells. (Kusumi et al., 1993) With these methods researcher are able to identify and characterize moving membrane proteins in live cells. Single molecule detection techniques revealed that receptor diffusion was slower than expected suggesting a system which interacts with the membrane proteins. (Bussell et al., 1995) Receptors tend to move freely in small compartments and frequently shift to another compartment. (Sako and Kusumi, 1994) One possible theory of the non-free movement of proteins is that their intracellular domains interact with the submembrane actin network directly or through anchoring proteins that restricts receptor movement. This hypothesis is termed as „fence model", in which the actin filaments act as fence creating compartments and the transition of receptors between these regions is called hop diffusion. (Kusumi et al., 1993) Receptor movements based on their mean square displacement (MSD, μ^2m) plot can be dividied into 4 groups: 1: Brownian or simple diffusion when free moving is observed; 2: restricted when the receptor undergoes Brownian diffusion within an enclosed area; 3: directed when the receptor constantly moving toward a direction with a steady speed; 4: immobile or stationary mode when the receptor shows no or minimal motion and possibly anchored to the submembrane actin filaments. (Kusumi et al., 1993) Actin fenced domains can range from 40 to 300 nm. Its ability to restrain molecule movement greatly depends on the number and forms of anchoring proteins, the density of actin filaments or the ongoing signaling events. (Kusumi et al., 2014; Tsunoyama et al., 2018) Other membrane structures that influence protein movements are the dynamically assembled and disassembled lipid raft domains. Lipid rafts are membrane microdomains rich

in sphingomyelin and cholesterol. Their size ranges from 5 to 500 nm. (Sezgin et al., 2017) Lipid rafts are densely packed with transmembrane receptors and act as a signal transduction initialization complex. It was shown that membrane receptors are moving slower inside the lipid rafts and it is connected to alterations in their signaling activity. (Spencer et al., 2017; Marchetti et al., 2019)

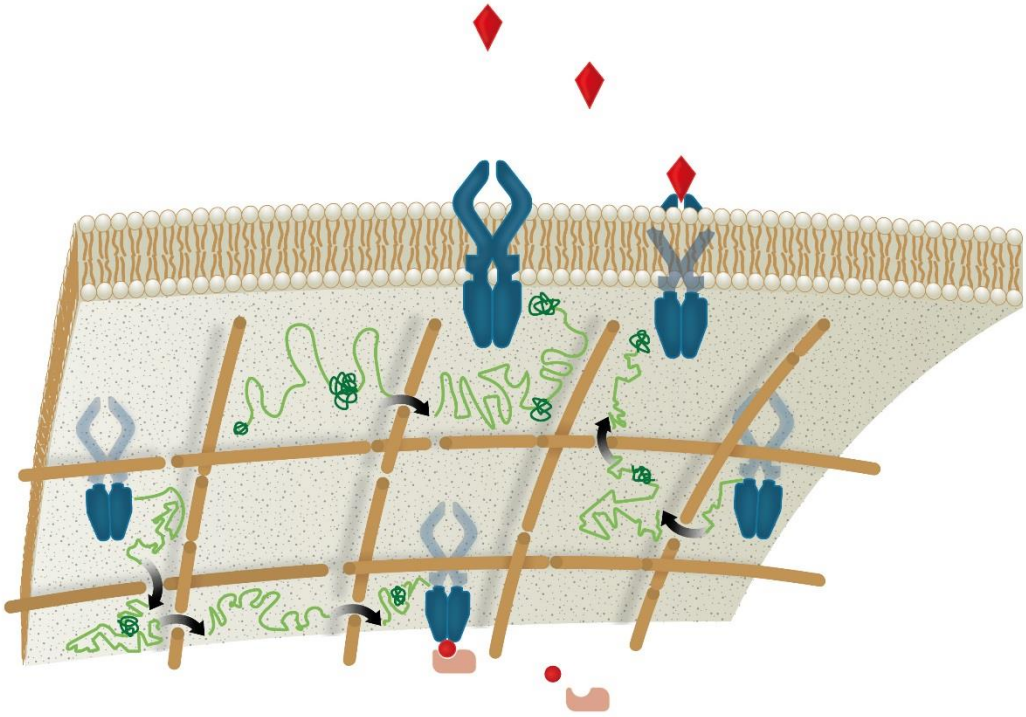

Figure 2. Schematic representation of the members and compartments of the cellular membrane and the lateral movement of transmembrane proteins. The movement of membrane receptors (blue shapes) are influenced by the cortical actin network (brown noodles) and ligant binding (red rhombus). When the continuity of the actin filament is broken, the receptor is able to transit into an other compartment via hop diffusion (black arrows). (Barabás et al., 2018)

2.8.1. Superresolution microscope techniques

Live-cell single molecule imaging techniques allow us to study cellular events at molecular level in real time. Stimulated Emission Depletion (STED) microscopy enables a spatial resolution of ~50 nm in live cells. This technique utilizes a depletion laser which selectively deactivates fluorescence in a doughnut shape and photons only from the center of excited area are detected. (Klar et al., 2000; Hein et al., 2008) Stohastical Optical

Resolution Microscopy (STORM) is able to reach a resolution of approximately 20 nm in spatial and 50 nm in axial axis. STORM captures series of images of photoswitchable dyes. In one image only a subset of these dyes are activated and localized. A STORM image is generated by summarizing the localization points from thousands of fluorescence images. (Rust et al., 2006) STORM and STED are excellent tools to investigate subcellular elements such as actin network, nuclear pores, mitochondrial structure, membrane microdomains as well as membrane receptor localization. (Petersen et al., 2016; Sidenstein et al., 2016) However, the temporal resolution of the above mentioned techniques is not enough to detect detailed membrane receptor movements. To follow receptor and membrane proteins in live cells, Total Internal Reflection Fluorescence Microscopy (TIRFM) and Highly Inclined Laminated Optical Sheet Microscopy (HILOM) are widely used techniques. The excitation laser is set to reach total reflection in TIRFM or a deep angle in HILOM. Due to these laser settings only a 100 nm or a 300-500 nm layer is illuminated, respectively. The rest of the cell will be dark that results in a low signal-to-noise ratio. TIRFM or HILOM are usually coupled with a fast and sensitive camera to make recordings of moving receptors. With superresolution methods, many processes became observable in live cells such as protein complex formation, dimerization, transiently existing domains, actin filament assembly and disassembly as well as receptor redistribution in the plasma membrane that is indispensible for LTP.

2.8.2. Glutamate receptor movement in synapse

The movement of glutamate receptors in the synapse under physiological conditions as well as during LTP was described in the last decades with the use of live-cell single molecule imaging and tracking. The localization and movement properties of NMDA receptors depends on their subunit composition. GluN2A-NMDA receptors are colocalized with PSD and mostly restricted or immobile while GluN2B-NMDA receptors are equally frequent in the perisynaptic area as well as in the active zone and exhibit Brownian movement. (van Zundert et al., 2004; Groc et al., 2006) During LTP GluN2B-NMDA receptors transit to the perisynaptic zone, while GluN2-NMDA receptors remain close to the PSD. (Dupuis et al., 2014; Ladépêche et al., 2014) The difference in subunit distribution arises from the intracellular domains of NMDA subunits. GluN2A prefers the interaction with PSD-95, the

main PSD protein, while GluN2B binds to SAP102, which is located perisynaptically. (Bard and Groc, 2011)

The turnover of AMPA receptors between the synaptic and perisynaptic areas is more dominant and faster during LTP than the lateral diffusion of NMDA receptors (Fig. 3). Inside the active site of the synapse AMPA receptors are either immobile and possibly bound to PSD95 or exhibit Brownian diffusion (Lee et al., 2017), while extrasynaptic AMPA receptors are moving mostly with Brownian diffusion and rarely enter immobile state. (Borgdorff and Choquet, 2002) The high mobility of extrasynaptic AMPA receptors enables them to serve as a reservoir during LTP. Extrasynaptic AMPA receptors laterally diffuse into the PSD where they are trapped by anchoring proteins. (Triller and Choquet, 2005) The reservoirs are refilled with AMPA receptors stored in endosomes inside the postsynaptic button. After LTP induction the dynamic balance of the synaptic, extrasynaptic and endosomatic AMPA receptor pool is shifted to a more dominant synaptic AMPA receptor content. (Barabás et al., 2018; Pereyra and Medina, 2021)

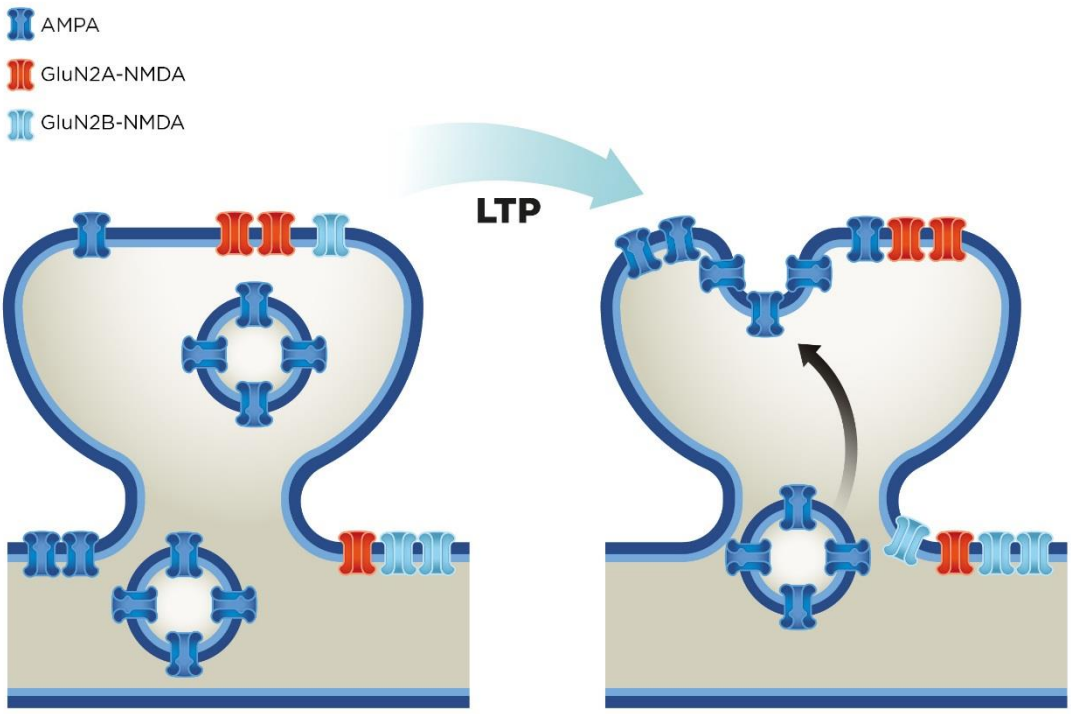

Figure 3. Schematic image showing the redistribution of ionotropic glutamate receptors during LTP. Intracellularly and perisynaptically stored AMPA receptors are recruited into the active site of the synapse while NMDA receptors exchange based on their subunit composition. (Barabás et al., 2018)

2.9.Effect of E2 on synaptic plasticity

In the last decades several studies described that E2 treatment potentiates glutamaterg neurotransmission in the hippocampus. (Teyler et al., 1980; Maggi et al., 1989; Gould et al., 1990; Wong and Moss, 1992) The physiological relevance of this effect was unknown until the discovery of neurosteroids which are synthesized in the brain in both sexes. (Roselli et al., 1985) Since then understanding of the molecular mechanisms of E2-induced synaptic potentiation is in the focus of neuroscience.

The effect of E2 on synaptic potentiation is a complex mechanism, which is probably due to the neuron-type specific expression pattern of ERs. (Kramár et al., 2009; Kumar et al., 2015) E2 acts at the level of pre- and postsynaptic membrane as well. It was demonstrated

that E2 treatment increases the probability of glutamate release in synapses, generating a higher excitatory postsynaptic current (EPSC). (Smejkalova and Woolley, 2010) Postsynaptically E2 was found to modulate dendritic spine formation, synapse size and the number of glutamate receptors in the PSD. For instance, E2 quickly increases the number of new dendrites in hippocampal neurons via actin network remodeling. These newly formed dendrites serve as a site of development of so called „silent" synapse. (Srivastava and Penzes, 2011; Phan et al., 2015) If continuous presynaptic inputs reach this silent synapse, it causes the strengthening and maintenance of the connection, but if there is no presynaptic input, the synapse collapses. (Sheppard et al., 2019) The morphology of the already existing dendrites are also affected by E2. E2 increases the size of the head and the active zone of the dendritic spines as well as shortens the neck region. (Li et al., 2004) In addition, E2 affects the redistribution of glutamate receptors on the dendritic spines. It has been demonstrated that 30 minutes after the E2 treatment, AMPA receptors are transiently removed from the active site and accumulated perisynaptically and AMPA receptor localization is recovered after 60 minutes. (Srivastava et al., 2008) Contrarily, synaptic NMDA receptor levels are only temporarly and shortly increased after E2 application. (Smith and McMahon, 2005) These events lead to decreased synaptic transmission, lower amplitude of miniature EPSCs and increase of the NMDA/AMPA ratio, which is characteristic of a silent synapse. If glutamate release from the presynaptic site activates NMDA receptors within the time frame of E2 effect, the synapse is enhanced and stabilized. This synaptic strengthening is acquired through the reinsertion of AMPA receptors into the active site. In summary, E2 can rewire the neuronal connectivity via potentiating the more active and weakening or abolishing the less used synapses. (Xie et al., 2007; Srivastava et al., 2008)

The continuous movement of glutamate receptors inside and outside of the synapse is a fundamental part of the effect of E2 on synaptic plasticity, however the precise mechanism in live cells has not been described. There are studies examining the effect of E2 on NMDA receptors or the effect of glucocorticoid hormones on the movement AMPA receptor. NMDA receptors diffuse slower in the neuronal membrane after E2 treatment, while corticosterone increases the surface diffusion of AMPA receptors and enchances LTP formation (Groc et al., 2008; Potier et al., 2016), but the ability of E2 to modulate the membrane movement of AMPA receptors is unknown.

3. Aims of the study

The major scope of this study was to determine the non-classical effects of E2 on the membrane movement of AMPA and mGluR1 glutamate receptors in order to better understand the molecular mechanism of E2 improved synaptic plasticity.

Our aims were:

1. to determine the E2 effect on diffusion coefficient (D) of AMPA and mGluR1 receptors in differentiated PC12 cells

2. to explore which ERs are responsible for the E2 effect

3. to test the role of cortical actin network in the E2 effect

4. to measure the effect of E2 on the D and synaptic dwell time of AMPA receptors in cultured hippocampal neurons

4. Materias and methods

4.1. Cell culture and neuronal differentiation

For single-molecule tracking of glutamate receptors, rat pheochromocytoma cells (PC12, Sigma-Aldrich) were differentiated into dPC12. PC12 cells were plated at a density of 2 x 10^3 cells/cm^2 on collagen IV-coated 35-mm glass-bottom dishes (MatTek Corporation) in phenol red-free RPMI 1640 medium supplemented with 10% horse serum (HS), 5% fetal bovine serum (FBS), and 2 mM L-glutamine (culture RPMI, cRPMI). Twelve hours after plating, the medium was replaced with phenol red-free RPMI 1640 medium supplemented with 1% HS, 2 mM L-glutamine, and 50 ng/mL nerve growth factor (NGF-2.5S, Sigma-Aldrich). The cells were fed with cRPMI after 2 days and used for imaging after 4 days of differentiation.

For antibody specificity testing chinese hamster ovary cells (CHO) were cultured in phenol-red free F12 medium supplemented with 10% fetal bovine serum (FBS), and 2 mM L-glutamine (culture F12, cF12). A day before transfection 2 x 10^5 CHO cells were plated onto untreated coverslip.

Cultures of the hippocampal neurons were prepared from C57BL/6 mouse embryos (E17-18) to examine the surface movement of extrasynaptic and synaptic GluR2-AMPAR molecules. The brains were aseptically removed from the skull, meninges were pulled off, and both hippocampi were separated from the cortex. Dissected hippocampi were incubated in pre-warmed MEM (Thermo Fischer Scientific) containing 0.05% trypsin (Gibco) and 0.05% DNaseI (Gibco) at 37 °C for 15 min. Two milliliters of FBS was added to stop the digestion, and the mixture was centrifuged for 5 min at 1200 rpm. Cells were triturated in Neurobasal (NB, Thermo Fischer Scientific) supplemented with B27 (Thermo Fischer Scientific), 5% FBS, 1% penicillin-streptomycin (Thermo Fischer Scientific). Then, 100.000 cells were plated on glass bottoms coated with poly-D-lysine (PDL)- and laminin-coated 35-mm glass-bottom dishes (Kovács et al., 2018). Neurons were cultured in an incubator at 95% relative humidity and 5% CO_2. After 3 days of seeding, one-third of the medium was replaced with pre-warmed MEM every third-day until day *in vitro* 19-21.

4.2. Characterization of neuronal properties of dPC12 and synapse detection on hippocampal culture

To validate the neuronal differentiation of PC12 cells, immunofluorescent staining was performed with microtubule-associated protein 2 (MAP2) and β-III tubulin antibodies. Cells were fixed in 4% paraformaldehyde (PFA) for 15 min and permeabilized with 0.03% Triton X-100 for 30 min after 4 days of differentiation. The cells were then incubated overnight at 4 °C with either mouse anti-MAP2 antibody (1:1000, MAB3418, Millipore) or mouse neuron-specific anti-β-III tubulin antibody (1:1000, MAB1195, RD Systems), before being incubated with biotinylated donkey anti-mouse $F(ab')_2$ (1:200, Jackson ImmunoResearch) and Alexa Fluor 647-conjugated streptavidin (1:2000, Thermo Fisher Scientific).

The electrophysiological properties of dPC12 were tested using whole-cell patch-clamp recording. Patch pipettes (1.5 mm outer diameter and 1.1 inner diameter) with a resistance of 6 MΩ were pulled from borosilicate glass capillaries with a micropipette puller (Sutter Instruments). The pipette recording solution contained (in mM) 10 KCl, 130 K-gluconate, 1.8 NaCl, 0.2 EGTA, 10 HEPES, and 2 Na-ATP, 0.2% biocytin and the pH was adjusted to 7.3 with KOH. All recordings were performed at 32°C in a chamber perfused with oxygenated artificial cerebrospinal fluid (ACSF) containing (in mM) 2.5 KCl, 10 glucose, 126 NaCl, 1.25 NaH_2PO_4, 2 $MgCl_2$, 2 $CaCl_2$, and 26 $NaHCO_3$. Whole-cell recordings were made with an Axopatch 700B amplifier (Molecular Devices) using an upright microscope (Nikon Eclipse FN1) equipped with infrared differential interference contrast optics. Cells with access resistance below 20 MΩ were used for analysis. Signals were low-pass filtered at 5 kHz and digitized at 20 kHz (Digidata 1550B, Molecular Devices). Acquisition and subsequent analysis of the data were performed using Clampex9 and Clampfit software (Axon Instruments). After measurement cells were fixed with 4% PFA for 15 min and permeabilized with 0.03% Triton X-100 for 30 min and Alexa Fluor 488 conjugated Streptavidin (1:2000) was applied for 2 hours at room temperature.

Dual-label immunofluorescence was performed to detect mature synapses in hippocampal neurons. Cells were treated as described above except that they were incubated overnight at 4 °C with anti-homer1 (1:1000, 160006, Synaptic Systems) and anti-β-III tubulin (1:1000, MAB1195, RD Systems) antibodies followed by Alexa Fluor 488-conjugated anti-chicken antibody and Alexa Fluor 647-conjugated anti-mouse antibody, respectively.

All immunofluorescence images were taken on confocal laser scanning microscope (CLSM) (Zeiss LSM710, 100X). A helium-neon laser with 488 and 633 nm wavelength was used to excite Alexa Fluor 488 and Alexa Fluor 647, respectively. Images were captured at 2048x2048 pixel resolution with a 2 μm optical thickness.

We applied MitoTracker Deep Red, carbocyanine-based MitoTracker dye, for synaptic labeling of live neurons. Previous experiments showed that MitoTracker effectively labels mitochondria live presynaptic terminals (Ehlers et al., 2007). To validate Mitotracker Deep Red as a synapse labeling in our experiments, hippocampal neurons were incubated with MitoTracker Deep Red (1 nM, Thermo Fischer Scientific) at 37 °C for 10 min. After washing neurons were fixed as described above and incubated overnight at 4 °C with anti-bassoon antibody (1:1000, ab82958, Abcam) followed by abberior STAR ORANGE conjugated anti-mouse secondary antibody (1:500, STORANGE, Abberior). 2 dimensional stimulated emission depletion (STED) images were taken on Abberior Expert Line STED system equipped with Plan Apo 100X/1.45 objective (Nikon). STAR ORANGE and MitoTracker were excited at 561 nm and 640 nm, respectively. The wavelength of the depletion laser was 775 nm. Super-resolution images were captured with 20 nm pixel size, 20 msec dwell time, and the pinhole was set to 1 A.U.

4.3.E2 receptor detection

Expression levels of estrogen receptor α (ERα), estrogen receptor β (ERβ), and the membrane estrogen receptor, GPER1, were examined in the dPC12. Total ribonucleic acid (RNA) was extracted from dPC12 with a conventional TRIzol (Thermo Fisher Scientific)-based protocol, and complementary deoxyribonucleic acid (cDNA) was constructed using a High-Capacity RNA-to-cDNA Kit (Thermo Fisher Scientific). The following polymerase chain reaction (PCR) primers were used: ERα, 5'-CGTAGCCAGCAACATGTCAA-3', and 5'-AATGGGCACTTCAGGAGACA-3'; ERβ, 5'-GAGGTGCTAATGGTGGGACT-3' and 5'-CTGAGCAGATGTTCCATGCC-3'; and GPER1, 5'-TGCACCTTCATGTCCCTCTT-3' and 5'-AAGGACCACTGCGAAGATCA-3'.

4.4. Single molecule glutamate receptor labeling in live dPC12 and hippocampal culture

To detect GluR2-AMPAR and mGluR1 molecules in the plasma membranes of dPC12, live-cell immunofluorescent labeling was performed. Before single-molecule imaging, dPC12 were incubated in dRPMI with ATTO 488-labeled antibodies directed against the extracellular N-terminal domain of either rat GluR2 (1:100, Alomone Labs) or rat mGluR1 (1:100, Alomone Labs) at 37 °C for 6 min. Specificity of ATTO 488-labeled GluR2-AMPAR antibody has been reported previously in brain sections of GluR2 knockout mice (Egbenya et al., 2018). The specificity of the antibodies was also tested with control peptides ($GluA2_{179-193}$ peptide and $mGluR1_{501-516}$ peptide, Alomone Labs), and no immunoreactivity was observed. In order to further test the specificity of anti-GluR2 antibody CHO cells were transfected with plasmid encoding GluR2 subunit using Lipofectamine 3000 (Sigma) according to the manufacturer's protocol. Rat GluR2 cDNA sequence was subcloned into a pCl mammalian expression vector under XhoI-NotI place. The GluR2 cDNA sequence was a gift from Jeremy Henley (Addgene plasmid #64941). The construct was verified with Sanger sequencing. 24 hours after transfection cells were labeled and imaged the same manner as detailed above.

To simultaneously label live synapses and GluR2-AMPAR, cultured hippocampal neurons were incubated in MEM containing MitoTracker Deep Red (1 nM, Thermo Fisher Scientific) and ATTO 488-labeled antibodies directed against the extracellular N-terminal domain of rat GluR2 (1:100, Alomone Labs) at 37 °C for 10 min. Neurons were imaged after they were carefully washed 3 times with pre-warmed MEM.

4.5. Drug application and cell viability assay

The following drugs were applied immediately before imaging the dPC12 in dRPMI: 17β-estradiol (E2, Sigma-Aldrich, 100 pM in 10^{-5}% EtOH, 1 nM and 100 nM in 10^{-3}% EtOH); G1, a selective GPER1 agonist (Tocris, 100 nM in 10^{-5}% dimethyl sulfoxide (DMSO)) (M. et al., 2009); and diarylpropionitrile (DPN), a selective ERβ agonist (Tocris, 10 pM in 2 x 10^{-5}% DMSO) (Bálint et al., 2016). To block GPER1, dPC12 were incubated in dRPMI containing G15, a selective GPER1 antagonist (Tocris, 1 μM in $2x10^{-3}$ % DMSO) (M. et al., 2009), for 10 minutes before E2 application and imaging. To inhibit actin polymerization, we applied latrunculin A (latA, Sigma-Aldrich, 1 μM in 0.1% DMSO) for

5 min before E2 addition and imaging. We also inhibited the actin polymerization regulator cofilin (Bamburg and Bernstein, 1000), via application of a selective Rho-associated protein kinase (ROCK) inhibitor, GSK429286 (Tocris, 1 μM in 0.1% DMSO) for 1 h (Liu et al., 2018) or selective c-Jun N-terminal kinase (JNK) inhibitor, SP600125 (Tocris, 1 μM in 0.1% DMSO) for 1 hour (Kim et al., 2019).

At the end of the experiments, the viability of the dPC12 was tested with a LIVE/DEAD viability/cytotoxicity kit (Thermo Fisher Scientific) according to the manufacturer's instructions. The results demonstrated that the cells retained their plasma membrane integrity during the experiments.

The hippocampal neurons were treated with E2 in the same manner as detailed above, with the exception that chemical long term potentiation (cLTP) was induced by incubating the neurons in MEM containing glycine (200 μM) and picrotoxin (1 μM) for 3 min (Groc et al., 2008) at room temperature. After washing 3 times, the cells were placed back at 37 °C for 20 min.

4.6. Single-molecule imaging of glutamate receptors with TIRF and HILO microscopy

Single-molecule imaging of labeled glutamate receptors was carried out on an Olympus IX81 fiber total internal reflection fluorescence microscope (TIRFM) equipped with Z-drift compensation (ZDC2) stage control, a plan apochromat objective (100X, numerical apertura: 1.49, Olympus), and a humidified chamber heated to 37 °C and containing 5% CO_2.

The dish containing dPC12 was mounted in the humidified chamber of the TIRF microscope immediately after *in vivo* labeling. A 491 nm diode laser (Olympus) was used to excite ATTO 488, and emission was detected above the 510 nm emission wavelength range. The angle of the excitation laser beam was set to reach a 100 nm penetration depth of the evanescent wave.

Hippocampal neurons were imaged using an Olympus IX81 fiber TIRF microscope with highly inclined laminated optical sheet (HILO) illumination (Tokunaga et al., 2008). The ATTO 488 dye was excited with the same laser as described above, and emission was detected with a 518QM32 filter. MitoTracker was excited with a 633 diode laser (Olympus), and emission was detected with a 655WB20 filter. A Hamamatsu 9100-13 electron-

multiplying charge-coupled device (EMCCD) camera and Olympus Excellence Pro imaging software were used for image acquisition by TIRF and HILO microscopy.

Experiments were performed for 20 min. During the measurement period of ATTO 488-GluR2-AMPAR and ATTO 488-mGluR1, 20-30 images were recorded with 10-second sampling intervals and 33-ms acquisition times. Single-molecule tracking of ATTO 488-GluR2-AMPAR and ATTO 488-mGluR1 was performed with custom-made software written in C++ (WinATR (Kusumi Lab, Membrane Cooperativity Unit, OIST). The center of each particle was localized by two-dimensional Gaussian fitting, and the trajectory for each signal was created by a minimum step size linking algorithm that connected the localized dots in subsequent images. The trajectories were individually checked, and artifacts or tracks shorter than 15 frames were excluded from further analysis. A minimum of 400 trajectories was collected in each experiment from both the soma and neurites. To examine the effect of E2 or vehicle (EtOH), 100-150 trajectories were collected in every consecutive 5-minute interval for up to 20 min (0-5, 5-10, 10-15, and 15-20 min). To identify the live synapses in hippocampal neurons, the MitoTracker Deep Red signal was detected as time-lapse stacks for 10 seconds. Time-lapse stacks were defined as Z-stacks, and an average intensity Z-projection was applied to increase the image quality and optimize the signal-to-noise ratio of the MitoTracker Deep Red signal.

4.7.Characterization of the surface movement of glutamate receptors

The mean square displacement curve for each trajectory was calculated by the following equation:

$$MSD(m\Delta T) = \frac{1}{N-m}\sum_{i=1}^{N-m}((x_{i+m}-x_i)^2+(y_{i+m}-y_i)^2)$$

where x_i and y_i are the coordinates of the signal's center, ΔT *is* the time interval between two consecutive frames, *N is* the total number of frames, and *m* represents the time delay.

The maximum likelihood estimation (Berglund, 2010) was applied to obtain the corresponding diffusion coefficient (D) value for each trajectory. Δx_k and Δy_k represent the observed displacements ($\Delta x_k = x_{k+1} - x_k$ and $\Delta y_k = y_{k+1} - y_k$) arranged in *N*-component column vectors, where the total number of frames is equal to *N*+1, and x_n and y_n are the

coordinates of the signal center on the *n*th frame. Σ is the $N \times N$ covariance matrix defined by the following equation:

$$\Sigma_{ij} = \begin{cases} 2D\Delta t - 2(2DR\Delta t - \sigma^2), \text{if } i = j \\ 2DR\Delta t - \sigma^2, \quad \text{if } i = j \pm 1 \\ 0, \quad \text{otherwise} \end{cases}$$

where D is the diffusion coefficient, Δ*t* is the frame integration time, σ is the static localization noise, and *R* summarizes the motion blur effect. In our case, *R*=1/6 as a consequence of continuous illumination.

The likelihood was defined by the following function:

$$L(\Delta x, \Delta y) = -log|\Sigma| - \frac{1}{2}(\Delta x)^T \Sigma^{-1}(\Delta x) - \frac{1}{2}(\Delta y)^T \Sigma^{-1}(\Delta y)$$

D and σ, which provide the maximal likelihood, are the estimated diffusion coefficient and static localization noise, respectively. The calculation of the determinant and the inverse of the covariance matrix at each step of the optimization method can be a severe computational difficulty at high values of *N*. An approximation (Gray, 2006) based on the theory of circulant matrices is applicable (Berglund, 2010). The global optimization of the likelihood function based on this approximation was implemented in MATLAB. The goodness of optimization was judged by evaluating the static localization noise. An optimization was considered to be inaccurate, and the corresponding trajectory was excluded from further analysis when the estimated static localization noise was out of ±90% range of the group's mean.

To examine the synaptic movements of GluR2-AMPAR, the maximum intensity Z-projected MitoTracker labeled synaptic area was determined manually. GluR2-AMPAR molecules were identified as synaptic if the trajectory was colocalized at least on one frame with the MitoTracker signal, and extrasynaptic if there was no co-localization (Groc et al., 2006, 2007). D values were calculated as described above for both synaptic and extrasynaptic GluR2-AMPAR (Groc et al., 2008). The synaptic dwell time for each treatment was determined as the mean time spent by synaptic receptors within the synaptic (MitoTracker labeled) area. The relative surface distribution of synaptic GluR2-AMPAR content (synaptic/total GluR2-AMPAR molecule trajectories) was calculated for each recording after vehicle or E2 treatment.

4.8. Dual-color imaging of AMPAR and GPER1 with Stohastical Optical Reconstruction Microscopy (STORM)

Super-resolution 3D STORM imaging was performed to examine the number of receptors and the probability of interaction between GluR2-AMPAR and GPER1 in dPC12. PC12 cells were plated onto poly-D-lysine (PDL)- and laminin-coated coverslips (Kovács et al., 2018), and differentiated into neurons as described above. The neurons were incubated in dRPMI medium containing either vehicle (EtOH) or E2 (100 pM or 100 nM) at 37 °C for 10 min. Immediately after treatment, GluR2-AMPAR was applied to live PC12 cells with mouse anti-GluR2-AMPAR antibody (1:1000, MAB397, raised in mouse, Millipore) at 37 °C for 20 min, followed by fixation in 4% PFA. After a thorough wash, the cells were incubated with anti-GPER1 primary antibody (1:5000, AF5534, Novus Biological) at 4 °C for 48 h. CF-568-labeled donkey anti-goat antibody (1:400, Biotium) was applied at room temperature for 2 h. Following three consecutive washes, Alexa Fluor 647-labeled anti-mouse antibody was applied at room temperature for 2 h (1:200, Jackson ImmunoResearch). The coverslips were washed, covered with imaging medium prepared from the following reagents in Dulbecco' phosphate buffer saline (PBS): 5% glucose, 0.1 M mercaptoethylamine, 1 mg/mL glucose oxidase and μl/mL 2.5 catalase (1500 U/mL) (Dudok et al., 2015), and transferred onto standard glass slides immediately before imaging. Using a CFI Apochromat TIRF 100X objective, corresponding confocal and super-resolution images were collected with a Nikon N-STORM/C2+ super-resolution system based on the platform of a Nikon Ti-E inverted microscope equipped with Nikon Perfect Focus System and a Nikon C2 confocal scan head. 3D STORM images were captured with an Andor iXon Ultra 897 EMCCD camera (pixel size: 160 nm/pixel) using an astigmatic imaging method which enables us to localize molecules within an axial distance of -300 to 300 nm from the center plane. STORM images were acquired by illuminating the samples with high-power lasers (561 and 647 nm). Image acquisition and processing were performed using the Nikon NIS-Elements AR software with the N-STORM module. The obtained 3D STORM localization points were filtered for the collected photon number, z-position (within an axial distance of -300 to 300 nm from the center plane), and local density using the VividSTORM software (Barna et al., 2016). Localization points were selected according to the regions of interest (ROIs) that were manually defined based on the correlated high-resolution confocal images. The clusters of selected localization points were determined using the density-based

spatial clustering of applications with noise (DBSCAN) algorithm. A cluster was defined if 3 or more localization points were detected within a 100 nm radius. The center of mass representing a single molecule was calculated for each cluster. In order to examine the number of GPER1 molecules relative to GluR2-AMPAR molecules, the ratio between the number of GPER1 and GluR2-AMPAR molecules (GPER1/GluR2-AMPAR) was calculated for both the soma and neurites.

4.9. Imaging of GPER1 distribution in dPC12 with Stimulated Emission Depletion Microscopy (STED)

To examine whether GPER1 is internalized after E2 administration, super-resolution 2D-STED microscopy was used. After 10 min of treatment with vehicle (10^{-3}% EtOH) or 100 nM E2, dPC12 was fixed with 4% PFA. Then, GPER1 immunocytochemistry was performed in the same manner as detailed in the section on STORM, with the exception that Alexa Fluor 647 conjugated anti-goat secondary antibody was used (1:2000) to visualize GPER1. To determine the boundary between the membrane and cytoplasm, dPC12 were treated with a vehicle or 100 nM E2 and cell surface biotin labeling was performed prior to GPER1 immunocytochemistry. Cells were washed with PBS containing 1 mM Ca^{+} and 1 mM Mg^{+} and incubated with biotin (0.5 mg/mL in PBS, EZ-Link Sulfo-NHS-LC-Biotin, ThermoFisher) for 10 minutes at room temperature followed by wash and fixation with 4% PFA for 20 minutes. After washing, cells were incubated with Alexa Fluor 594 conjugated streptavidin (1:2000, Thermofisher) for 20 minutes at room temperature. STED images were taken as described above. Based on the result of STED microscopy, 1 μm thick membrane area was defined from the outer edge of GPER1 signal. For image analysis of GPER1 internalization we used cells labeled with GPER1 antibody alone. The captured images were analyzed using Fiji software (Schindelin et al., 2012). After background subtraction, the mean intensity value was calculated with the plot profile algorithm within a specified rectangle (ROI size: 12 μm^2). From each cell (n=15 total) one ROI (with 2 μm^2 membrane and 10 μm^2 cytoplasmic area) was selected, integrated density was calculated and normalized to the area (μm^2).

4.10. Imaging of cortical actin network

To validate the effect of latA, GSK429286 and SP600125 on dPC12, the morphology of the cortical actin network of dPC12, were examined after drug administration. After 10 min of treatment with 1 μM of latA, or after 60 min of treatment with 1 μM of GSK429286, 1 μM of SP600125, or vehicle (in 10^{-3}% DMSO), dPC12 were fixed in 4% PFA, permeabilized with 0.1% Triton X-100 for 30 min, and incubated with Alexa Fluor 488 phalloidin (1:200, Thermo Fisher Scientific) for 45 min at room temperature. Imaging was performed on CLSM (Zeiss LSM710, 100X), and Alexa Fluor 488 was excited with an argon laser at a wavelength of 488 nm. Images with 2 μm optical thickness and 4096x4096 (X/Y) resolution were captured with the use of ZEN software applying the same settings (laser power, digital gain) to all images. 6 cells were selected from each treatment group (vehicle, latA, GSK, SP6001235). Three ROIs (ROI size: 4.3 μm^2) were selected from each cell and the average integrated density was calculated from raw images using FIJI software. Results are expressed in the percentage of ROI in order to obtain the integrated density values per μm^2 (in arbitrary units).

4.11. Statistics

To compare the surface movements of GluR2-AMPAR and mGluR1 in soma and neurites, D values were expressed as cumulative probability functions. In the rest of the experiments, the D values were expressed as the mean percentage of control (vehicle) + standard error of mean (SEM) in figures. GPER1/AMPAR ratios and extrasynaptic/synaptic D_{AMPAR} values were expressed as the median ± 25% -75% (interquartile range). To compare the distributions of D values of vehicle control and treatment and extrasynaptic/synaptic D_{AMPAR} values the Kolmogorov-Smirnov test was used. The integrated GPER1/AMPAR ratios of the soma and neurites and densities of Alexa Fluor 488-phalloidin and Alexa Fluor 647-GPER1 immunolabeling were compared with the Mann-Whitney U test. Synaptic dwell time and exchange frequency of GluR2-AMPAR were compared using the Kruskal-Wallis test followed by Dunn's post hoc test. Statistical differences were considered significant at a *p*-value of <0.05. All statistical analyses were performed with Statistica version 13.3 for Windows (TIBCO Software Inc.).

5. Results

5.1. Characterization of neuronal properties of dPC12

We characterized the PC12 cells after 4 days of NGF treatment when neurite outgrowth was pronounced (Fig. 4*A*). Immunocytochemistry showed that dPC12 expressed neuronal markers such as β-III tubulin and MAP-2 (Fig. 4*B*). In addition, we examined the passive electrophysiological parameters of 10 cells using whole-cell patch clamp technique. We found that the resting membrane potential, the input resistance and the cell capacitance were -55.5 ±7.7 mV, 1072.7 ±854.9 MΩ and 60.2±32.9 pF, respectively (values are represented as mean ± SD). Finally, we recorded that step current injection elicited a single abortive action potential in dPC12 (Fig. 4*C*). Moreover, *in vivo* labeling of dPC12 demonstrated GluR2-AMPAR and mGluR1 in neurites and soma (Fig. 5).

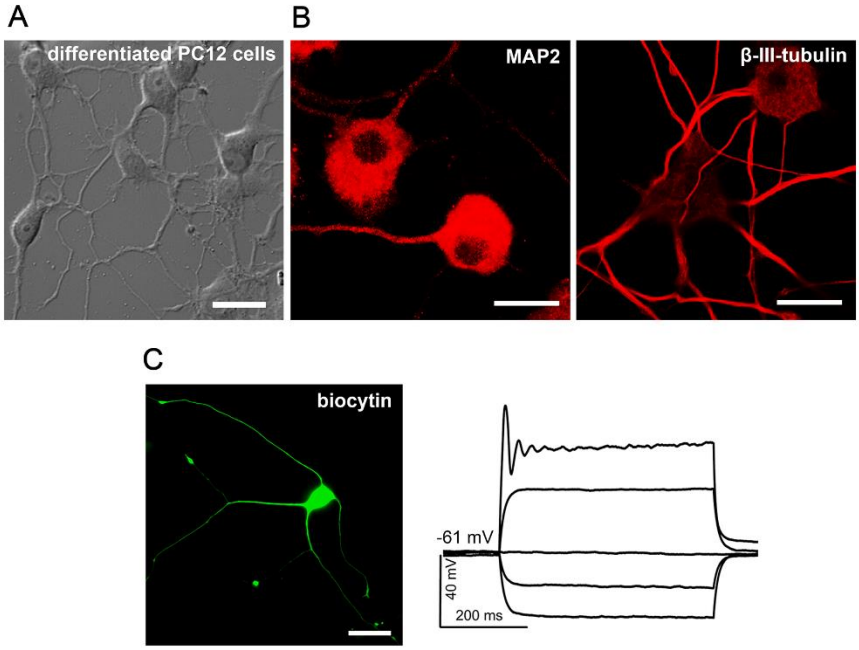

Figure 4. **Characterization of neuronal properties of differentiated PC12 cells.** ***A***, Differential interference contrast microscopy image depicts PC12 cells after 4 days of NGF treatment. ***B***, Immunofluorescence staining of microtubule-associated protein 2 (MAP2) and β-III tubulin shows the presence of neuronal markers. Scale bars: 20 µm. ***C,*** Left: immunofluorescence image of a biocytin loaded dPC12. Right: representative traces of the membrane potential in response to step current injection in dPC12. Scale bar: 20 µm

5.2. Characterization of the labeling of glutamate receptors

In single-molecule tracking experiments, the fluorescence intensity versus time function showed one-step photobleaching, representing single ATTO 488 fluorophores for GluR2-AMPAR and mGluR1. The fluorescence intensity histograms of both GluR2-AMPAR and mGluR1 had peak intensities similar to those of the step sizes for photobleaching (Fig 5*A*, *B*). These results suggest that most of the spots represented single fluorophores and single receptors.

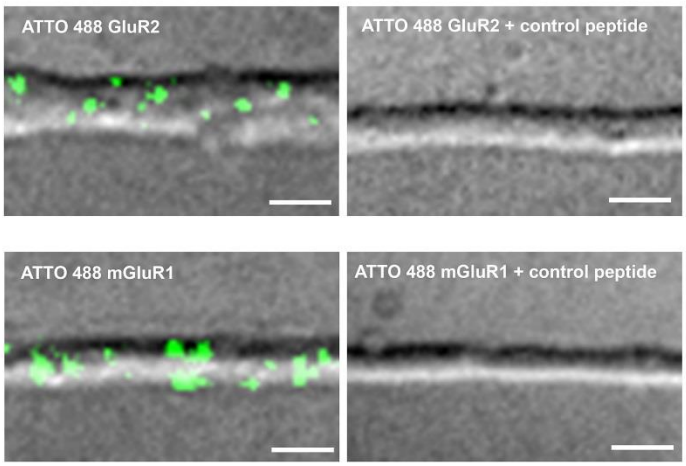

Figure 5. **The specificity of ATTO 488-labeled anti-GluR2-AMPAR and mGluR1 antibodies**. Left, Live-cell labeling of dPC12 neurites with ATTO 488-labeled anti-GluR2-AMPAR and anti-mGluR1 antibodies. Right, No immunoreactivity was observed after pre-incubating with blocking peptides (control peptides) ($GluA2_{179\text{-}193}$ peptide and $mGluR1_{501\text{-}516}$ peptide, Alomone Labs). Scale bar: 2 μm

5.3. E2 rapidly decreases the surface movement of AMPAR in dPC12

5.3.1. *Surface movement of GluR2-AMPAR and mGluR1 in dPC12*

The surface movement of glutamate receptors was detected in the plasma membrane of live dPC12 (Fig. 5*C*). Based on the mean square displacement functions of GluR2-AMPARs and mGluR1 receptors, they exhibited two main types of movements: Brownian diffusion, when receptors moved freely between barriers and confined motion when receptors were restricted to a small area (Fig. 5*D*). The diffusion coefficients of both receptors are

significantly higher on the neurite than on soma (Fig. 5*E, F*), indicating that the surface movement of glutamate receptors is faster on neurites.

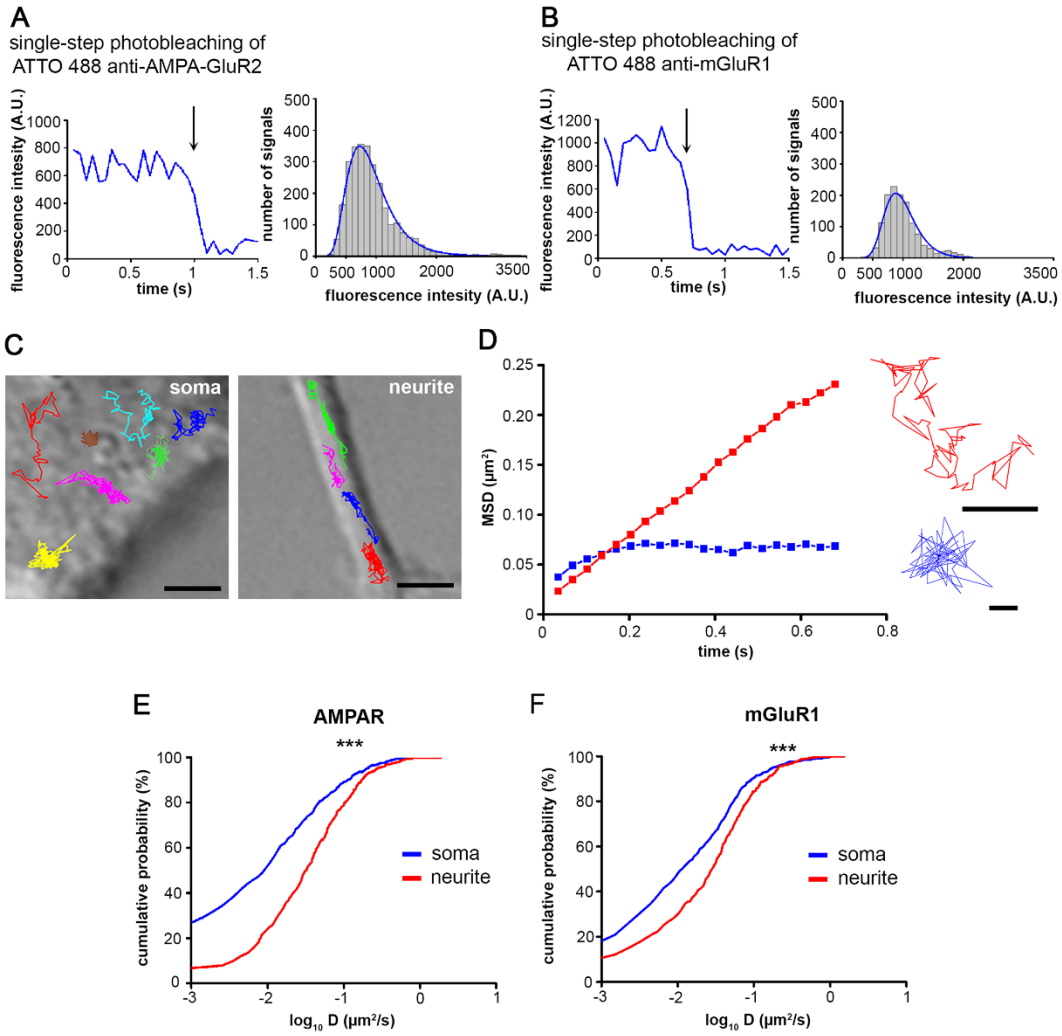

Figure 6. **Characterization of differentiated PC12 cells and validation of single-molecule labeling.** ***A, B,*** Left, Intensity profiles of a single ATTO 488-labeled GluR2-AMPAR (***A***) and mGluR1 (***B***) signal. The arrows indicate single-step photobleaching. Right**,** Histogram showing the intensity value of every spot found in a recording of ATTO 488-labeled GluR2-AMPAR (***A***) and mGluR1 (***B***), superimposed with a single fitted lognormal curve (blue line). ***C***, Representative trajectories of AMPAR molecules on somas and neurites. Scale bar: 2 µm. ***D***, The mean square displacement (MSD) functions and trajectories represent AMPAR molecules with Brownian motion (red) and confined motion (blue). Scale bars: 0.1 µm. ***E,F,*** The cumulative probability functions of D values of AMPAR (***E***) and mGluR1 (***F***) on neurites and somas (n = 510-676 trajectories). ****p*<0.001

5.3.2. *Dose dependence*

Administration of 100 pM, 1 nM and 100 nM doses of E2 evoked a clear dose-dependent decrease in D_{AMPAR} in neurites as measured in the first 20 minutes after treatment with a maximum decrease of 55% ($p<0.01$) (vehicle mean D_{AMPAR} ± SEM ($\mu m^2/s$) on neurite: 0.058±0.003) (Fig 7*A*). In soma, 100 pM of E2 significantly decreased D_{AMPAR} (68%, $p<0.01$), while 1 nM and 100 nM of E2 were ineffective (vehicle mean D_{AMPAR} ± SEM [$\mu m^2/s$] on soma: 0.024±0.002) (Fig 7*A*). In contrast, E2 (100 nM, 1 nM or 100 pM) did not change D_{mGluR1} either in soma or in neurites (Fig. 7*B*) (vehicle mean D_{mGluR1} ± SEM ($\mu m^2/s$); soma: 0.032±0.003, neurite: 0.049±0.005).

To investigate whether a low concentration of EtOH (10^{-3} %) (vehicle) affects GluR2-AMPAR and mGluR1 surface trafficking, we compared D_{AMPAR} and D_{mGluR1} in a culture medium (control) without or with vehicle (20 min after application). There was no significant effect of vehicle on D_{AMPAR} and D_{mGluR1} in dPC12 (values are expressed as the mean D ± SEM [$\mu m^2/s$]; on soma: control D_{AMPAR}: 0.024±0.003 (n = 590 trajectories), vehicle D_{AMPAR}: 0.022±0.002 (n = 612 trajectories); neurite: control D_{AMPAR}: 0.073±0.006 (n = 545 trajectories), vehicle D_{AMPAR}: 0.069±0.007, (n = 647 trajectories); soma: control D_{mGluR1}: 0.033±0.003 (n = 751 trajectories), vehicle D_{mGluR1}: 0.034±0.002, (n = 622 trajectories); neurite: control D_{mGluR1}: 0.051±0.004 (n = 513 trajectories), vehicle: 0.050±0.003, (n = 496 trajectories)).

5.3.3. *Time course*

To examine the time dependence of the effect evoked by E2 on D_{AMPAR} or D_{mGluR1}, we applied the most effective E2 doses on soma and neurites and measured D at different time points. The application of 100 pM of E2 resulted in a significant decrease ($p<0.01$) in D_{AMPAR} on soma within 5 min. This remained reduced at 10 min, 15 min, and 20 min (vehicle mean D_{AMPAR} ± SEM ($\mu m^2/s$) on soma: 5 min, 0.064±0.007; 10 min, 0.054±0.008; 15 min, 0.03±0.004; 20 min, 0.042±0.008). In contrast, 100 nM of E2 only reduced D_{AMPAR} on neurites at 10 min, 15 min, and 20 min (vehicle mean D_{AMPAR} ± SEM [$\mu m^2/s$] on neurites: 5 min: 0.063±0.007; 10 min: 0.051±0.005; 15 min: 0.050±0.007; 20 min: 0.051±0.007) (Fig 7*C*). In contrast, 100 pM or 100 nM of E2 did not affect D_{mGluR1} on neurites or soma, respectively, at any time point (vehicle mean D_{mGluR1} ± SEM [$\mu m^2/s$] on soma: 5 min: 0.033±0.006; 10 min: 0.042±0.006 15 min: 0.031±0.005; 20 min: 0.036±0.007; on neurites:

5 min: 0.061±0.006; 10 min: 0.053±0.007; 15 min: 0.052±0.004; 20 min: 0.038±0.004) (Fig. 7*D*).

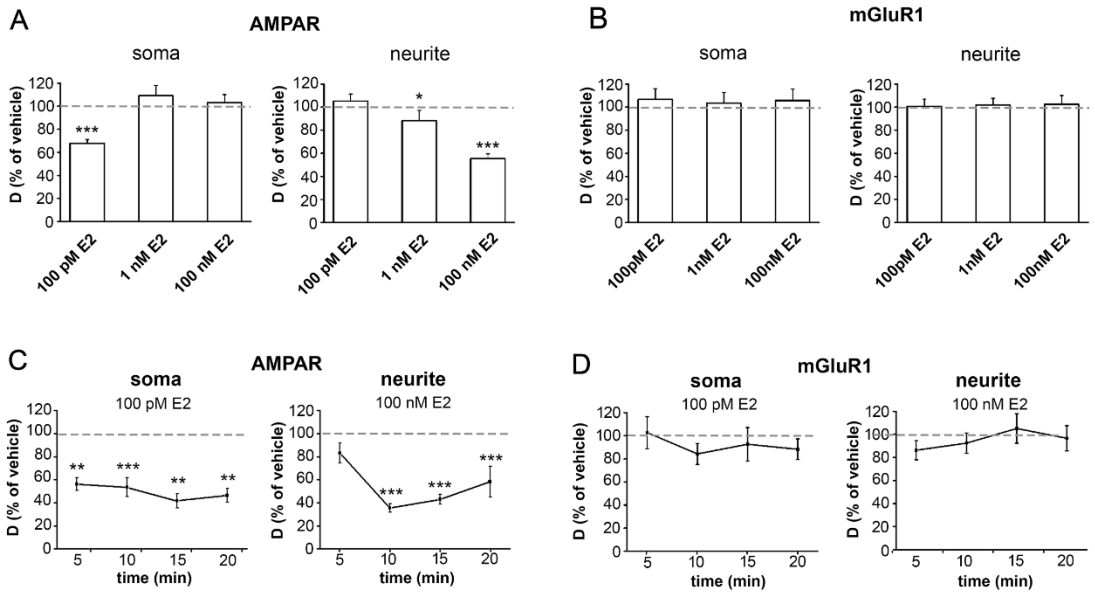

Figure 7. **Effect of E2 on the surface movement of GluR2-AMPAR and mGluR1.** ***A,*** Effect of different concentrations of E2 on the diffusion coefficient (D, $\mu m^2/s$) of GluR2-AMPAR (**A**) and mGluR1 (**B**) (% of vehicle treatment as the mean ± SEM, n = 425-1145 trajectories per group). ***C, D,*** Line graphs depict changes in D of GluR2-AMPAR (***C***) and mGluR1 (***D***) molecules at different time points after the administration of the most effective concentration of E2 (% of vehicle treatment as the mean D ± SEM, n = 117-187 trajectories per time point).

5.4.E2 effect is mediated by GPER1 and ERβ in dPC12

Our PCR results revealed that dPC12 expresses ERβ and GPER1, but not ERα (Fig. 8*A*). Although the addition of ERβ agonist DPN (10 pM) or specific GPER1 agonist G1 (100 nM) alone did not affect the surface movement of somatic GluR2-AMPAR molecules (vehicle mean D_{AMPAR} ± SEM ($\mu m^2/s$) on soma; DPN vehicle: 0.04±0.003; G1 vehicle: 0.023±0.002), co-administration of DPN and G1 decreased D_{AMPAR} (DPN+G1 vehicle D_{AMPAR} mean ± SEM ($\mu m^2/s$) on soma: 0.075±0.009) similar to 100 pM of E2 (Fig 8*B*). G1 (100 nM) mimicked the effect of 100 nM of E2 without and with 10 pM of DPN (vehicle mean D_{AMPAR}

± SEM (μm^2/s) on neurite; G1 vehicle: 0.056±0.003; G1+DPN vehicle: 0.1±0.004) in neurites (Fig 8*B*). However, 10 pM of DPN alone did not alter the D_{AMPAR} in neurites (DPN vehicle mean D_{AMPAR} ± SEM (μm^2/s) on neurite: 0.056±0.004) (Fig 5*B*). In addition, prior application of 1 μM of G15 blocked the effect of 100 pM of E2 on soma and 100 nM of E2 on neurites (vehicle mean D_{AMPAR} ± SEM (μm^2/s); soma: 0.025±0.002, neurite: 0.048±0.003, Fig. 8*B*). G15 application alone did not alter the surface movement of GluR2-AMPAR in either neurites or soma (vehicle mean D_{AMPAR} ± SEM (μm^2/s); soma: 0.020±0.002, neurite: 0.062±0.004, Fig 8*B*).

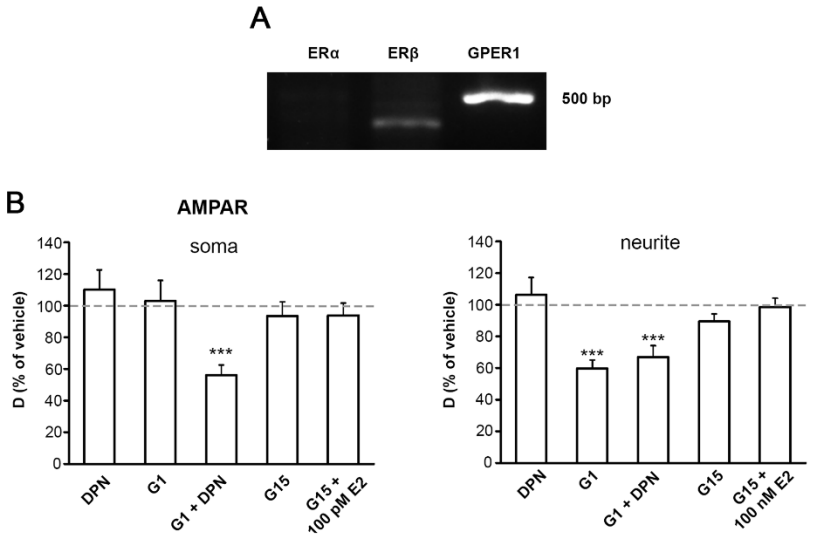

Figure 8. **Effect of estrogen receptor modulation on the surface movement of GluR2-AMPAR.** ***A***, Representative PCR gel electrophoresis image depicting the expression of estrogen receptor beta (ERβ) and G protein-coupled estrogen receptor 1 (GPER1) mRNA in dPC12. Estrogen receptor alpha (ERα) mRNA was not detected. ***B***, Histograms demonstrate the mean D_{AMPAR} as a percentage of vehicle control on somas and neurites in the presence of the estrogen receptor, β (ERβ) agonist diarylpropionitrile (DPN), a GPER1 agonist (G1), G1+DPN together, a GPER1 antagonist (G15) and G15+E2 (with 100 pM of E2 on the somas and 100 nM of E2 on the neurites) (mean ± SEM; n = 215-641 trajectories).

Since we applied DMSO as a vehicle in these experiments, we also tested whether the 0.1 % DMSO alone affected D_{AMPAR}. We compared D_{AMPAR} in a culture medium (control) with or without vehicle (20 min after application). There was no significant effect of DMSO on D_{AMPAR} in dPC12 (values are expressed as the mean D±SEM [μm^2/s] on soma: medium

D_{AMPAR}: 0.024±0.003 (n = 590 trajectories), vehicle D_{AMPAR}: 0.023±0.002 (n = 645 trajectories); on neurite: medium D_{AMPAR}: 0.073±0.006 (n = 545 trajectories), vehicle D_{AMPAR}: 0.062±0.004, (n = 524 trajectories).

Our results show that GPER1 mediates the effect of E2 on GluR2-AMPAR on both soma and neurites. To further analyze the relationship between GluR2-AMPAR and GPER1, we used STORM super-resolution imaging to examine the expression GPER1 and GluR2-AMPAR. STORM imaging revealed that GPER1 and GluR2-AMPAR receptors are expressed on both soma and neurites (Fig. 9*A*). In order to examine the number of GPER1 in relation to GluR2-AMPAR we normalized the number of GPER1 to GluR2-AMPAR using GPER1/GluR2-AMPAR ratio. Our analysis demonstrated that the GPER1/GluR2-AMPAR ratio was significantly higher in soma than in neurites of dPC12 (Fig 9B).

E2 can induce rapid internalization and consequent desensitization of GPER1 (Filardo and Thomas, 2012). The internalization of GPER1 may explain the different effects of E2 on the soma and neurites. To visualize whether GPER1 is internalized after E2 administration in soma, stimulated emission depletion (STED) microscopy was used (Fig 9 *C1, C2*). Super-resolution STED imaging revealed that the intensity of immunostaining of GPER1 was approximately 2 times higher in the membrane region than in the cytoplasm of vehicle-treated dPC12 (Fig 9*C1, C2, D*). After 10 min of 100 nM of E2 treatment, the intensity profile of GPER1 showed a significant decrease in the membrane region (Fig. 9*C1, C2*, *D, E*). In contrast, the majority of GPER1 immunoreactivity was located in the cytoplasm (Fig. 9*C1*, *C2*, *D, E*) after treatment with 100 nM of E2, suggesting rapid internalization of GPER1 in response to high E2 exposure. There was no internalization of GPER1 observed in neurites after 100 nM of E2 treatment.

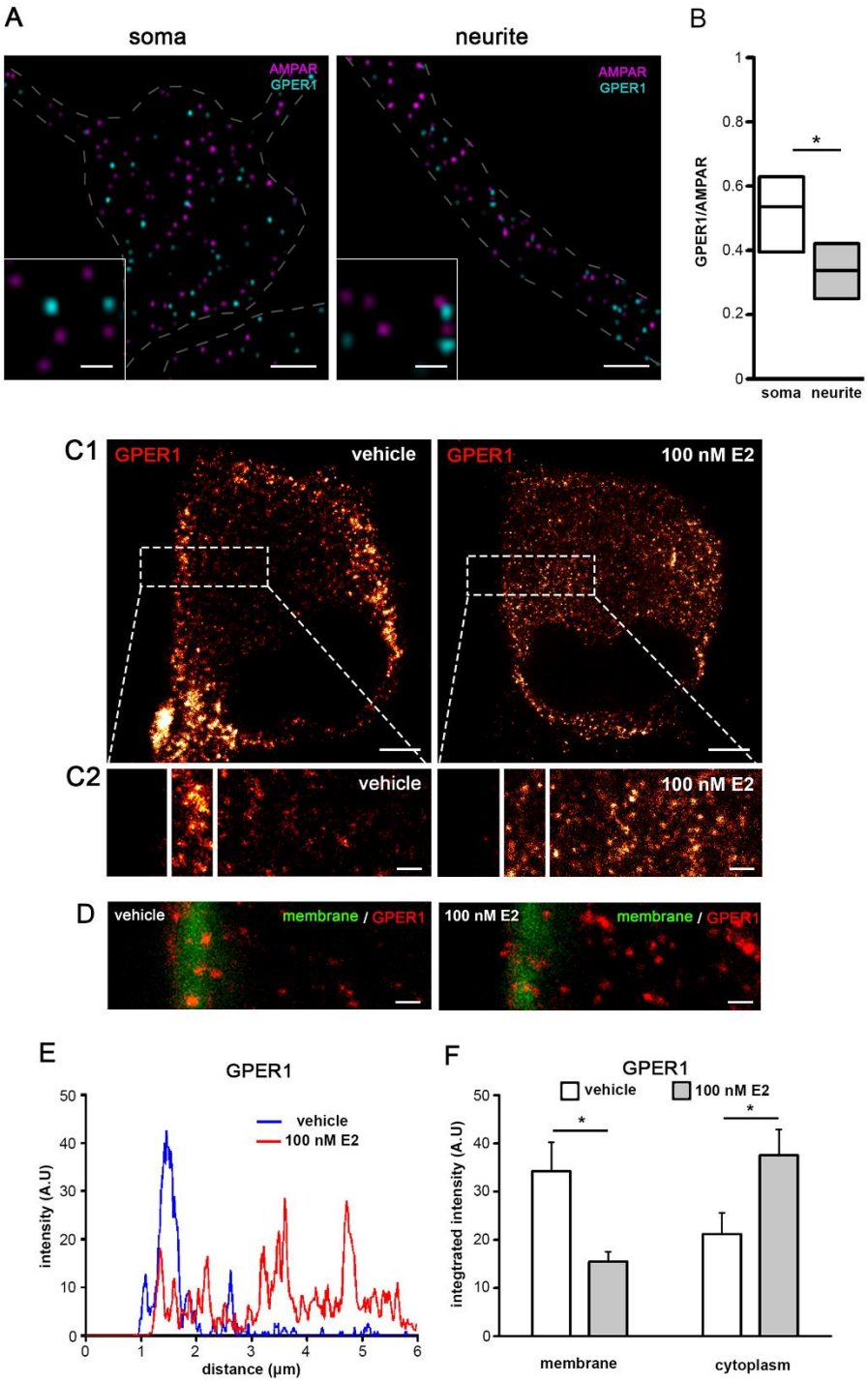

Figure 9. **The GluR2-AMPAR/GPER1 ratio and molecular distance between GPER1 and GluR2-AMPAR in the membrane.** ***A***, STORM images depicting immunolabeled AMPAR (magenta) and GPER1 (cyan) molecules on dPC12. Dashed lines delineate the borders of the neurites and somas. Scale bar: 2 µm; inset scale bar: 0.5 µm. ***B***, The ratio between the number of GPER1 and AMPAR molecules (GPER1/GluR2-AMPAR) on the neurites and somas (n = 11 somas or neurites). ***C1,*** Photomicrographs depict GPER1

immunoreactivity (visualized with STED microscopy) in dPC12 after 10 minutes of vehicle (left) or of 100 nM of E2 treatment (right). Scale bar: 2 μm. ***C2,*** One 2 μm^2 (between parallel white bars) and one 10 μm^2 (to the left) areas were selected within each ROI for the membrane and cytoplasmic regions of each cell, respectively. Integrated density was calculated and normalized to the area. Scale bar: 0.5 μm. ***D,*** Dual labeling of plasma membrane and GPER1 molecules defines the membrane regions (approximately 1 μm wide). Scale bar: 0.5 μm. ***E****,* Line graph of the fluorescent intensity calculated from the magnified STED inserts (C2). ***F****,* Integrated density graphs of GPER1 show the effect of vehicle and 100 nM of E2 treatment in the membrane and in the cytoplasm (n=15 cells were evaluated in each group).

5.5. Function of cortical actin network in the effect of E2 on the membrane diffusion of AMPAR in dPC12

Cortical actin is a thin actin network that lies directly underneath the plasma membrane. The cortical actin network is essential in the organization of neuronal compartments and plays a crucial role in membrane receptor movement (Schevzov et al., 2012), thus we speculated that the cortical actin network may play a role in the effect of E2 on the receptor dynamics. Previous studies show that E2 induces cytoskeleton assembly mediated by GPER1 receptors via different intracellular signaling pathways, including the ROCK-cofilin (Gowrishankar et al., 2012; Wang et al., 2019) and JNK-cofilin (Kim et al., 2019) pathways. To determine the possible role of cortical actin in the effects of E2 on glutamate receptors, we treated cells with the actin polymerization inhibitor, latrunculinA (latA; 1 μM). To examine the role of the ROCK-cofilin and JNK-cofilin pathways in E2 action, we applied the ROCK inhibitor, GSK429286 (1 μM) (Wang et al., 2019), and JNK inhibitor, SP600125 (1 μM) (Kim et al., 2019), respectively.

First, we validated whether latA, or ROCK and JNK inhibitors altered the morphology of cortical actin. Phalloidin immunostaining demonstrated cortical F-actin in dPC12 (Fig. 10*A*). The density of the cortical actin network in dPC12 was decreased by latA, GSK429286, or SP600125 administration (Fig. 10*A*). In single-molecule tracking experiments, 10 min of latA, or pretreatment with GSK429286 or SP600125 for 60 min significantly increased D_{AMPAR} on soma (vehicle D_{AMPAR} mean ± SEM [$\mu m^2/s$]: 0.021±0.002, Fig. 10*B1*) without affecting D_{AMPAR} on neurites in dPC12 (vehicle D_{AMPAR} mean ± SEM [$\mu m^2/s$]: 0.049±0.003, Fig. 10*B2*). Pretreatment with latA, GSK429286, or

SP600125 decreased the effect of 100 pM of E2 on soma and 100 nM of E2 on neurites on the surface movement of GluR2-AMPAR molecules (D_{AMPAR} mean ± SEM [$\mu m^2/s$] on soma: vehicle E2: 0.03±0.004; vehicle E2+latA: 0.062±0.006; vehicle E2+GSK429286: 0.087±0.007; vehicle E2+SP600125: 0.093±0.008; on neurites: vehicle E2: 0.074±0.006; vehicle E2+latA: 0.06±0.004; vehicle E2+GSK429286: 0.113±0.015; vehicle E2+SP600125: 0.128±0.012, Fig. 10*C1,C2*). In experiments with latA, ROCK and JNK cRPMI containing 0.1 % DMSO was used as vehicle control. Cell viability was not altered by DMSO nor latA treatment.

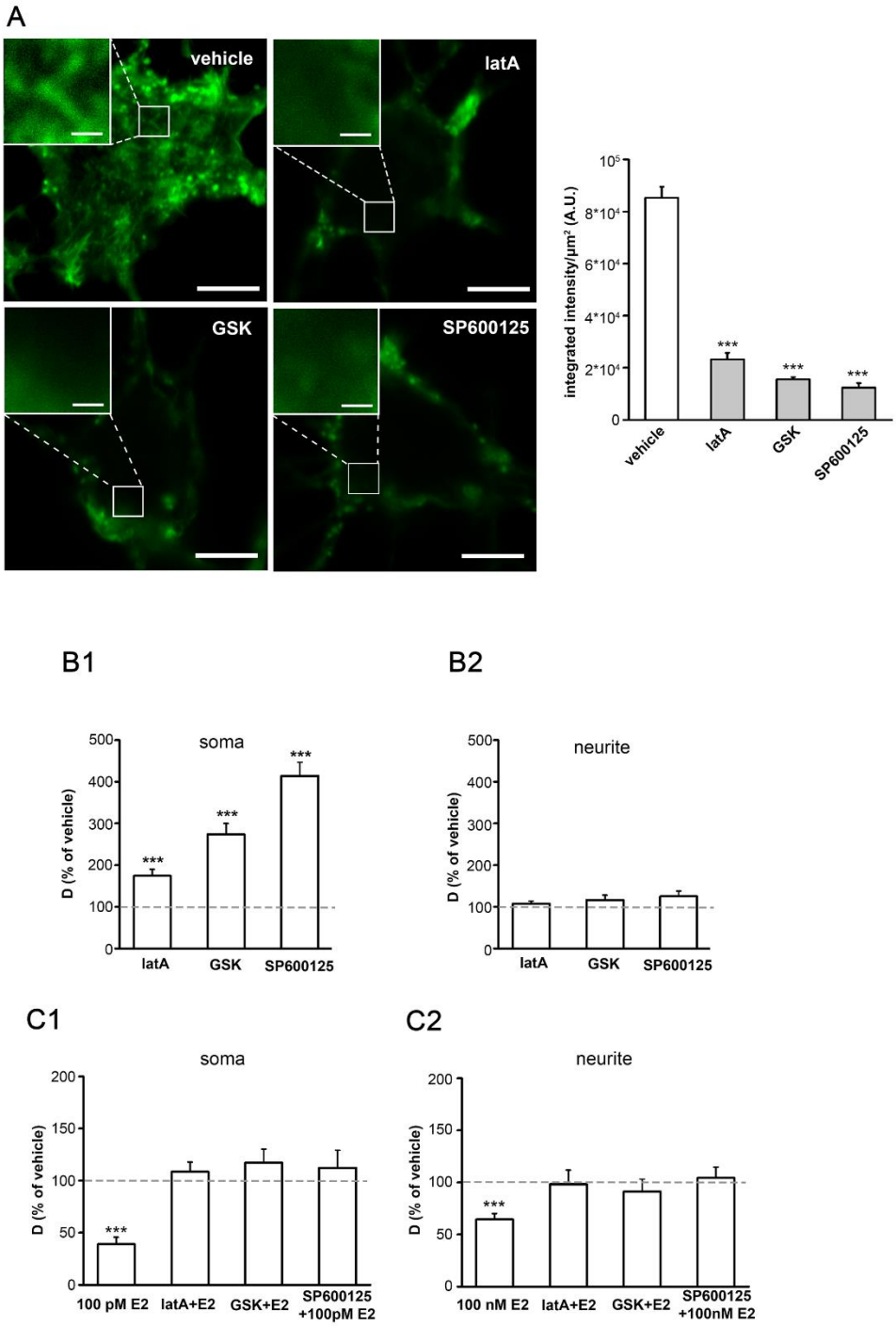

Figure 10. **The role of the cortical actin in the rapid effect of E2.** ***A***, Left, confocal images depict Alexa Fluor 488 phalloidin-labeled cortical actin network in dPC12 after treatment with vehicle, 1 µM of latA, 1 µM of SP600125 or 1 µM of GSK429286. Scale bar: 5 µm; insert scale bar: 0.5 µm. Right, the bar graph shows the effect of LatA, GSK429286, and SP600125 on the integrated density of the fluorescently labeled cortical actin network (n = 3 cells per group (3 ROIs per cell)). ***B1-2***, Effect of LatA, GSK429286, and SP600125 treatment on D_{AMPAR} (% of vehicle treatment as the mean ± SEM; n = 215-544 trajectories).

C1-2, Effect of 100 pM of E2 on somas and 100 nM of E2 on neurites with or without LatA, GSK429286, and SP600125 (% of vehicle treatment as the mean ± SEM; n = 184-277 trajectories). ****p*<0.001

5.6.E2 rapidly decreases the surface movement and increases the synaptic dwell time of AMPAR in hippocampal neurons

To validate the effect of E2 on the surface movement of GluR2-AMPAR in another *in vitro* neuron system and examine the effect of E2 on synaptic GluR2-AMPAR, we performed single-molecule tracking experiments on primary hippocampal neuron culture (Fig. 11*A*).

Immunocytochemical labeling revealed that β-III tubulin-expressing hippocampal neurons have multiple homer-1 positive synapses along their neurites at day *in vitro* 18-21. (Fig. 11*A*). The live-cell presynaptic MitoTracker Deep Red labeling was validated with co-immunostaining of presynaptic protein bassoon. STED imaging showed that every single MitoTracker Deep Red labeled synapse exhibited colocalization with presynaptic marker bassoon. Only 10% of the bassoon labeled synapses showed no colocalization with MitoTracker Deep Red labeling (Fig. 11*B*).

Our single-molecule imaging experiment revealed the surface movement of ATTO 488-labeled GluR2-AMPAR on neurites in extrasynaptic and synaptic regions. D values of GluR2-AMPAR molecules were significantly lower in synapse compared to extrasynaptic regions (Fig 11*C*). Fluorescence intensity histograms and step sizes for photobleaching suggest that most of the spots represented single fluorophores and single receptors. Our *in vivo* labeling failed to show GluR2-AMPAR molecules on soma of hippocampal neurons using HILO.

Both 100 pM and 100 nM of E2 decreased extrasynaptic and synaptic D_{AMPAR} in neurites (Fig. 11*D*). Similar to E2, chemical strengthening of synapses (chemical long term potentiation (cLTP)) elicited a decrease in synaptic D_{AMPAR} (Fig 11*D*) (vehicle D_{AMPAR} mean ± SEM ($\mu m^2/s$): synaptic: 0.253±0.038, extrasynaptic: 0.247±0.014). Furthermore, 100 nM, but not 100 pM of E2, increased the synaptic dwell time of GluR2-AMPAR to a similar extent as cLTP (Fig. 11*D*). Treatment with 100 nM of E2 did not change the cLTP-induced increase in the synaptic dwell time of GluR2-AMPAR. E2 (100 nM, 100 pM) did not affect

synaptic AMPAR content (Fig. 11*E*), and it did not alter cLTP-induced increase in synaptic AMPAR content (Fig. 11*F*).

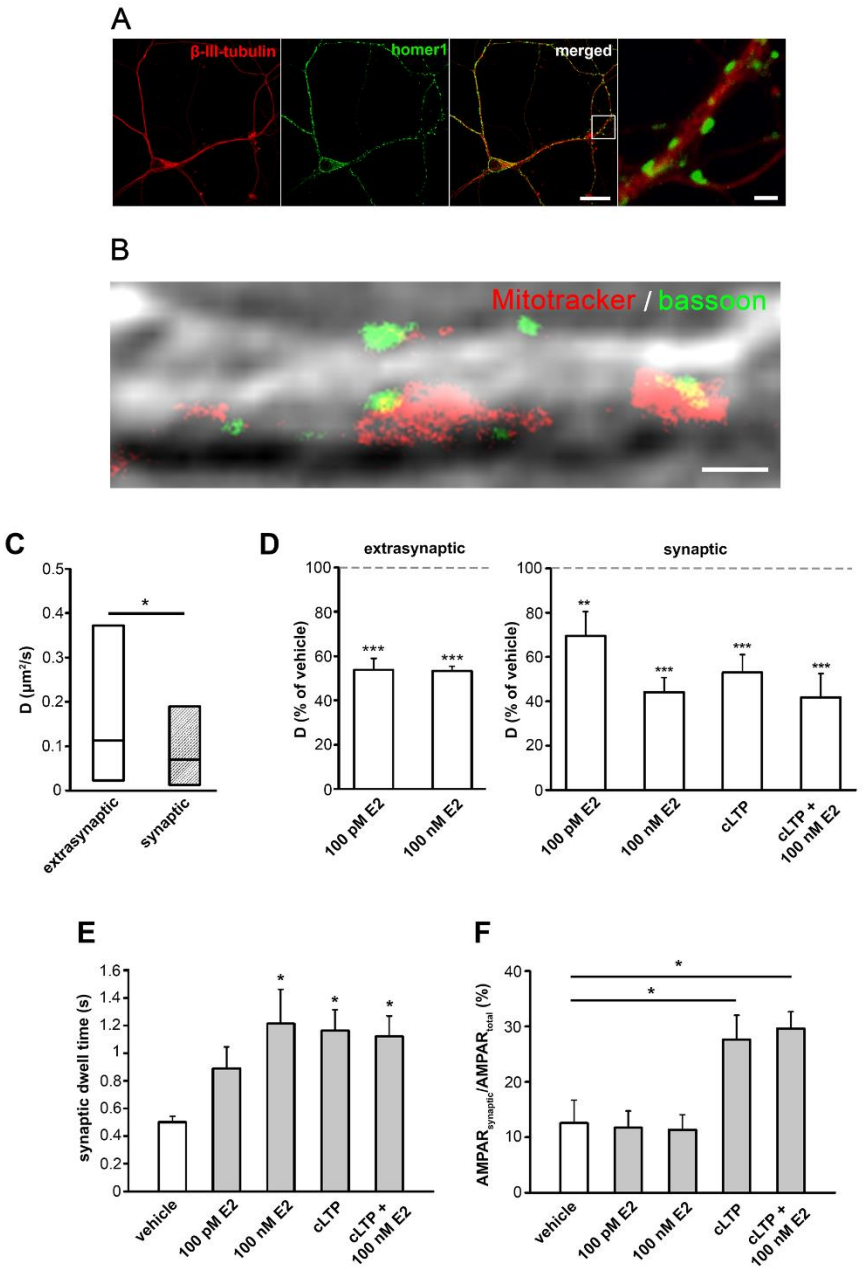

Figure 11. **Effect of E2 on the surface movement of GluR2-AMPA on primary hippocampal neurons.** ***A***, Photomicrograph shows a primary hippocampal neuron labeled with homer-1 (synapse) and β-III tubulin (neuron). Scale bar: 10 μm, insert scale bar: 2 μm. ***B***, Dual color STED image of a hippocampal neuron overlayed to differential interference contrast microscopy image depicts live-cell synapse labeling MitoTracker Deep Red (red) and presynaptic protein bassoon (green). Scale bar: 1 μm. ***C,*** Distribution of D values of extrasynaptic and synaptic GluR2-AMPAR under control conditions (median ± IQR, n =

754 extrasynaptic trajectories and n = 104 synaptic trajectories) ***D***, Effect of E2 (100 pM and 100 nM) on D of extrasynaptic and synaptic GluR2-AMPA with or without chemical LTP (cLTP) induced by glycine/picrotoxin (gly/pic) (% of vehicle treatment as the mean ± SEM; n = 742-928 extrasynaptic trajectories and n = 104-155 synaptic trajectories). ***E, F,*** Effect of vehicle, E2 (100 n, 100 pM) with or without cLTP (gly/pic) on synaptic dwell time (mean ± SEM (s); n= 104-155) (***E***) and relative surface distribution of synaptic GluR2-AMPAR content (synaptic/total GluR2-AMPA molecule trajectories) (mean ± SEM, n= 8-18 recordings) (***F***).

6. Discussion

We found that E2 rapidly decreased the D_{AMPAR} in live dPC12 via rapid membrane-initiated GPER1 signaling in neurites but both GPER1 and ERβ was required for the effect of E2 in soma. Nevertheless, different dose was effective on soma compared to neurites. On soma 100 pM E2, while on neurites 1 nM or 100 nM E2 decreased the D_{AMPAR}. This difference may be the consequence of GPER1 internalization in soma induced by 100 nM E2. We showed that D_{AMPAR} was affected by the cortical actin network in dPC12 cells. Furthermore, the effects of E2 on D_{AMPAR} in soma were mediated by actin via the ROCK-cofilin and JNK-cofilin pathways. Importantly, we confirmed our results on live hippocampal neurons: we showed that E2 also decreases $D_{AMPAR.}$ Similarly to cLTP induction, E2 decreases D_{AMPAR} and increases the synaptic dwell time of GluR2-AMPAR.

PC12 cells are an extensively used model in neurobiology because they dramatically change their phenotype when they are exposed to NGF. They exit the cell cycle, project long neurite-like processes and take on many properties of differentiated sympathetic neurons including synthesis, storage, and release of catecholamines (principally dopamine). (Wiatrak et al., 2020). Previous experiments demonstrated that dPC12 cells can generate action potentials (Hu et al., 2018), and express GluR2-AMPA, mGluR1 mRNA and protein (Kane et al., 1998; Mehmood et al., 2013). Our results confirmed that dPC12 has abortive action potential similar to immature neurons with moderate amount of sodium current (Belinsky et al., 2011) and expresses GluR2-AMPAR and mGluR1 in soma and neurites, providing an effective platform to examine the surface movement of glutamate receptors. Although previous findings demonstrated that dPC12 exhibits synapse-like structures (Jeon et al., 2010), it does not form classical synapses. Therefore, we used cultured hippocampal neurons to study synaptic GluR2-AMPAR. Our results demonstrated that these neurons were effectively labeled with pre- and postsynaptic markers, MitoTracker Deep Red and homer-1, respectively. Experiments performed by Ehlers et al demonstrated that *in vivo* MitoTracker labeling exhibited around 84% colocalization with the presynaptic marker bassoon (Ehlers et al., 2007). Our immunofluorescence stainings showed that MitoTracker Deep Red entirely colocalized with bassoon, although some synapses were labeled with bassoon alone in our hippocampal culture. In agreement with previous studies (Groc et al., 2008), our results demonstrated that synaptic D_{AMPAR} is lower than extrasynaptic D_{AMPAR} suggesting that GluR2-AMPAR exhibited a more confined motion in the synapses.

6.1. Compartment specific effect of E2

Besides its classical genomic action, E2 exerts rapid non-classical effects on glutamate receptors. The surface movement of glutamate receptors plays critical roles in functions such as glutamatergic neurotransmission and synaptic plasticity. It has been described that AMPAR, the most abundant glutamate receptor in excitatory synapses, shows immobile or relatively slow diffusion in the postsynaptic density but exhibits Brownian movement outside the synapse (Borgdorff and Choquet, 2002). It has also been reported that E2 decreases the surface movement of NMDA receptor (Potier et al., 2016). However, the effect of E2 on surface movement of AMPAR is unknown. In this study, we examined whether E2 alters the surface movement of GluR2-AMPAR molecules, the most ample AMPAR subunit in neurons. Here, we show that E2 decreases D_{AMPAR} in a concentration-dependent manner, with distinct effects on soma and neurites in dPC12. However, E2 alters only D_{AMPAR} but not D_{mGluR1}, suggesting that the rapid modulation of glutamatergic receptor surface diffusion by E2 is type-dependent. It is worth noting that the rapidity of E2 action on D_{AMPAR} ($\leq$ 5 min) indicates a non-classical mechanism.

ERs, namely GPER1, ERα, and ERβ, are of great interest and have been suggested to be involved in non-classical E2 actions. Our PCR results showed the expression of GPER1 and ERβ but not ERα in dPC12. Interestingly, in our experiments, ER agonists and antagonists demonstrated a compartment-specific effect on dPC12, as they had different effects on soma and neurites. In soma, the ability of E2 to reduce D_{AMPAR} requires both ERβ and GPER1 since this response was observed after the co-application of ERβ and GPER1 agonists (DPN and G1) but not after application of DPN or G1 alone. The complementary effect of liganded ERβ and GPER1 on soma is also corroborated by the fact that GPER1 blocker G15 inhibited the effect of E2 on somatic D_{AMPAR}. In contrast, on neurites G1 reduced D_{AMPAR}, DPN was not effective, and G15 antagonized the effect of E2. In summary, both ERβ and GPER1 are required for E2 effect on soma, but on neurite E2 effect occurs through GPER1 only. Studies have revealed that cortical actin network differs in soma and neurite and its dynamics is regulated by ERβ (Y et al., 2017). As discussed later, we found in dPC12 that the actin structure influences the membrane movement of receptors differently on soma and neurite. We assume that on soma ERβ and GPER1 regulates receptor dynamics through cortical actin rearrangement, while on neurite GPER1 alone affects receptor movements via an unknown mechanism unrelated to cortical actin network.

The concentration dependence of E2 action differs between soma and neurites in dPC12. While 100 pM of E2 reduced D_{AMPAR} in soma, higher concentrations (1 nM or 100 nM) were required to decrease the D_{AMPAR} in neurites. One possible reason for the compartement-specific E2 action may be the difference in the distribution of GPER1 molecules on the membrane of soma and neurites. Indeed, our STORM experiments showed that the GPER1/GluR2-AMPAR ratio was higher in soma than in neurites, indicating that neurites express less GPER1 than soma. These observations are consistent with our finding showing a significant decrease in D_{AMPAR} in neurites after exposure to high E2 (1 nM and 100 nM).

Interestingly, high doses of E2 (1 nM, 100 nM) did not alter D_{AMPAR} in soma. Previous studies have indicated that GPER1 undergoes desensitization after the administration of the ligand at high concentrations (Brailoiu et al., 2007). Thus, it is likely that a high concentration of E2 induces GPER1 desensitization in the soma. Previous experiments demonstrated that E2 administration could induce translocation of GPER1 from the cell membrane to the cytoplasm, resulting in the desensitization of the receptor (Filardo and Thomas, 2012). Our STED experiments corroborated these findings because 10 min after administration of 100 nM of E2, GPER1 immunolabeling relocated from the membrane region to the cytoplasm (Funakoshi et al., 2006), indicating a rapid internalization of GPER1 on soma. Rapid internalization indicates the desensitization of GPER1, which may explain why high doses of E2 were ineffective on the soma. We hypothesize that an even higher concentration of E2 would be sufficient to induce internalization due to the low level of GPER1.

6.2. Role of cortical actin network in the effect of E2

It has been shown earlier that the actin cytoskeleton can interact with the intracellular domains of membrane receptors, thus regulating their movement (Kusumi et al., 2014). Single-particle tracking studies of lipid-anchored molecules demonstrated reduced mobility in the axon initial segment and showed that the confined motion was due to actin structures (Albrecht et al., 2016). Our present findings confirm these previous observations (Hanley, 2014a), as the disruption of cortical actin by latA increased D_{AMPAR} in soma. Interestingly, latA has a compartment-specific effect because it is not effective in neurites. Furthermore, we found that D_{AMPAR} and D_{mGluR1} were higher for neurites than for soma. Super-resolution imaging studies revealed that soma and neurites have different cortical actin structures (Lukinavičius et al., 2014; Han et al., 2017). Actin has a polygonal lattice structure in soma

(Han et al., 2017), and its associated proteins such as adducin and spectrin form 190-nm-spaced ring-like structures around the circumference of neurites (Xu et al., 2013; Han et al., 2017). We hypothesize that the higher D values measured on neurites arise from the difference between the structural arrangement of actin in soma and neurites. This may also provide an effective basis for the compartment-specific effect of latA and surface dynamics of GluR2-AMPARs.

Recent evidence implicates that cortical actin is important in receptor crosstalk through modulation of protein dynamics (Mattila et al., 2016). Cofilin is a highly abundant constitutively active actin-binding protein that alters the properties of F-actin and is regulated by the ROCK-cofilin and JNK-cofilin pathways (Hu et al., 2018; Kim et al., 2019). Phosphorylation inactivates cofilin and facilitates actin filament assembly. E2 increases the activity of cofilin (Kramár et al., 2009; Brandt and Rune, 2019) and stabilizes the F-actin cytoskeleton via GPER1 (Wang et al., 2019). Cofilin has been reported to mediate cortical actin dynamics that regulate AMPAR trafficking in synaptic plasticity (Gu et al., 2010). Therefore, we investigated the role of actin in the effect of E2 on D_{AMPAR}. Our results demonstrated that latA diminished the effect of E2, indicating that cortical actin plays a pivotal role in E2 action on D_{AMPAR}. Our results also demonstrated that the E2-induced decrease in D_{AMPAR} is completely blocked by the inhibition of the ROCK-cofilin or JNK-cofilin pathways in soma and neurites. We suggest that E2 binding to GPER1 activates both the ROCK-cofilin and JNK-cofilin pathways, which then change the cortical actin dynamics and decrease the surface movement of GluR2-AMPAR.

6.3. E2 effect on AMPAR in hippocampal neurons

The pressing question related to the rapid E2 effect on AMPARs is that of explaining the physiological relevance of the observed changes.

To confirm the effect of E2 on D_{AMPAR} in another *in vitro* neuron system and examine the effect of E2 on synaptic GluR2-AMPAR, we performed single-molecule tracking experiments on a primary hippocampal neuron culture. Cultured hippocampal neurons expressing ERα, ERβ, and GPER1 (Wehrenberg et al., 2001; Prange-Kiel et al., 2003; Zhao et al., 2016) provide physiologically relevant *in vitro* model for studying E2 effect. Our results showed that E2 administration (100 pM and 100 nM) rapidly decreased the synaptic and extrasynaptic D_{AMPAR} in hippocampal neurons similar to dPC12.

LTP of excitatory synaptic transmission is a well-known form of synaptic plasticity and is considered a cellular model for learning and memory. Although several studies have demonstrated that E2 plays an essential role in LTP and alters memory formation (Spencer et al., 2008; Fester and Rune, 2015), the precise molecular mechanism is not clear. AMPAR plays a pivotal role in synaptic alterations involved in synaptic transmission, synaptic plasticity, LTP, learning, and memory. Using single-molecule tracking experiments and AMPAR immobilization techniques, Penn and colleagues (2017) have shown that the surface movement of AMPARs is a key factor in the modulation of synaptic potentiation and learning (Phan et al., 2015). At the molecular level, the recruitment and slow diffusion of glutamate receptors at the postsynaptic site have been shown after LTP (Kovács et al., 2018). Indeed, our single-molecule tracking of hippocampal neurons demonstrated that cLTP decreased D_{AMPAR} in synapses and increased the synaptic dwell time and content of GluR2-AMPARs. Similar to cLTP, 100 nM of E2 decreased D_{AMPAR} and increased the dwell time of GluR2-AMPA in the synapse. Although recent morphological studies have demonstrated that E2 increased the expression of GluR2 in mushroom spines at 120 min *in vivo* (Avila et al., 2017) our results show that E2 did not affect the GluR2-AMPAR content in the synapses within 20 min. We suggest that E2 can rapidly enhance the synaptic efficacy of glutamatergic synapses by decreasing D_{AMPAR}. Interestingly, E2 did not change the effect of cLTP on D_{AMPAR}, dwell time, and synaptic content of GluR2-AMPAR. However, E2 can likely increase the efficacy of cLTP by retaining the AMPARs in the synapses.

In conclusion, our study demonstrates that E2 rapidly and dose-dependently decreases the surface movement of GluR2-AMPARs via compartment-specific ER-mediated mechanisms in live neurons. Our results also suggest that cortical actin mediates liganded GPER1 action on the surface movement of GluR2-AMPARs via the ROCK-cofilin and JNK-cofilin pathways. This study provides the first evidence that E2 decreases the surface movement and increases the dwell time of GluR2-AMPARs in the synapses. These results provide a strong foundation for understanding the molecular mechanism by which E2 affects neuronal plasticity and glutamatergic neurotransmission. Finally, these observations will likely be of physiological importance for cognitive functions and of particular relevance to E2 action on memory formation.

7. Conclusions

While many studies have investigated the rapid action of gonadal steroid E2 on cell signaling and synaptic plasticity, its effect on the surface trafficking of excitatory receptors such as AMPAR, which plays a critical role in excitatory neurotransmission and synaptic plasticity is unknown.

By means of TIRFM we demonstrated that E2 rapidly and dose dependently decrease the membrane movement of AMPAR. This effect was compartment specific: only the lower dose was effective on the soma and higher dose had an effect on the neurite.

E2 effect was mediated by only GPER1 on the neurite but required both GPER1 and ERβ on the soma.

In further experiments utilizing superresolution microscopy we showed that E2 was ineffective on the soma in a higher dose because it triggered internalization of GPER1. On the neurite, the lower dose of E2 was ineffective possibly due to the low GPER1/AMPAR ratio.

E2 effect required an intact cortical actin network and functional ROCK/JNK/cofilin system.

We confirmed the effect of E2 on the membrane movement of AMPAR in hippocampal neurons and we also showed that E2 decreases the synaptic dwell time of AMPAR in hippocampal neurons revealing its physiological relevance.

These results bring us closer to understand the molecular mechanism of E2 action on neuronal plasticity and glutamatergic neurotransmission.

8. Acknowledgement

I would first like to thank my supervisors Prof. Dr. István Ábrahám and Dr. Klaudia Barabás whose expertise guided me through the PhD years. Their experience, caring and patience were greatly precious for me during research.

I am deeply greatful to every member of the Molecular Neuroendocrinology Research Group. They were always there when I nedded support or professional advice. I always felt that working in this group with amazing people is a real privilege.

I am also greatful to my friends and colleagues Dr. Tamás Kovács, Dr. Dávid Ernszt and Dr. Zoltán Somogyi. Their impact on my scientific and personal life is invaluable. They were always ready for an hour-long coffee break to discuss the most non-scientific topics in the most scientific way.

Finally, I would like to thank my family their continuous support during my entire university life.

Unfortunately, the sudden and tragic pass of István didn't let him see the success of this PhD. I would like to dedicate this dissertation for him.

May He rest in peace.

9. List of publications

This dissertation is based on the following articles:

Godó, S., Barabás, K., Lengyel, F., Ernszt, D., Kovács, T., Kecskés, M., et al. (2021). Single-Molecule Imaging Reveals Rapid Estradiol Action on the Surface Movement of AMPA Receptors in Live Neurons. *Front. Cell Dev. Biol.* 9, 2698.

impact factor: 6.684

Barabás, K., Godó, S., Lengyel, F., Ernszt, D., Pál, J., and Ábrahám, I. M. (2018). Rapid non-classical effects of steroids on the membrane receptor dynamics and downstream signaling in neurons. Horm. Behav., 0–1

impact factor: 3.949

Other publication:

Payrits, M., Borbely, E., Godo, S., Ernszt, D., Kemeny, A., Kardos, J., et al. (2020). Genetic deletion of TRPA1 receptor attenuates amyloid beta- 1-42 (Aβ(1-42))-induced neurotoxicity in the mouse basal forebrain in vivo. Mech. Ageing Dev. 189, 111268.

impact factor: 4.304

Total impact factor: 14.3829

10. References

Ábrahám, I. M., Kőszegi, Z., Tolod-Kemp, E., and Szegő, É. M. (2009). Action of estrogen on survival of basal forebrain cholinergic neurons: Promoting amelioration. *Psychoneuroendocrinology* 34, S104–S112. doi:https://doi.org/10.1016/j.psyneuen.2009.05.024.

Albrecht, D., Winterflood, C. M., Sadeghi, M., Tschager, T., Noé, F., and Ewers, H. (2016). Nanoscopic compartmentalization of membrane protein motion at the axon initial segment. *J. Cell Biol.* 215, 1–10. doi:10.1083/jcb.201603108.

Ashby, M. C., De La Rue, S. A., Ralph, G. S., Uney, J., Collingridge, G. L., and Henley, J. M. (2004). Removal of AMPA receptors (AMPARs) from synapses is preceded by transient endocytosis of extrasynaptic AMPARs. *J. Neurosci.* 24, 5172–5176. doi:10.1523/JNEUROSCI.1042-04.2004.

Avila, J. A., Alliger, A. A., Carvajal, B., Zanca, R. M., Serrano, P. A., and Luine, V. N. (2017). Estradiol rapidly increases GluA2-mushroom spines and decreases GluA2-filopodia spines in hippocampus CA1. *Hippocampus* 27, 1224–1229. doi:10.1002/hipo.22768.

Baglietto-Vargas, D., Prieto, G. A., Limon, A., Forner, S., Rodriguez-Ortiz, C. J., Ikemura, K., et al. (2018). Impaired AMPA signaling and cytoskeletal alterations induce early synaptic dysfunction in a mouse model of Alzheimer's disease. *Aging Cell* 17, e12791. doi:10.1111/acel.12791.

Bálint, F., Liposits, Z., and Farkas, I. (2016). Estrogen Receptor Beta and 2-arachidonoylglycerol Mediate the Suppressive Effects of Estradiol on Frequency of Postsynaptic Currents in Gonadotropin-Releasing Hormone Neurons of Metestrous Mice: An Acute Slice Electrophysiological Study. *Front. Cell. Neurosci.* 10, 77. doi:10.3389/fncel.2016.00077.

Bamburg, J. R., and Bernstein, B. W. (1000). Roles of ADF/cofilin in actin polymerization and beyond. doi:10.3410/B2-62.

Barabás, K., Godó, S., Lengyel, F., Ernszt, D., Pál, J., and Ábrahám, I. M. (2018). Rapid non-classical effects of steroids on the membrane receptor dynamics and downstream signaling in neurons. *Horm. Behav.* 104. doi:10.1016/j.yhbeh.2018.05.008.

Bard, L., and Groc, L. (2011). Glutamate receptor dynamics and protein interaction:

Lessons from the NMDA receptor. *Mol. Cell. Neurosci.* 48, 298–307. doi:10.1016/j.mcn.2011.05.009.

Barna, L., Dudok, B., Miczán, V., Horváth, A., László, Z. I., and Katona, I. (2016). Correlated confocal and super-resolution imaging by VividSTORM. *Nat. Protoc.* 11, 163–83. doi:10.1038/nprot.2016.002.

Bechtholt-Gompf, A. J., Walther, H. V, Adams, M. A., Carlezon, W. A. J., Ongür, D., and Cohen, B. M. (2010). Blockade of astrocytic glutamate uptake in rats induces signs of anhedonia and impaired spatial memory. *Neuropsychopharmacol. Off. Publ. Am. Coll. Neuropsychopharmacol.* 35, 2049–2059. doi:10.1038/npp.2010.74.

Belinsky, G. S., Moore, A. R., Short, S. M., Rich, M. T., and Antic, S. D. (2011). Physiological properties of neurons derived from human embryonic stem cells using a dibutyryl cyclic AMP-based protocol. *Stem Cells Dev.* 20, 1733–1746. doi:10.1089/scd.2010.0501.

Ben Zablah, Y., Merovitch, N., and Jia, Z. (2020). The Role of ADF/Cofilin in Synaptic Physiology and Alzheimer's Disease . *Front. Cell Dev. Biol.* 8, 1337. Available at: https://www.frontiersin.org/article/10.3389/fcell.2020.594998.

Bendel, O., Meijer, B., Hurd, Y., and von Euler, G. (2005). Cloning and expression of the human NMDA receptor subunit NR3B in the adult human hippocampus. *Neurosci. Lett.* 377, 31–36. doi:10.1016/j.neulet.2004.11.064.

Berglund, A. J. (2010). Statistics of camera-based single-particle tracking. *Phys. Rev. E - Stat. Nonlinear, Soft Matter Phys.* 82, 1–8. doi:10.1103/PhysRevE.82.011917.

Björnström, L., and Sjöberg, M. (2005). Mechanisms of Estrogen Receptor Signaling: Convergence of Genomic and Nongenomic Actions on Target Genes. *Mol. Endocrinol.* 19, 833–842. doi:10.1210/me.2004-0486.

Bliss, T. V, and Gardner-Medwin, A. R. (1973). Long-lasting potentiation of synaptic transmission in the dentate area of the unanaestetized rabbit following stimulation of the perforant path. *J. Physiol.* 232, 357–374. doi:10.1113/jphysiol.1973.sp010274.

Borgdorff, A. J., and Choquet, D. (2002). Regulation of AMPA receptor lateral movements. *Nature* 417, 649. Available at: http://dx.doi.org/10.1038/nature00780.

Bourdeau, V., Deschênes, J., Métivier, R., Nagai, Y., Nguyen, D., Bretschneider, N., et al. (2004). Genome-wide identification of high-affinity estrogen response elements in human and mouse. *Mol. Endocrinol.* 18, 1411–1427. doi:10.1210/me.2003-0441.

Brailoiu, E., Dun, S. L., Brailoiu, G. C., Mizuo, K., Sklar, L. A., Oprea, T. I., et al. (2007). Distribution and characterization of estrogen receptor G protein-coupled receptor 30

in the rat central nervous system. *J. Endocrinol.* 193, 311–321. doi:10.1677/JOE-07-0017.

Brandt, N., and Rune, G. M. (2019). Sex-dependency of oestrogen-induced structural synaptic plasticity: Inhibition of aromatase versus application of estradiol in rodents. *Eur. J. Neurosci.* n/a. doi:10.1111/ejn.14541.

Bredt, D. S., and Nicoll, R. A. (2003). AMPA receptor trafficking at excitatory synapses. *Neuron* 40, 361–379. doi:10.1016/s0896-6273(03)00640-8.

Burnashev, N., Monyer, H., Seeburg, P. H., and Sakmann, B. (1992). Divalent ion permeability of AMPA receptor channels is dominated by the edited form of a single subunit. *Neuron* 8, 189–198. doi:https://doi.org/10.1016/0896-6273(92)90120-3.

Bussell, S. J., Koch, D. L., and Hammer, D. A. (1995). Effect of hydrodynamic interactions on the diffusion of integral membrane proteins: tracer diffusion in organelle and reconstituted membranes. *Biophys. J.* 68, 1828–1835. doi:10.1016/S0006-3495(95)80359-0.

Carmeci, C., Thompson, D. A., Ring, H. Z., Francke, U., and Weigel, R. J. (1997). Identification of a gene (GPR30) with homology to the G-protein-coupled receptor superfamily associated with estrogen receptor expression in breast cancer. *Genomics* 45, 607–617. doi:10.1006/geno.1997.4972.

Castellucci, V., Pinsker, H., Kupfermann, I., and Kandel, E. R. (1970). Neuronal mechanisms of habituation and dishabituation of the gill-withdrawal reflex in Aplysia. *Science* 167, 1745–1748. doi:10.1126/science.167.3926.1745.

Chatterton, J. E., Awobuluyi, M., Premkumar, L. S., Takahashi, H., Talantova, M., Shin, Y., et al. (2002). Excitatory glycine receptors containing the NR3 family of NMDA receptor subunits. *Nature* 415, 793–798. doi:10.1038/nature715.

Choi, D. W. (1994). Glutamate receptors and the induction of excitotoxic neuronal death. *Prog. Brain Res.* 100, 47–51. doi:10.1016/s0079-6123(08)60767-0.

Citri, A., and Malenka, R. C. (2008). Synaptic Plasticity: Multiple Forms, Functions, and Mechanisms. *Neuropsychopharmacology* 33, 18–41. doi:10.1038/sj.npp.1301559.

Collingridge, G. L., Isaac, J. T. R., and Wang, Y. T. (2004). Receptor trafficking and synaptic plasticity. *Nat. Rev. Neurosci.* 5, 952–962. doi:10.1038/nrn1556.

Conn, P. J., and Pin, J. P. (1997). Pharmacology and functions of metabotropic glutamate receptors. *Annu. Rev. Pharmacol. Toxicol.* 37, 205–237. doi:10.1146/annurev.pharmtox.37.1.205.

Danbolt, N. C. (2001). Glutamate uptake. *Prog. Neurobiol.* 65, 1–105. doi:10.1016/s0301-

0082(00)00067-8.

Diering, G. H., and Huganir, R. L. (2018). The AMPA Receptor Code of Synaptic Plasticity. *Neuron* 100, 314–329. doi:https://doi.org/10.1016/j.neuron.2018.10.018.

Doble, A. (1999). The role of excitotoxicity in neurodegenerative disease: implications for therapy. *Pharmacol. Ther.* 81, 163–221. doi:10.1016/s0163-7258(98)00042-4.

Dos Santos, E. G., Dieudonne, M. N., Pecquery, R., Le Moal, V., Giudicelli, Y., and Lacasa, D. (2002). Rapid nongenomic E2 effects on p42/p44 MAPK, activator protein-1, and cAMP response element binding protein in rat white adipocytes. *Endocrinology* 143, 930–940. doi:10.1210/endo.143.3.8678.

Dudok, B., Barna, L., Ledri, M., Szabó, S. I., Szabadits, E., Pintér, B., et al. (2015). Cell-specific STORM super-resolution imaging reveals nanoscale organization of cannabinoid signaling. *Nat. Neurosci.* 18, 75–86. doi:10.1038/nn.3892.

Dupuis, J. P., Ladépêche, L., Seth, H., Bard, L., Varela, J., Mikasova, L., et al. (2014). Surface dynamics of GluN2B-NMDA receptors controls plasticity of maturing glutamate synapses. *EMBO J.* 33, 842–861. doi:10.1002/embj.201386356.

Egbenya, D. L., Hussain, S., Lai, Y. C., Xia, J., Anderson, A. E., and Davanger, S. (2018). Changes in synaptic AMPA receptor concentration and composition in chronic temporal lobe epilepsy. *Mol. Cell. Neurosci.* 92, 93–103. doi:10.1016/j.mcn.2018.07.004.

Ehlers, M. D., Heine, M., Groc, L., Lee, M. C., and Choquet, D. (2007). Diffusional Trapping of GluR1 AMPA Receptors by Input-Specific Synaptic Activity. *Neuron* 54, 447–460. doi:10.1016/j.neuron.2007.04.010.

Fester, L., and Rune, G. M. (2015). Sexual neurosteroids and synaptic plasticity in the hippocampus. *Brain Res.* 1621, 162–169. doi:10.1016/j.brainres.2014.10.033.

Filardo, E. J., Quinn, J. A., Frackelton, A. R., and Bland, K. I. (2002). Estrogen Action Via the G Protein-Coupled Receptor, GPR30: Stimulation of Adenylyl Cyclase and cAMP-Mediated Attenuation of the Epidermal Growth Factor Receptor-to-MAPK Signaling Axis. *Mol. Endocrinol.* 16, 70–84. doi:10.1210/mend.16.1.0758.

Filardo, E. J., and Thomas, P. (2012). Minireview: G Protein-Coupled Estrogen Receptor-1, GPER-1: Its Mechanism of Action and Role in Female Reproductive Cancer, Renal and Vascular Physiology. *Endocrinology* 153, 2953–2962. doi:10.1210/en.2012-1061.

Fisher, S. A., Fischer, T. M., and Carew, T. J. (1997). Multiple overlapping processes underlying short-term synaptic enhancement. *Trends Neurosci.* 20, 170–177. doi:10.1016/s0166-2236(96)01001-6.

Fuentes, N., and Silveyra, P. (2019). Estrogen receptor signaling mechanisms. *Adv. Protein Chem. Struct. Biol.* 116, 135–170. doi:10.1016/bs.apcsb.2019.01.001.

Fujimoto, N., and Kitamura, S. (2004). Effects of environmental estrogenic chemicals on AP1 mediated transcription with estrogen receptors alpha and beta. *J. Steroid Biochem. Mol. Biol.* 88, 53–59. doi:10.1016/j.jsbmb.2003.10.006.

Funakoshi, T., Yanai, A., Shinoda, K., Kawano, M. M., and Mizukami, Y. (2006). G protein-coupled receptor 30 is an estrogen receptor in the plasma membrane. *Biochem. Biophys. Res. Commun.* 346, 904–910. doi:10.1016/j.bbrc.2006.05.191.

Fusi, S., Drew, P. J., and Abbott, L. F. (2005). Cascade models of synaptically stored memories. *Neuron* 45, 599–611. doi:10.1016/j.neuron.2005.02.001.

Gibney, E. R., and Nolan, C. M. (2010). Epigenetics and gene expression. *Heredity (Edinb).* 105, 4–13. doi:10.1038/hdy.2010.54.

Glidewell-Kenney, C., Hurley, L. A., Pfaff, L., Weiss, J., Levine, J. E., and Jameson, J. L. (2007). Nonclassical estrogen receptor α signaling mediates negative feedback in the female mouse reproductive axis. *Proc. Natl. Acad. Sci.* 104, 8173 LP – 8177. doi:10.1073/pnas.0611514104.

Gould, E., Woolley, C. S., Frankfurt, M., and McEwen, B. S. (1990). Gonadal steroids regulate dendritic spine density in hippocampal pyramidal cells in adulthood. *J. Neurosci.* 10, 1286–1291. doi:10.1523/JNEUROSCI.10-04-01286.1990.

Gowrishankar, K., Ghosh, S., Saha, S., Mayor, S., and Rao, M. (2012). Active Remodeling of Cortical Actin Regulates Spatiotemporal Organization of Cell Surface Molecules. *Cell* 149, 1353–1367. doi:10.1016/j.cell.2012.05.008.

Gray, R. M. (2006). Toeplitz and Circulant Matrices: A Review. *Found. Trends® Commun. Inf. Theory* 2, 155–239. doi:10.1561/0100000006.

Groc, L., Choquet, D., and Chaouloff, F. (2008). The stress hormone corticosterone conditions AMPAR surface trafficking and synaptic potentiation. *Nat. Neurosci.* 11, 868. Available at: http://dx.doi.org/10.1038/nn.2150.

Groc, L., Choquet, D., Stephenson, F. A., Verrier, D., Manzoni, O. J., and Chavis, P. (2007). NMDA Receptor Surface Trafficking and Synaptic Subunit Composition Are Developmentally Regulated by the Extracellular Matrix Protein Reelin. *J. Neurosci.* 27, 10165–10175. doi:10.1523/JNEUROSCI.1772-07.2007.

Groc, L., Heine, M., Cognet, L., Brickley, K., Stephenson, F. A., Lounis, B., et al. (2004). Differential activity-dependent regulation of the lateral mobilities of AMPA and NMDA receptors. *Nat. Neurosci.* 7, 695–696. doi:10.1038/nn1270.

Groc, L., Heine, M., Cousins, S. L., Stephenson, F. A., Lounis, B., Cognet, L., et al. (2006). NMDA receptor surface mobility depends on NR2A-2B subunits. *Proc. Natl. Acad. Sci. U. S. A.* 103, 18769–18774. doi:10.1073/pnas.0605238103.

Gruber, C. J., Tschugguel, W., Schneeberger, C., and Huber, J. C. (2002). Production and actions of estrogens. *N. Engl. J. Med.* 346, 340–352. doi:10.1056/NEJMra000471.

Gu, J., Lee, C. W., Fan, Y., Komlos, D., Tang, X., Sun, C., et al. (2010). ADF/Cofilin-Mediated Actin Dynamics Regulate AMPA Receptor Trafficking during Synaptic Plasticity HHS Public Access Author manuscript. *Nat Neurosci* 13, 1208–1215. doi:10.1038/nn.2634.

Gu, Q., and Moss, R. L. (1996). 17β-Estradiol Potentiates Kainate-Induced Currents via Activation of the cAMP Cascade. *J. Neurosci.* 16, 3620 LP – 3629. doi:10.1523/JNEUROSCI.16-11-03620.1996.

Hammes, A., Andreassen, T. K., Spoelgen, R., Raila, J., Hubner, N., Schulz, H., et al. (2005). Role of endocytosis in cellular uptake of sex steroids. *Cell* 122, 751–762. doi:10.1016/j.cell.2005.06.032.

Hammond, G. L., and Bocchinfuso, W. P. (1995). Sex hormone-binding globulin/androgen-binding protein: Steroid-binding and dimerization domains. *J. Steroid Biochem. Mol. Biol.* 53, 543–552. doi:https://doi.org/10.1016/0960-0760(95)00110-L.

Han, B., Zhou, R., Xia, C., and Zhuang, X. (2017). Structural organization of the actin-spectrin-based membrane skeleton in dendrites and soma of neurons. *Proc. Natl. Acad. Sci. U. S. A.* 114, E6678–E6685. doi:10.1073/pnas.1705043114.

Hanley, J. G. (2014a). Actin-dependent mechanisms in AMPA receptor trafficking. *Front. Cell. Neurosci.* 8, 381. doi:10.3389/fncel.2014.00381.

Hanley, J. G. (2014b). Actin-dependent mechanisms in AMPA receptor trafficking . *Front. Cell. Neurosci.* 8, 381. Available at: https://www.frontiersin.org/article/10.3389/fncel.2014.00381.

Hein, B., Willig, K. I., and Hell, S. W. (2008). Stimulated emission depletion (STED) nanoscopy of a fluorescent protein-labeled organelle inside a living cell. *Proc. Natl. Acad. Sci. U. S. A.* 105, 14271–14276. doi:10.1073/pnas.0807705105.

Henson, M. A., Roberts, A. C., Salimi, K., Vadlamudi, S., Hamer, R. M., Gilmore, J. H., et al. (2008). Developmental regulation of the NMDA receptor subunits, NR3A and NR1, in human prefrontal cortex. *Cereb. Cortex* 18, 2560–2573. doi:10.1093/cercor/bhn017.

Hu, R., Cao, Q., Sun, Z., Chen, J., Zheng, Q., and Xiao, F. (2018). A novel method of neural differentiation of PC12 cells by using Opti-MEM as a basic induction medium. *Int. J. Mol. Med.* 41, 195–201. doi:10.3892/ijmm.2017.3195.

Izquierdo, I. (1994). Pharmacological evidence for a role of long-term potentiation in memory. *FASEB J. Off. Publ. Fed. Am. Soc. Exp. Biol.* 8, 1139–1145.

Jeon, C. Y., Jin, J. K., Koh, Y. H., Chun, W., Choi, I. G., Kown, H. J., et al. (2010). Neurites from PC12 cells are connected to each other by synapse-like structures. *Synapse* 64, 765–772. doi:10.1002/syn.20789.

Kane, M. D., Vanden Heuvel, J. P., Isom, G. E., and Schwarz, R. D. (1998). Differential expression of group I metabotropic glutamate receptors (mGluRs) in the rat pheochromocytoma cell line PC12: Role of nerve growth factor and ras. *Neurosci. Lett.* 252, 1–4. doi:10.1016/S0304-3940(98)00484-4.

Katzenellenbogen, B. S., Montano, M. M., Ediger, T. R., Sun, J., Ekena, K., Lazennec, G., et al. (2000). Estrogen receptors: selective ligands, partners, and distinctive pharmacology. *Recent Prog. Horm. Res.* 55, 163–165.

Kelly, M. J., and Rønnekleiv, O. K. (2009). Control of CNS neuronal excitability by estrogens via membrane-initiated signaling. *Mol. Cell. Endocrinol.* 308, 17–25. doi:10.1016/j.mce.2009.03.008.

Kim, C. H., Lee, J., Lee, J.-Y., and Roche, K. W. (2008). Metabotropic glutamate receptors: phosphorylation and receptor signaling. *J. Neurosci. Res.* 86, 1–10. doi:10.1002/jnr.21437.

Kim, J., Schalk, J. C., Koss, W. A., Gremminger, R. L., Taxier, L. R., Gross, K. S., et al. (2019). Dorsal Hippocampal Actin Polymerization Is Necessary for Activation of G-Protein-Coupled Estrogen Receptor (GPER) to Increase CA1 Dendritic Spine Density and Enhance Memory Consolidation. *J. Neurosci.* 39, 9598–9610. doi:10.1523/JNEUROSCI.2687-18.2019.

Klar, T. A., Jakobs, S., Dyba, M., Egner, A., and Hell, S. W. (2000). Fluorescence microscopy with diffraction resolution barrier broken by stimulated emission. *Proc. Natl. Acad. Sci. U. S. A.* 97, 8206–8210. doi:10.1073/pnas.97.15.8206.

Klinge, C. M. (2001). Estrogen receptor interaction with estrogen response elements. *Nucleic Acids Res.* 29, 2905–2919. doi:10.1093/nar/29.14.2905.

Kovács, G., Környei, Z., Tóth, K., Baranyi, M., Brunner, J., Neubrandt, M., et al. (2018). Modulation of P2X7 purinergic receptor activity by extracellular Zn2+ in cultured mouse hippocampal astroglia. *Cell Calcium* 75, 1–13.

doi:10.1016/j.ceca.2018.07.010.

Kramár, E. A., Chen, L. Y., Brandon, N. J., Rex, C. S., Liu, F., Gall, C. M., et al. (2009). Cytoskeletal changes underlie estrogen's acute effects on synaptic transmission and plasticity. *J. Neurosci.* 29, 12982–93. doi:10.1523/JNEUROSCI.3059-09.2009.

Kumar, A. (2015). NMDA Receptor Function During Senescence: Implication on Cognitive Performance . *Front. Neurosci.* 9, 473. Available at: https://www.frontiersin.org/article/10.3389/fnins.2015.00473.

Kumar, A., Bean, L. A., Rani, A., Jackson, T., and Foster, T. C. (2015). Contribution of estrogen receptor subtypes, ERα, ERβ, and GPER1 in rapid estradiol-mediated enhancement of hippocampal synaptic transmission in mice. *Hippocampus* 25, 1556–1566. doi:10.1002/hipo.22475.

Kumar, P., Kale, R. K., and Baquer, N. Z. (2011). Estradiol modulates membrane-linked ATPases, antioxidant enzymes, membrane fluidity, lipid peroxidation, and lipofuscin in aged rat liver. *J. Aging Res.* 2011, 580245. doi:10.4061/2011/580245.

Kusumi, A., Sako, Y., and Yamamoto, M. (1993). Confined Lateral Diffusion of Membrane-Receptors as Studied by Single-Particle Tracking (Nanovid Microscopy) - Effects of Calcium-Induced Differentiation in Cultured Epithelial-Cells. *Biophys. J.* 65, 2021–2040.

Kusumi, A., Tsunoyama, T. A., Hirosawa, K. M., Kasai, R. S., and Fujiwara, T. K. (2014). Tracking single molecules at work in living cells. *Nat. Chem. Biol.* 10, 524. Available at: http://dx.doi.org/10.1038/nchembio.1558.

Kuzmiski, J. B., and Bains, J. S. (2010). Metabotropic glutamate receptors: gatekeepers of homeostasis. *J. Neuroendocrinol.* 22, 785–792. doi:10.1111/j.1365-2826.2010.02020.x.

Ladépêche, L., Dupuis, J. P., and Groc, L. (2014). Surface trafficking of NMDA receptors: Gathering from a partner to another. *Semin. Cell Dev. Biol.* 27, 3–13. doi:10.1016/j.semcdb.2013.10.005.

Le Dily, F., and Beato, M. (2018). Signaling by Steroid Hormones in the 3D Nuclear Space. *Int. J. Mol. Sci.* 19. doi:10.3390/ijms19020306.

Lee, S. H., Jin, C., Cai, E., Ge, P., Ishitsuka, Y., Teng, K. W., et al. (2017). Super-resolution imaging of synaptic and extra-synaptic AMPA receptors with Different-Sized fluorescent probes. *Elife* 6. doi:10.7554/eLife.27744.

Lesage, A., and Steckler, T. (2010). Metabotropic glutamate mGlu1 receptor stimulation and blockade: therapeutic opportunities in psychiatric illness. *Eur. J. Pharmacol.*

639, 2–16. doi:10.1016/j.ejphar.2009.12.043.

Li, C., Brake, W. G., Romeo, R. D., Dunlop, J. C., Gordon, M., Buzescu, R., et al. (2004). Estrogen alters hippocampal dendritic spine shape and enhances synaptic protein immunoreactivity and spatial memory in female mice. *Proc. Natl. Acad. Sci.* 101, 2185 LP – 2190. doi:10.1073/pnas.0307313101.

Lisman, J. (1989). A mechanism for the Hebb and the anti-Hebb processes underlying learning and memory. *Proc. Natl. Acad. Sci. U. S. A.* 86, 9574–9578. doi:10.1073/pnas.86.23.9574.

Liu, S., Wang, X., Pan, L., Wu, W., Yang, D., Qin, M., et al. (2018). Endogenous hydrogen sulfide regulates histone demethylase JMJD3-mediated inflammatory response in LPS-stimulated macrophages and in a mouse model of LPS-induced septic shock. *Biochem. Pharmacol.* 149, 153–162. doi:https://doi.org/10.1016/j.bcp.2017.10.010.

Lukinavičius, G., Reymond, L., D'Este, E., Masharina, A., Göttfert, F., Ta, H., et al. (2014). Fluorogenic probes for live-cell imaging of the cytoskeleton. *Nat. Methods* 11, 731–733. doi:10.1038/nmeth.2972.

M., S., M., S. É., K., B., A., J., Tóth, S., Z., K., et al. (2009). Genistein Induces Phosphorylation of cAMP Response Element-binding Protein in Neonatal Hypothalamus In Vivo. *J. Neuroendocrinol.* 21, 1024–1028. doi:10.1111/j.1365-2826.2009.01925.x.

Maggi, A., Susanna, L., Bettini, E., Mantero, G., and Zucchi, I. (1989). Hippocampus: a target for estrogen action in mammalian brain. *Mol. Endocrinol.* 3, 1165–1170. doi:10.1210/mend-3-7-1165.

Makhinson, M., Chotiner, J. K., Watson, J. B., and O'Dell, T. J. (1999). Adenylyl cyclase activation modulates activity-dependent changes in synaptic strength and Ca2+/calmodulin-dependent kinase II autophosphorylation. *J. Neurosci.* 19, 2500–2510. doi:10.1523/JNEUROSCI.19-07-02500.1999.

Malenka, R. C. (1991). Postsynaptic factors control the duration of synaptic enhancement in area CA1 of the hippocampus. *Neuron* 6, 53–60. doi:10.1016/0896-6273(91)90121-f.

Malenka, R. C., and Bear, M. F. (2004). LTP and LTD: an embarrassment of riches. *Neuron* 44, 5–21. doi:10.1016/j.neuron.2004.09.012.

Marchetti, L., Bonsignore, F., Gobbo, F., Amodeo, R., Calvello, M., Jacob, A., et al. (2019). Fast-diffusing p75NTR monomers support apoptosis and growth cone

collapse by neurotrophin ligands. *Proc. Natl. Acad. Sci. U. S. A.*, 201902790. doi:10.1073/pnas.1902790116.

Marino, M., Galluzzo, P., and Ascenzi, P. (2006). Estrogen signaling multiple pathways to impact gene transcription. *Curr. Genomics* 7, 497–508. doi:10.2174/138920206779315737.

Marino, M., Pallottini, V., and Trentalance, A. (1998). Estrogens cause rapid activation of IP3-PKC-alpha signal transduction pathway in HEPG2 cells. *Biochem. Biophys. Res. Commun.* 245, 254–258. doi:10.1006/bbrc.1998.8413.

Mattila, P. K., Batista, F. D., and Treanor, B. (2016). Dynamics of the actin cytoskeleton mediates receptor cross talk: An emerging concept in tuning receptor signaling. *J. Cell Biol.* 212, 267–280. doi:10.1083/jcb.201504137.

McDevitt, M. A., Glidewell-Kenney, C., Jimenez, M. A., Ahearn, P. C., Weiss, J., Jameson, J. L., et al. (2008). New insights into the classical and non-classical actions of estrogen: evidence from estrogen receptor knock-out and knock-in mice. *Mol. Cell. Endocrinol.* 290, 24–30. doi:10.1016/j.mce.2008.04.003.

Mehmood, T., Schneider, A., Pannetier, S., and Hanauer, A. (2013). Rsk2 knockdown in PC12 cells results in Sp1 dependent increased expression of the Gria2 gene, encoding the AMPA receptor subunit GluR2. *Int. J. Mol. Sci.* 14, 3358–3375. doi:10.3390/ijms14023358.

Monyer, H., Burnashev, N., Laurie, D. J., Sakmann, B., and Seeburg, P. H. (1994). Developmental and regional expression in the rat brain and functional properties of four NMDA receptors. *Neuron* 12, 529–540. doi:10.1016/0896-6273(94)90210-0.

Mulkey, R. M., and Malenka, R. C. (1992). Mechanisms underlying induction of homosynaptic long-term depression in area CA1 of the hippocampus. *Neuron* 9, 967–975. doi:10.1016/0896-6273(92)90248-c.

N, H., A, P., S, A., J, M., G, C., J, H., et al. (2007). Estrogen receptors: how do they signal and what are their targets. *Physiol. Rev.* 87, 905–931. doi:10.1152/PHYSREV.00026.2006.

Nakanishi, S. (1992). Molecular diversity of glutamate receptors and implications for brain function. *Science* 258, 597–603. doi:10.1126/science.1329206.

Niciu, M. J., Kelmendi, B., and Sanacora, G. (2012). Overview of glutamatergic neurotransmission in the nervous system. *Pharmacol. Biochem. Behav.* 100, 656–664. doi:10.1016/j.pbb.2011.08.008.

Nilsson, B.-O., Olde, B., and Leeb-Lundberg, L. M. F. (2011). G protein-coupled

oestrogen receptor 1 (GPER1)/GPR30: a new player in cardiovascular and metabolic oestrogenic signalling. *Br. J. Pharmacol.* 163, 1131–9. doi:10.1111/j.1476-5381.2011.01235.x.

Nowak, L., Bregestovski, P., Ascher, P., Herbet, A., and Prochiantz, A. (1984). Magnesium gates glutamate-activated channels in mouse central neurones. *Nature* 307, 462–465. doi:10.1038/307462a0.

O'Shea, R. D. (2002). Roles and regulation of glutamate transporters in the central nervous system. *Clin. Exp. Pharmacol. Physiol.* 29, 1018–1023. doi:10.1046/j.1440-1681.2002.03770.x.

Olde, B., and Leeb-Lundberg, L. M. F. (2009). GPR30/GPER1: searching for a role in estrogen physiology. *Trends Endocrinol. Metab.* 20, 409–416. doi:10.1016/j.tem.2009.04.006.

Olive, M. F. (2009). Metabotropic glutamate receptor ligands as potential therapeutics for addiction. *Curr. Drug Abuse Rev.* 2, 83–98. doi:10.2174/1874473710902010083.

Palmada, M., and Centelles, J. J. (1998). Excitatory amino acid neurotransmission. Pathways for metabolism, storage and reuptake of glutamate in brain. *Front. Biosci.* 3, d701-18. doi:10.2741/a314.

Pang, Z. P., and Südhof, T. C. (2010). Cell biology of Ca2+-triggered exocytosis. *Curr. Opin. Cell Biol.* 22, 496–505. doi:10.1016/j.ceb.2010.05.001.

Pavlov, D., Muhlrad, A., Cooper, J., Wear, M., and Reisler, E. (2006). Severing of F-actin by yeast cofilin is pH-independent. *Cell Motil. Cytoskeleton* 63, 533–542. doi:10.1002/cm.20142.

Pellerin, L., and Magistretti, P. J. (2004). Neuroenergetics: calling upon astrocytes to satisfy hungry neurons. *Neurosci. a Rev. J. bringing Neurobiol. Neurol. psychiatry* 10, 53–62. doi:10.1177/1073858403260159.

Pereyra, M., and Medina, J. H. (2021). AMPA Receptors: A Key Piece in the Puzzle of Memory Retrieval . *Front. Hum. Neurosci.* 15, 527. Available at: https://www.frontiersin.org/article/10.3389/fnhum.2021.729051.

Petersen, E. N., Chung, H. W., Nayebosadri, A., and Hansen, S. B. (2016). Kinetic disruption of lipid rafts is a mechanosensor for phospholipase D. *Nat. Commun.* 7, 1–8. doi:10.1038/ncomms13873.

Pettit, D. L., Perlman, S., and Malinow, R. (1994). Potentiated transmission and prevention of further LTP by increased CaMKII activity in postsynaptic hippocampal slice neurons. *Science* 266, 1881–1885. doi:10.1126/science.7997883.

Phan, A., Suschkov, S., Molinaro, L., Reynolds, K., Lymer, J. M., Bailey, C. D. C., et al. (2015). Rapid increases in immature synapses parallel estrogen-induced hippocampal learning enhancements. *Proc. Natl. Acad. Sci. U. S. A.* 112, 16018–23. doi:10.1073/pnas.1522150112.

Portela, A., and Esteller, M. (2010). Epigenetic modifications and human disease. *Nat. Biotechnol.* 28, 1057–1068. doi:10.1038/nbt.1685.

Potier, M., Georges, F., Brayda-Bruno, L., Ladépêche, L., Lamothe, V., Al Abed, A. S., et al. (2016). Temporal Memory and Its Enhancement by Estradiol Requires Surface Dynamics of Hippocampal CA1 N-Methyl-D-Aspartate Receptors. *Biol. Psychiatry* 79, 735–745. doi:10.1016/j.biopsych.2015.07.017.

Prange-Kiel, J., Wehrenberg, U., Jarry, H., and Rune, G. M. (2003). Para/autocrine regulation of estrogen receptors in hippocampal neurons. *Hippocampus* 13, 226–234. doi:10.1002/hipo.10075.

Roselli, C. E., Horton, L. E., and Resko, J. A. (1985). Distribution and regulation of aromatase activity in the rat hypothalamus and limbic system. *Endocrinology* 117, 2471–2477. doi:10.1210/endo-117-6-2471.

Rudolph, L. M., Cornil, C. A., Mittelman-Smith, M. A., Rainville, J. R., Remage-Healey, L., Sinchak, K., et al. (2016). Actions of Steroids: New Neurotransmitters. *J. Neurosci.* 36, 11449–11458. doi:10.1523/JNEUROSCI.2473-16.2016.

Rust, M. B. (2015). ADF/cofilin: a crucial regulator of synapse physiology and behavior. *Cell. Mol. Life Sci.* 72, 3521–3529. doi:10.1007/s00018-015-1941-z.

Rust, M. J., Bates, M., and Zhuang, X. (2006). Sub-diffraction-limit imaging by stochastic optical reconstruction microscopy (STORM). *Nat. Methods* 3, 793–795. doi:10.1038/nmeth929.

Sako, Y., and Kusumi, A. (1994). Compartmentalized structure of the plasma membrane for receptor movements as revealed by a nanometer-level motion analysis. *J. Cell Biol.* 125, 1251–1264. doi:10.1083/jcb.125.6.1251.

Schevzov, G., Curthoys, N. M., Gunning, P. W., and Fath, T. (2012). *Functional Diversity of Actin Cytoskeleton in Neurons and its Regulation by Tropomyosin*. 1st ed. Elsevier Inc. doi:10.1016/B978-0-12-394309-5.00002-X.

Schindelin, J., Arganda-Carreras, I., Frise, E., Kaynig, V., Longair, M., Pietzsch, T., et al. (2012). Fiji: an open-source platform for biological-image analysis. *Nat. Methods* 9, 676–682. doi:10.1038/nmeth.2019.

Schwenk, J., Baehrens, D., Haupt, A., Bildl, W., Boudkkazi, S., Roeper, J., et al. (2014).

Regional diversity and developmental dynamics of the AMPA-receptor proteome in the mammalian brain. *Neuron* 84, 41–54. doi:10.1016/j.neuron.2014.08.044.

Sezgin, E., Levental, I., Mayor, S., and Eggeling, C. (2017). The mystery of membrane organization: Composition, regulation and roles of lipid rafts. *Nat. Rev. Mol. Cell Biol.* 18, 361–374. doi:10.1038/nrm.2017.16.

Sheppard, P. A. S., Choleris, E., and Galea, L. A. M. (2019). Structural plasticity of the hippocampus in response to estrogens in female rodents. *Mol. Brain* 12, 22. doi:10.1186/s13041-019-0442-7.

Shi, S., Hayashi, Y., Esteban, J. A., and Malinow, R. (2001). Subunit-specific rules governing AMPA receptor trafficking to synapses in hippocampal pyramidal neurons. *Cell* 105, 331–343. doi:10.1016/s0092-8674(01)00321-x.

Sidenstein, S. C., D'Este, E., Böhm, M. J., Danzl, J. G., Belov, V. N., and Hell, S. W. (2016). Multicolour multilevel STED nanoscopy of actin/spectrin organization at synapses. *Sci. Rep.* 6. doi:10.1038/srep26725.

Smejkalova, T., and Woolley, C. S. (2010). Estradiol acutely potentiates hippocampal excitatory synaptic transmission through a presynaptic mechanism. *J. Neurosci.* 30, 16137–16148. doi:10.1523/JNEUROSCI.4161-10.2010.

Smith, C. C., and McMahon, L. L. (2005). Estrogen-induced increase in the magnitude of long-term potentiation occurs only when the ratio of NMDA transmission to AMPA transmission is increased. *J. Neurosci.* 25, 7780–7791. doi:10.1523/JNEUROSCI.0762-05.2005.

Sobolevsky, A. I., Rosconi, M. P., and Gouaux, E. (2009). X-ray structure, symmetry and mechanism of an AMPA-subtype glutamate receptor. *Nature* 462, 745–756. doi:10.1038/nature08624.

Spencer, A., Yu, L., Guili, V., Reynaud, F., Ding, Y., Ma, J., et al. (2017). Nerve growth factor signaling from membrane microdomains to the nucleus: Differential regulation by caveolins. *Int. J. Mol. Sci.* 18. doi:10.3390/ijms18040693.

Spencer, J. L., Waters, E. M., Romeo, R. D., Wood, G. E., Milner, T. A., and McEwen, B. S. (2008). Uncovering the mechanisms of estrogen effects on hippocampal function. *Front. Neuroendocrinol.* 29, 219–237. doi:10.1016/j.yfrne.2007.08.006.

Srivastava, D. P., Woolfrey, K. M., Jones, K. A., Shum, C. Y., Lash, L. L., Swanson, G. T., et al. (2008). Rapid enhancement of two-step wiring plasticity by estrogen and NMDA receptor activity. *Proc. Natl. Acad. Sci.* 105, 14650 LP – 14655. doi:10.1073/pnas.0801581105.

Srivastava, D., and Penzes, P. (2011). Rapid Estradiol Modulation of Neuronal Connectivity and Its Implications for Disease . *Front. Endocrinol.* 2, 77. Available at: https://www.frontiersin.org/article/10.3389/fendo.2011.00077.

Storey, E., Kowall, N. W., Finn, S. F., Mazurek, M. F., and Beal, M. F. (1992). The cortical lesion of Huntington's disease: further neurochemical characterization, and reproduction of some of the histological and neurochemical features by N-methyl-D-aspartate lesions of rat cortex. *Ann. Neurol.* 32, 526–534. doi:10.1002/ana.410320408.

Szego, C. M., and Davis, J. S. (1967). Adenosine 3',5'-monophosphate in rat uterus: acute elevation by estrogen. *Proc. Natl. Acad. Sci. U. S. A.* 58, 1711–1718. Available at: http://www.ncbi.nlm.nih.gov/pmc/articles/PMC223984/.

Teyler, T. J., Vardaris, R. M., Lewis, D., and Rawitch, A. B. (1980). Gonadal steroids: Effects on excitability of hippocampal pyramidal cells. *Science (80-.).* 209, 1017–1018. doi:10.1126/science.7190730.

Thomas, P., Pang, Y., Filardo, E. J., and Dong, J. (2005). Identity of an estrogen membrane receptor coupled to a G protein in human breast cancer cells. *Endocrinology* 146, 624–632. doi:10.1210/en.2004-1064.

Tokunaga, M., Imamoto, N., and Sakata-Sogawa, K. (2008). Highly inclined thin illumination enables clear single-molecule imaging in cells. *Nat. Methods* 5, 159–161. doi:10.1038/nmeth1171.

Traynelis, S. F., Hartley, M., and Heinemann, S. F. (1995). Control of proton sensitivity of the NMDA receptor by RNA splicing and polyamines. *Science* 268, 873–876. doi:10.1126/science.7754371.

Traynelis, S. F., Wollmuth, L. P., McBain, C. J., Menniti, F. S., Vance, K. M., Ogden, K. K., et al. (2010). Glutamate receptor ion channels: structure, regulation, and function. *Pharmacol. Rev.* 62, 405–496. doi:10.1124/pr.109.002451.

Triller, A., and Choquet, D. (2005). Surface trafficking of receptors between synaptic and extrasynaptic membranes: and yet they do move! *Trends Neurosci.* 28, 133–139. doi:10.1016/j.tins.2005.01.001.

Tsien, J. Z., Huerta, P. T., and Tonegawa, S. (1996). The essential role of hippocampal CA1 NMDA receptor-dependent synaptic plasticity in spatial memory. *Cell* 87, 1327–1338. doi:10.1016/s0092-8674(00)81827-9.

Tsunoyama, T. A., Watanabe, Y., Goto, J., Naito, K., Kasai, R. S., Suzuki, K. G. N., et al. (2018). Super-long single-molecule tracking reveals dynamic-anchorage-induced integrin function. *Nat. Chem. Biol.* 14. doi:10.1038/s41589-018-0032-5.

Ubuka, T., and Tsutsui, K. (2014). Review: neuroestrogen regulation of socio-sexual behavior of males. *Front. Neurosci.* 0, 323. doi:10.3389/FNINS.2014.00323.

van Zundert, B., Yoshii, A., and Constantine-Paton, M. (2004). Receptor compartmentalization and trafficking at glutamate synapses: a developmental proposal. *Trends Neurosci.* 27, 428–437. doi:10.1016/J.TINS.2004.05.010.

Vrtačnik, P., Ostanek, B., Mencej-Bedrač, S., and Marc, J. (2014). The many faces of estrogen signaling. *Biochem. medica* 24, 329–342. doi:10.11613/BM.2014.035.

Wang, Z., Sun, L., Liang, S., Liu, Z. chao, Zhao, Z. yi, Yang, J., et al. (2019). GPER stabilizes F-actin cytoskeleton and activates TAZ via PLCβ-PKC and Rho/ROCK-LIMK-Cofilin pathway. *Biochem. Biophys. Res. Commun.* doi:10.1016/j.bbrc.2019.06.132.

Wehrenberg, U., Prange-Kiel, J., and Rune, G. M. (2001). Steroidogenic factor-1 expression in marmoset and rat hippocampus: Co-localization with StAR and aromatase. *J. Neurochem.* 76, 1879–1886. doi:10.1046/j.1471-4159.2001.00207.x.

Wenthold, R. J., Petralia, R. S., Blahos J, I. I., and Niedzielski, A. S. (1996). Evidence for multiple AMPA receptor complexes in hippocampal CA1/CA2 neurons. *J. Neurosci.* 16, 1982–1989. doi:10.1523/JNEUROSCI.16-06-01982.1996.

Wiatrak, B., Kubis-Kubiak, A., Piwowar, A., and Barg, E. (2020). PC12 Cell Line: Cell Types, Coating of Culture Vessels, Differentiation and Other Culture Conditions. *Cells* 9. doi:10.3390/cells9040958.

Wong, M., and Moss, R. L. (1992). Long-term and short-term electrophysiological effects of estrogen on the synaptic properties of hippocampal CA1 neurons. *J. Neurosci.* 12, 3217–3225. doi:10.1523/JNEUROSCI.12-08-03217.1992.

Xie, Z., Srivastava, D. P., Photowala, H., Kai, L., Cahill, M. E., Woolfrey, K. M., et al. (2007). Kalirin-7 controls activity-dependent structural and functional plasticity of dendritic spines. *Neuron* 56, 640–656. doi:10.1016/j.neuron.2007.10.005.

Xu, K., Zhong, G., and Zhuang, X. (2013). Actin, spectrin, and associated proteins form a periodic cytoskeletal structure in axons. *Science* 339, 452–456. doi:10.1126/science.1232251.

Y, Z., L, H., Y, Z., J, Z., Z, L., F, X., et al. (2017). Estrogen receptor alpha and beta regulate actin polymerization and spatial memory through an SRC-1/mTORC2-dependent pathway in the hippocampus of female mice. *J. Steroid Biochem. Mol. Biol.* 174, 96–113. doi:10.1016/J.JSBMB.2017.08.003.

Zhao, T. Z., Shi, F., Hu, J., He, S. M., Ding, Q., and Ma, L. T. (2016). GPER1 mediates

estrogen-induced neuroprotection against oxygen-glucose deprivation in the primary hippocampal neurons. *Neuroscience* 328, 117–126. doi:10.1016/j.neuroscience.2016.04.026.

Zhu, J. J., Esteban, J. A., Hayashi, Y., and Malinow, R. (2000). Postnatal synaptic potentiation: Delivery of GluR4-containing AMPA receptors by spontaneous activity. *Nat. Neurosci.* 3, 1098–1106. doi:10.1038/80614.

Zucker, R. S., and Regehr, W. G. (2002). Short-term synaptic plasticity. *Annu. Rev. Physiol*. 64, 355–405. doi:10.1146/annurev.physiol.64.092501.114547.

frontiers in Cell and Developmental Biology

ORIGINAL RESEARCH
published: 23 September 2021
doi: 10.3389/fcell.2021.708715

Single-Molecule Imaging Reveals Rapid Estradiol Action on the Surface Movement of AMPA Receptors in Live Neurons

Soma Godó[1], Klaudia Barabás[1], Ferenc Lengyel[1], Dávid Ernszt[1], Tamás Kovács[1], Miklós Kecskés[2], Csaba Varga[2], Tibor Z. Jánosi[1], Géza Makkai[1], Gergely Kovács[1], Barbara Orsolits[3], Takahiro Fujiwara[4], Akihiro Kusumi[5] and István M. Ábrahám[1]*

[1] PTE-NAP Molecular Neuroendocrinology Research Group, Centre for Neuroscience, Szentágothai Research Center, Medical School, Institute of Physiology, University of Pécs, Pécs, Hungary, [2] PTE-NAP Cortical Microcircuits Research Group, Institute of Physiology, Medical School, Centre for Neuroscience, Szentágothai Research Institute, Pécs, Hungary, [3] Laboratory of Neuroimmunology, Institute of Experimental Medicine of the Hungarian Academy of Sciences, Budapest, Hungary, [4] Institute for Integrated Cell-Material Sciences (WPI-iCeMS), Kyoto University, Kyoto, Japan, [5] Membrane Cooperativity Unit, Okinawa Institute of Science and Technology Graduate University (OIST), Onna, Japan

OPEN ACCESS

Edited by:
Bianca Marchetti, Università di Catania, Italy

Reviewed by:
Reyna Hernandez-Benitez, Salk Institute for Biological Studies, United States
Deepak Prakash Srivastava, King's College London, United Kingdom
Gyorgy Vereb, University of Debrecen, Hungary

****Correspondence:***
Soma Godó
soma.godo@aok.pte.hu

Specialty section:
This article was submitted to Signaling, a section of the journal Frontiers in Cell and Developmental Biology

Received: *12 May 2021*
Accepted: *07 September 2021*
Published: *23 September 2021*

Citation:
Godó S, Barabás K, Lengyel F, Ernszt D, Kovács T, Kecskés M, Varga C, Jánosi TZ, Makkai G, Kovács G, Orsolits B, Fujiwara T, Kusumi A and Ábrahám IM (2021) Single-Molecule Imaging Reveals Rapid Estradiol Action on the Surface Movement of AMPA Receptors in Live Neurons. Front. Cell Dev. Biol. 9:708715. doi: 10.3389/fcell.2021.708715

Gonadal steroid 17β-estradiol (E2) exerts rapid, non-genomic effects on neurons and strictly regulates learning and memory through altering glutamatergic neurotransmission and synaptic plasticity. However, its non-genomic effects on AMPARs are not well understood. Here, we analyzed the rapid effect of E2 on AMPARs using single-molecule tracking and super-resolution imaging techniques. We found that E2 rapidly decreased the surface movement of AMPAR via membrane G protein-coupled estrogen receptor 1 (GPER1) in neurites in a dose-dependent manner. The cortical actin network played a pivotal role in the GPER1 mediated effects of E2 on the surface mobility of AMPAR. E2 also decreased the surface movement of AMPAR both in synaptic and extrasynaptic regions on neurites and increased the synaptic dwell time of AMPARs. Our results provide evidence for understanding E2 action on neuronal plasticity and glutamatergic neurotransmission at the molecular level.

Keywords: 17β-estradiol, AMPAR, single-molecule tracking, diffusion, synapse

INTRODUCTION

The gonadal steroid, 17β-estradiol (E2), plays a role in a wide range of biological functions, from fertility to neuroprotection (McEwen, 2002; Kwakowsky et al., 2013; Marbouti et al., 2020a,b; Hokenson et al., 2021). The cellular effects of E2 have been proposed to be mediated by a slow transcriptional action through the nuclear receptors, ERα, and ERβ. In addition to its classical genomic effects, E2 exerts non-classical actions. It rapidly alters the function of receptors and the activity of second messengers through membrane estrogen receptors, such as membrane-associated ERα and ERβ, as well as the G protein-coupled estrogen receptor 1 (GPER1) (Rudolph et al., 2016).

Glutamatergic neurotransmission and synaptic plasticity are also promptly regulated by E2 (Teyler et al., 1980; Wong and Moss, 1992; Kramár et al., 2009b; Ledoux et al., 2009; Vierk et al., 2014; Murakami et al., 2018; Lu et al., 2019). Extracellularly recorded dendritic field potentials in

the hippocampal CA1 subfield and miniature excitatory synaptic currents (mEPSCs) recorded via whole-cell voltage-clamp in the CA1 pyramidal cells of adult rats are rapidly altered by E2 (Phan et al., 2015; Oberlander and Woolley, 2016). However, the E2 effect is selective to a subset of neurons and the molecular mechanism differs between sexes probably due to the different ER profile which can lead to different effect on neurons (Wong and Moss, 1992).

The surface movement of glutamate receptors, such as AMPARs, is crucial in excitatory neurotransmission and synaptic plasticity (Babayan and Kramár, 2013; Penn et al., 2017). The submembrane actin network affects excitatory neurotransmission and surface movement of AMPARs (Kramár et al., 2006; Gowrishankar et al., 2012). The amount, distribution, and movement of AMPAR molecules in the postsynaptic density and the extrasynaptic sites determine the efficiency and function of the synapse (Ashby et al., 2004; Groc and Choquet, 2006; Lee et al., 2017; Choquet, 2018). Steroid hormones such as corticosterone and aldosterone, have been shown to rapidly alter the membrane dynamics of AMPARs, as well as the synaptic dwell time (the time spent within the active site of synapse) (Groc et al., 2008). However, it is unknown whether E2 affects the surface movement of AMPARs. We applied E2 to live neurons and performed multiple super-resolution imaging and single-molecule tracking approaches to examine the effects of E2 on the surface movement of glutamate receptor molecules. Our findings demonstrated that E2 rapidly decreased the surface movements of GluR2-AMPAR molecules [the most abundant AMPAR subunit in neurons (Isaac et al., 2007)] in a dose-dependent manner without affecting mGluR1 molecules [a metabotropic glutamate receptor 1 involved in the rapid membrane action of E2 (Micevych and Mermelstein, 2008)] in neuronal cells differentiated from rat pheochromocytoma (PC12) cells (dPC12). The mechanism of the E2 action is compartment-specific and is mediated by ER mechanisms involving the cortical actin and cofilin pathways. Our results gained from dPC12 were confirmed by cultured hippocampal neurons, a more differentiated system with mature synapses. In hippocampal neurons E2 also decreased the surface movements of GluR2-AMPAR. This study provides the first evidence that E2 decreases the surface movement of synaptic GluR2-AMPAR and increases the dwell time of GluR2-AMPAR in the synapse. These findings broaden our knowledge of the molecular mechanism of E2 action on neuronal plasticity and glutamatergic neurotransmission.

RESULTS

Characterization of Neuronal Properties of dPC12 and Single-Molecule Tracking of ATTO 488-Labeled GluR2-AMPAR and mGluR1

We characterized the PC12 cells after 4 days of NGF treatment when neurite outgrowth was pronounced (**Supplementary Figure 1A**). Immunocytochemistry showed that dPC12 expressed neuronal markers such as β-III tubulin and MAP-2 (**Supplementary Figure 1B**). In addition, we examined the passive electrophysiological parameters of 10 cells using whole-cell patch clamp technique. We found that the resting membrane potential, the input resistance and the cell capacitance were -55.5 ± 7.7 mV, 1072.7 ± 854.9 MΩ and 60.2 ± 32.9 pF, respectively (values are represented as mean ± SD). Finally, we recorded that step current injection elicited a single abortive action potential in dPC12 (**Supplementary Figure 1C**). Moreover, *in vivo* labeling of dPC12 demonstrated GluR2-AMPAR and mGluR1 in neurites and soma (**Supplementary Movies 1–4**).

In single-molecule tracking experiments, the fluorescence intensity versus time function showed one-step photobleaching, representing single ATTO 488 fluorophores for GluR2-AMPAR and mGluR1. The fluorescence intensity histograms of both GluR2-AMPAR and mGluR1 had peak intensities similar to those of the step sizes for photobleaching (**Figures 1A,B**). These results suggest that most of the spots represented single fluorophores and single receptors.

E2 Rapidly Decreases the Surface Movement of GluR2-AMPAR Molecules in dPC12

Surface Movements of GluR2-AMPARs and mGluR1 on dPC12

The surface movement of glutamate receptors was detected in the plasma membrane of live dPC12 (**Figure 1C** and **Supplementary Movies 1–4**). Based on the mean square displacement functions of GluR2-AMPARs and mGluR1 receptors, they exhibited two main types of movements: Brownian diffusion, when receptors moved freely between barriers and confined motion when receptors were restricted to a small area (**Figure 1D**). The diffusion coefficients of both receptors are significantly higher on the neurite than on soma (**Figures 1E,F**), indicating that the surface movement of glutamate receptors is faster on neurites.

Dose Dependence

Administration of 100pM, 1 nM and 100 nM doses of E2 evoked a clear dose-dependent decrease in D_{AMPAR} in neurites as measured in the first 20 min after treatment with a maximum decrease of 55% ($p < 0.01$) (vehicle mean $D_{AMPAR} \pm$ SEM ($\mu m^2/s$) on neurite: 0.058 ± 0.003) (**Figure 2A** and **Supplementary Movie 5**). In soma, 100 pM of E2 significantly decreased D_{AMPAR} (68%, $p < 0.01$), while 1 nM and 100 nM of E2 were ineffective (vehicle mean $D_{AMPAR} \pm$ SEM [$\mu m^2/s$] on soma: 0.024 ± 0.002) (**Figure 2A**). In contrast, E2 (100 nM, 1 nM or 100 pM) did not change D_{mGluR1} either in soma or in neurites (**Figure 2B**) (vehicle mean $D_{mGluR1} \pm$ SEM ($\mu m^2/s$); soma: 0.032 ± 0.003, neurite: 0.049 ± 0.005).

To investigate whether a low concentration of EtOH (10^{-3} %) (vehicle) affects GluR2-AMPAR and mGluR1 surface trafficking, we compared D_{AMPAR} and D_{mGluR1} in a culture medium (control) without or with vehicle (20 min after application). There was no significant effect of vehicle on D_{AMPAR} and D_{mGluR1} in dPC12 [values are expressed as the mean D ± SEM [$\mu m^2/s$];

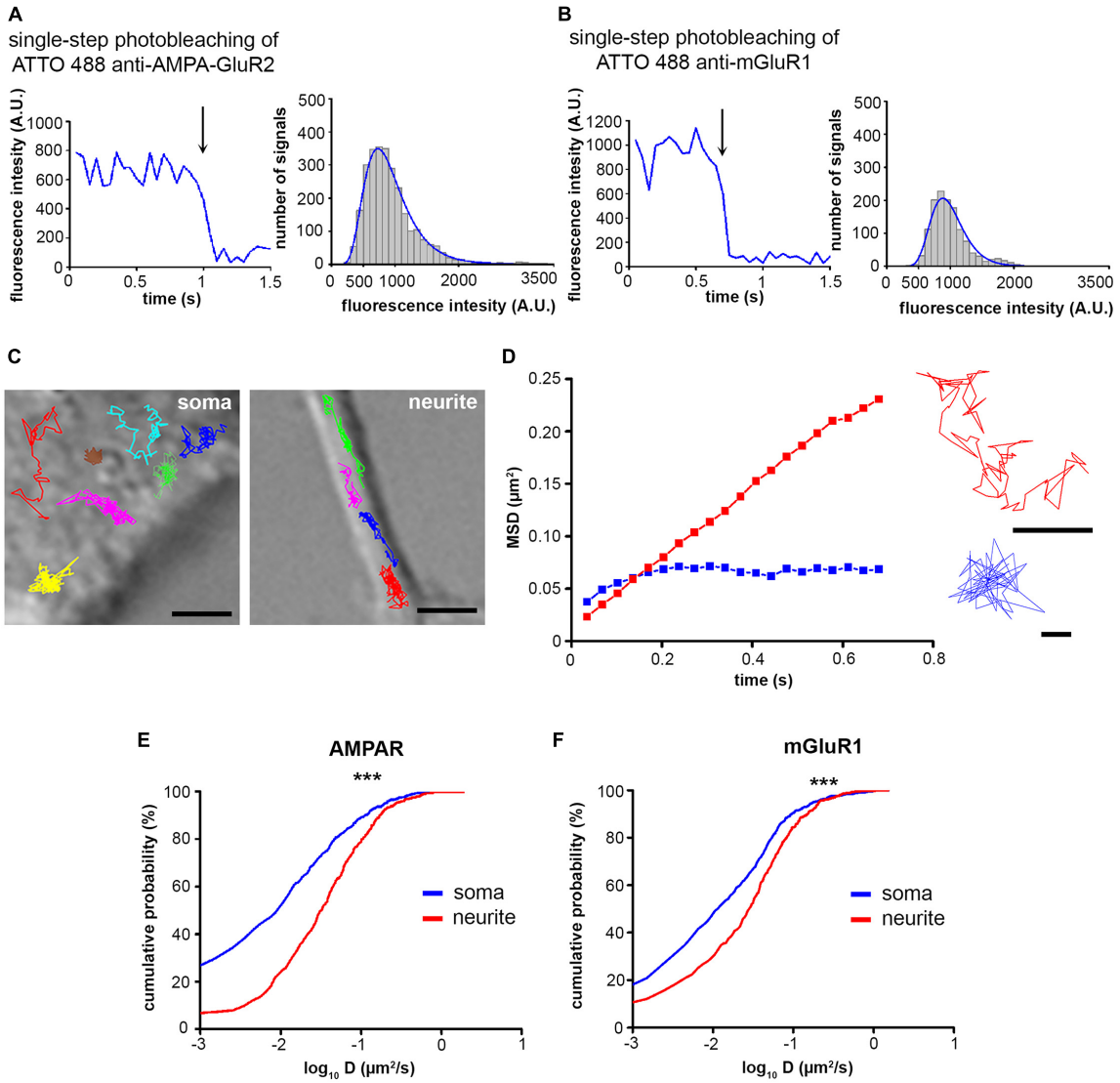

FIGURE 1 | Characterization of differentiated PC12 cells and validation of single-molecule labeling. **(A,B)** Left, Intensity profiles of a single ATTO 488-labeled GluR2-AMPAR **(A)** and mGluR1 **(B)** signal. The arrows indicate single-step photobleaching. Right, Histogram showing the intensity value of every spot found in a recording of ATTO 488-labeled GluR2-AMPAR **(A)** and mGluR1 **(B)**, superimposed with a single fitted lognormal curve (blue line). **(C)** Representative trajectories of AMPAR molecules on somas and neurites. Scale bar = 2 µm. **(D)** The mean square displacement functions and trajectories represent AMPAR molecules with Brownian motion (red) and confined motion (blue). Scale bar = 0.1 µm. **(E,F)** The cumulative probability functions of D values of AMPAR **(E)** and mGluR1 **(F)** on neurites and somas (n = 510–676 trajectories). ***$p < 0.001$.

on soma: control D_{AMPAR}: 0.024 ± 0.003 (n = 590 trajectories), vehicle D_{AMPAR}: 0.022 ± 0.002 (n = 612 trajectories); neurite: control D_{AMPAR}: 0.073 ± 0.006 (n = 545 trajectories), vehicle D_{AMPAR}: 0.069 ± 0.007, (n = 647 trajectories); soma: control D_{mGluR1}: 0.033 ± 0.003 (n = 751 trajectories), vehicle D_{mGluR1}: 0.034 ± 0.002, (n = 622 trajectories); neurite: control D_{mGluR1}: 0.051 ± 0.004 (n = 513 trajectories), vehicle: 0.050 ± 0.003, (n = 496 trajectories)].

Time Course

To examine the time dependence of the effect evoked by E2 on D_{AMPAR} or D_{mGluR1}, we applied the most effective E2 doses on soma and neurites and measured D at different time points. The application of 100 pM of E2 resulted in a significant decrease ($p < 0.01$) in D_{AMPAR} on soma within 5 min. This remained reduced at 10 min, 15 min, and 20 min (vehicle mean D_{AMPAR} ± SEM (µm²/s) on soma: 5 min, 0.064 ± 0.007; 10 min, 0.054 ± 0.008; 15 min, 0.03 ± 0.004; 20 min, 0.042 ± 0.008). In contrast, 100 nM of E2 only reduced D_{AMPAR} on neurites at 10, 15, and 20 min (vehicle mean D_{AMPAR} ± SEM [µm²/s] on neurites: 5 min: 0.063 ± 0.007; 10 min: 0.051 ± 0.005; 15 min: 0.050 ± 0.007; 20 min: 0.051 ± 0.007) (**Figure 2C**). In contrast, 100 pM or 100 nM of E2 did not affect D_{mGluR1} on neurites or soma, respectively, at any time point (vehicle mean

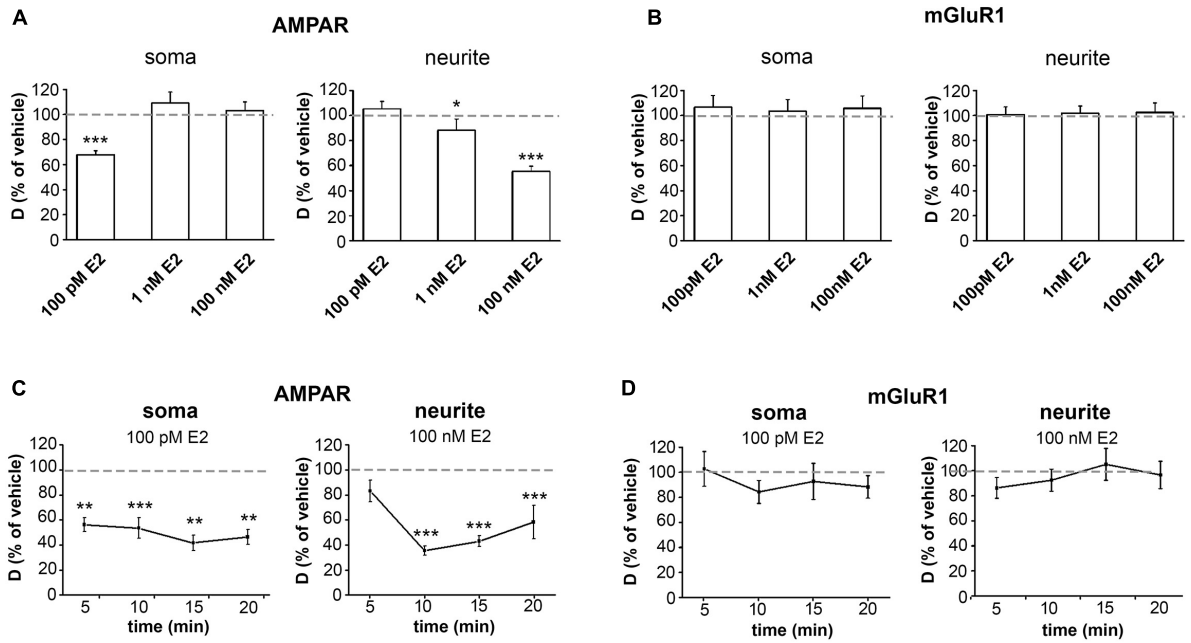

FIGURE 2 | Effect of E2 on the surface movement of GluR2-AMPAR and mGluR1. **(A)** Effect of different concentrations of E2 on the diffusion coefficient (D, $\mu m^2/s$) of GluR2-AMPAR **(A)** and mGluR1 **(B)** (% of vehicle treatment as the mean ± SEM, *n* = 425–1145 trajectories per group). **(C,D)** Line graphs depict changes in D of GluR2-AMPAR **(C)** and mGluR1 **(D)** molecules at different time points after the administration of the most effective concentration of E2 (% of vehicle treatment as the mean D ± SEM, *n* = 117–187 trajectories per time point). $^*p < 0.05$; $^{**}p < 0.01$; $^{***}p < 0.001$.

D_{mGluR1} ± SEM [$\mu m^2/s$] on soma: 5 min: 0.033 ± 0.006; 10 min: 0.042 ± 0.006 15 min: 0.031 ± 0.005; 20 min: 0.036 ± 0.007; on neurites: 5 min: 0.061 ± 0.006; 10 min: 0.053 ± 0.007; 15 min: 0.052 ± 0.004; 20 min: 0.038 ± 0.004) (**Figure 2D**).

GPER1 and ERβ Mediate the Effect of E2 on the Surface Movement of GluR2-AMPAR Molecules in dPC12

Our PCR results revealed that dPC12 expresses ERβ and GPER1, but not ERα (**Figure 3A**). Although the addition of ERβ agonist DPN (10 pM) or specific GPER1 agonist G1 (100 nM) alone did not affect the surface movement of somatic GluR2-AMPAR molecules (vehicle mean D_{AMPAR} ± SEM ($\mu m^2/s$) on soma; DPN vehicle: 0.04 ± 0.003; G1 vehicle: 0.023 ± 0.002), co-administration of DPN and G1 decreased D_{AMPAR} (DPN+G1 vehicle D_{AMPAR} mean ± SEM ($\mu m^2/s$) on soma: 0.075 ± 0.009) similar to 100 pM of E2 (**Figure 3B**). G1 (100 nM) mimicked the effect of 100 nM of E2 without and with 10 pM of DPN (vehicle mean D_{AMPAR} ± SEM ($\mu m^2/s$) on neurite; G1 vehicle: 0.056 ± 0.003; G1+DPN vehicle: 0.1 ± 0.004) in neurites (**Figure 3B**). However, 10 pM of DPN alone did not alter the D_{AMPAR} in neurites (DPN vehicle mean D_{AMPAR} ± SEM ($\mu m^2/s$) on neurite: 0.056 ± 0.004) (**Figure 3B**). In addition, prior application of 1 μM of G15 blocked the effect of 100 pM of E2 on soma and 100 nM of E2 on neurites (vehicle mean D_{AMPAR} ± SEM ($\mu m^2/s$); soma: 0.025 ± 0.002, neurite: 0.048 ± 0.003, **Figure 3B**). G15 application alone did not alter the surface movement of GluR2-AMPAR in either neurites or soma (vehicle mean D_{AMPAR} ± SEM ($\mu m^2/s$); soma: 0.020 ± 0.002, neurite: 0.062 ± 0.004, **Figure 3B**).

Since we applied DMSO as a vehicle in these experiments, we also tested whether the 0.1 % DMSO alone affected D_{AMPAR}. We compared D_{AMPAR} in a culture medium (control) with or without vehicle (20 min after application). There was no significant effect of DMSO on D_{AMPAR} in dPC12 (values are expressed as the mean D ± SEM [$\mu m^2/s$] on soma: medium D_{AMPAR}: 0.024 ± 0.003 (*n* = 590 trajectories), vehicle D_{AMPAR}: 0.023 ± 0.002 (*n* = 645 trajectories); on neurite: medium D_{AMPAR}: 0.073 ± 0.006 (*n* = 545 trajectories), vehicle D_{AMPAR}: 0.062 ± 0.004, (*n* = 524 trajectories).

Our results show that GPER1 mediates the effect of E2 on GluR2-AMPAR on both soma and neurites. To further analyze the relationship between GluR2-AMPAR and GPER1, we used STORM super-resolution imaging to examine the expression GPER1 and GluR2-AMPAR. STORM imaging revealed that GPER1 and GluR2-AMPAR receptors are expressed on both soma and neurites (**Figure 4A**). In order to examine the number of GPER1 in relation to GluR2-AMPAR we normalized the number of GPER1 to GluR2-AMPAR using GPER1/GluR2-AMPAR ratio. Our analysis demonstrated that the GPER1/GluR2-AMPAR ratio was significantly higher in soma than in neurites of dPC12 (**Figure 4B**).

E2 can induce rapid internalization and consequent desensitization of GPER1 (Filardo and Thomas, 2012). The internalization of GPER1 may explain the different effects of E2 on the soma and neurites. To visualize whether GPER1 is internalized after E2 administration in soma, stimulated emission

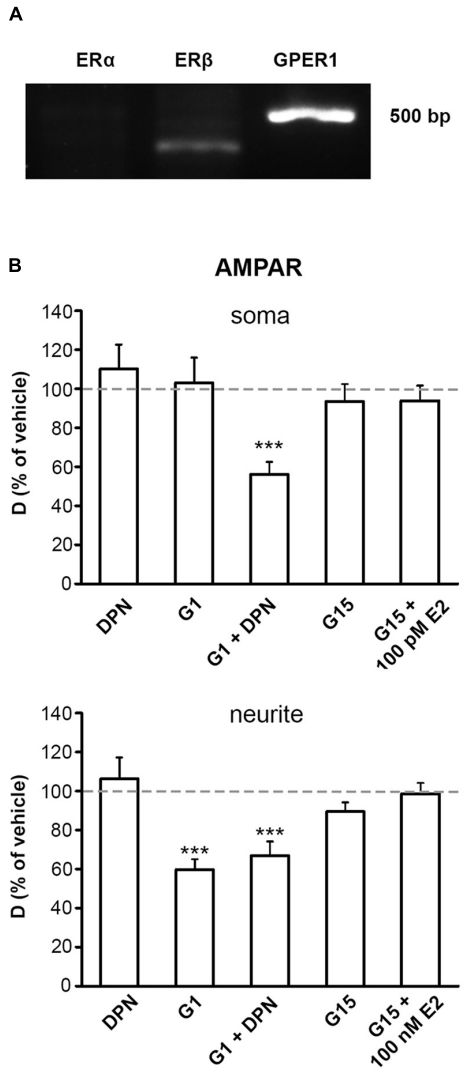

FIGURE 3 | Effect of estrogen receptor modulation on the surface movement of GluR2-AMPAR. **(A)** Representative PCR gel electrophoresis image depicting the expression of estrogen receptor beta (ERβ) and G protein-coupled estrogen receptor 1 (GPER1) mRNA in dPC12. Estrogen receptor alpha (ERα) mRNA was not detected. **(B)** Histograms demonstrate the mean D_{AMPAR} as a percentage of vehicle control on somas and neurites in the presence of the estrogen receptor, β (ERβ) agonist diarylpropionitrile (DPN), a GPER1 agonist (G1), G1+DPN together, a GPER1 antagonist (G15) and G15+E2 (with 100 pM of E2 on the somas and 100 nM of E2 on the neurites) (mean ± SEM; n = 215–641 trajectories). ***$p < 0.001$.

depletion (STED) microscopy was used (**Figures 4C1,C2**). Super-resolution STED imaging revealed that the intensity of immunostaining of GPER1 was approximately 2 times higher in the membrane region than in the cytoplasm of vehicle-treated dPC12 (**Figures 4C1,C2,D**). After 10 min of 100 nM of E2 treatment, the intensity profile of GPER1 showed a significant decrease in the membrane region (**Figures 4C1,C2,D,E**). In contrast, the majority of GPER1 immunoreactivity was located in the cytoplasm (**Figures 4C1,C2,D,E**) after treatment with 100 nM of E2, suggesting rapid internalization of GPER1 in response to high E2 exposure. There was no internalization of GPER1 observed in neurites after 100 nM of E2 treatment (**Supplementary Figure 2**).

Critical Role of the Cortical Actin Network in the Effect of E2 on GluR2-AMPAR in dPC12

Cortical actin is a thin actin network that lies directly underneath the plasma membrane. The cortical actin network is essential in the organization of neuronal compartments and plays a crucial role in membrane receptor movement (Schevzov et al., 2012), thus we speculated that the cortical actin network may play a pivotal role in the effect of E2 on the receptor dynamics. Previous studies show that E2 induces cytoskeleton assembly mediated by GPER1 receptors via different intracellular signaling pathways, including the Rho-associated protein kinase (ROCK)-cofilin (Gowrishankar et al., 2012; Wang et al., 2019) and c-Jun-N-terminal kinase (JNK)-cofilin (Kim et al., 2019) pathways. To determine the possible role of cortical actin in the effects of E2 on glutamate receptors, we treated cells with the actin polymerization inhibitor, latrunculinA (latA; l μM). To examine the role of the ROCK-cofilin and JNK-cofilin pathways in E2 action, we applied the ROCK inhibitor, GSK429286 (l μM) (Wang et al., 2019), and JNK inhibitor, SP600125 (l μM) (Kim et al., 2019), respectively.

First, we validated whether latA, or ROCK and JNK inhibitors altered the morphology of cortical actin. Phalloidin immunostaining demonstrated cortical F-actin in dPC12 (**Figure 5A**). The density of the cortical actin network in dPC12 was decreased by latA, GSK429286, or SP600125 administration (**Figure 5A**). In single-molecule tracking experiments, 10 min of latA, or pretreatment with GSK429286 or SP600125 for 60 min significantly increased D_{AMPAR} on soma (vehicle D_{AMPAR} mean ± SEM [$\mu m^2/s$]: 0.021 ± 0.002, **Figure 5B1**) without affecting D_{AMPAR} on neurites in dPC12 (vehicle D_{AMPAR} mean ± SEM [$\mu m^2/s$]: 0.049 ± 0.003, **Figure 5B2**). Pretreatment with latA, GSK429286, or SP600125 decreased the effect of 100 pM of E2 on soma and 100 nM of E2 on neurites on the surface movement of GluR2-AMPAR molecules (D_{AMPAR} mean ± SEM [$\mu m^2/s$] on soma: vehicle E2: 0.03 ± 0.004; vehicle E2+latA: 0.062 ± 0.006; vehicle E2+GSK429286: 0.087 ± 0.007; vehicle E2+SP600125: 0.093 ± 0.008; on neurites: vehicle E2: 0.074 ± 0.006; vehicle E2+latA: 0.06 ± 0.004; vehicle E2+GSK429286: 0.113 ± 0.015; vehicle E2+SP600125: 0.128 ± 0.012, **Figures 5C1,C2**). In experiments with latA, ROCK, and JNK cRPMI containing 0.1 % DMSO was used as vehicle control. Cell viability was not altered by DMSO nor latA treatment (**Supplementary Figure 3**).

E2 Rapidly Decreases the Surface Movement and Increases the Synaptic Dwell Time of GluR2-AMPAR in Mouse Primary Hippocampal Neurons

To validate the effect of E2 on the surface movement of GluR2-AMPAR in another *in vitro* neuron system and examine the

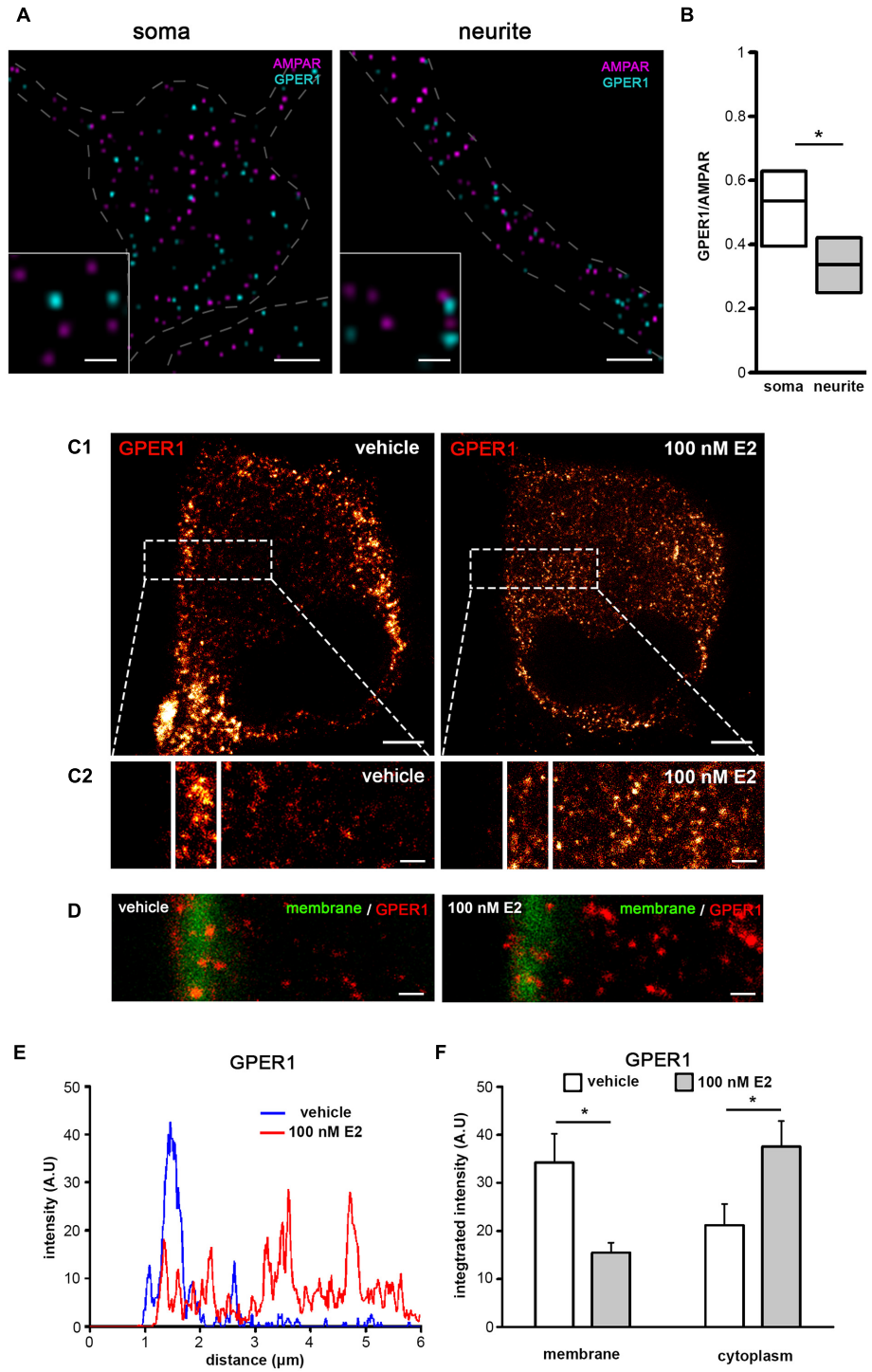

FIGURE 4 | The GluR2-AMPAR/GPER1 ratio and molecular distance between GPER1 and GluR2-AMPAR in the membrane. **(A)** STORM images depicting immunolabeled AMPAR (magenta) and GPER1 (cyan) molecules on dPC12. Dashed lines delineate the borders of the neurites and somas. Scale bar = 2 µm; inset Scale bar = 0.5 µm. **(B)** The ratio between the number of GPER1 and AMPAR molecules (GPER1/GluR2-AMPAR) on the neurites and somas (n = 11 somas or neurites). **(C1)** Photomicrographs depict GPER1 immunoreactivity (visualized with STED microscopy) in dPC12 after 10 min of vehicle (left) or of 100 nM of E2 treatment (right). Scale bar = 2 µm. **(C2)** One 2 μm^2 (between parallel white bars) and one 10 μm^2 (to the left) areas were selected within each ROI for the membrane and cytoplasmic regions of each cell, respectively. Integrated density was calculated and normalized to the area. Scale bar = 0.5 µm. **(D)** Dual labeling of plasma membrane and GPER1 molecules defines the membrane regions (approximately 1 µm wide). Scale bar = 0.5 µm. **(E)** Line graph of the fluorescent intensity calculated from the magnified STED inserts (C2). **(F)** Integrated density graphs of GPER1 show the effect of vehicle and 100 nM of E2 treatment in the membrane and in the cytoplasm (n = 15 cells were evaluated in each group). *$p < 0.05$.

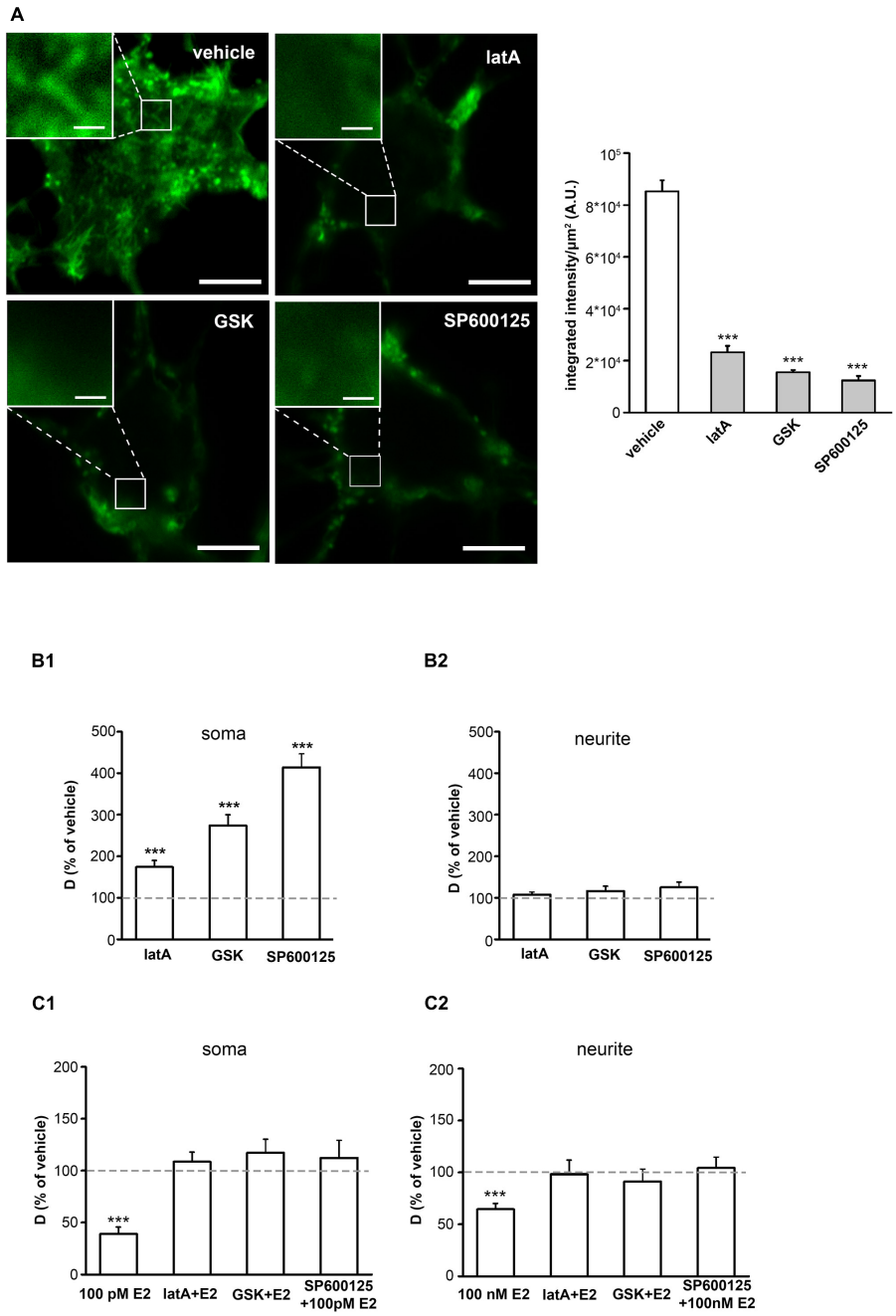

FIGURE 5 | The role of the cortical actin in the rapid effect of E2. **(A)** Left, confocal images depict Alexa Fluor 488 phalloidin-labeled cortical actin network in dPC12 after treatment with vehicle, 1 μM of latA, 1 μM of SP600125 or 1 μM of GSK429286. Scale bar = 5 μm; insert Scale bar = 0.5 μm. Right, the bar graph shows the effect of LatA, GSK429286, and SP600125 on the integrated density of the fluorescently labeled cortical actin network [n = 3 cells per group (3 ROIs per cell)]. **(B1,B2)** Effect of LatA, GSK429286, and SP600125 treatment on D_{AMPAR} (% of vehicle treatment as the mean ± SEM; n = 215–544 trajectories). **(C1,C2)** Effect of 100 pM of E2 on somas and 100 nM of E2 on neurites with or without LatA, GSK429286, and SP600125 (% of vehicle treatment as the mean ± SEM; n = 184–277 trajectories). ***$p < 0.001$.

effect of E2 on synaptic GluR2-AMPAR, we performed single-molecule tracking experiments on primary hippocampal neuron culture (**Figure 6A**).

Immunocytochemical labeling revealed that β-III tubulin-expressing hippocampal neurons have multiple homer-1 positive synapses along their neurites at day *in vitro* 18–21 (**Figure 6A**). The live-cell presynaptic MitoTracker Deep Red labeling was validated with co-immunostaining of presynaptic protein bassoon. STED imaging showed that every single MitoTracker Deep Red labeled synapse exhibited colocalization

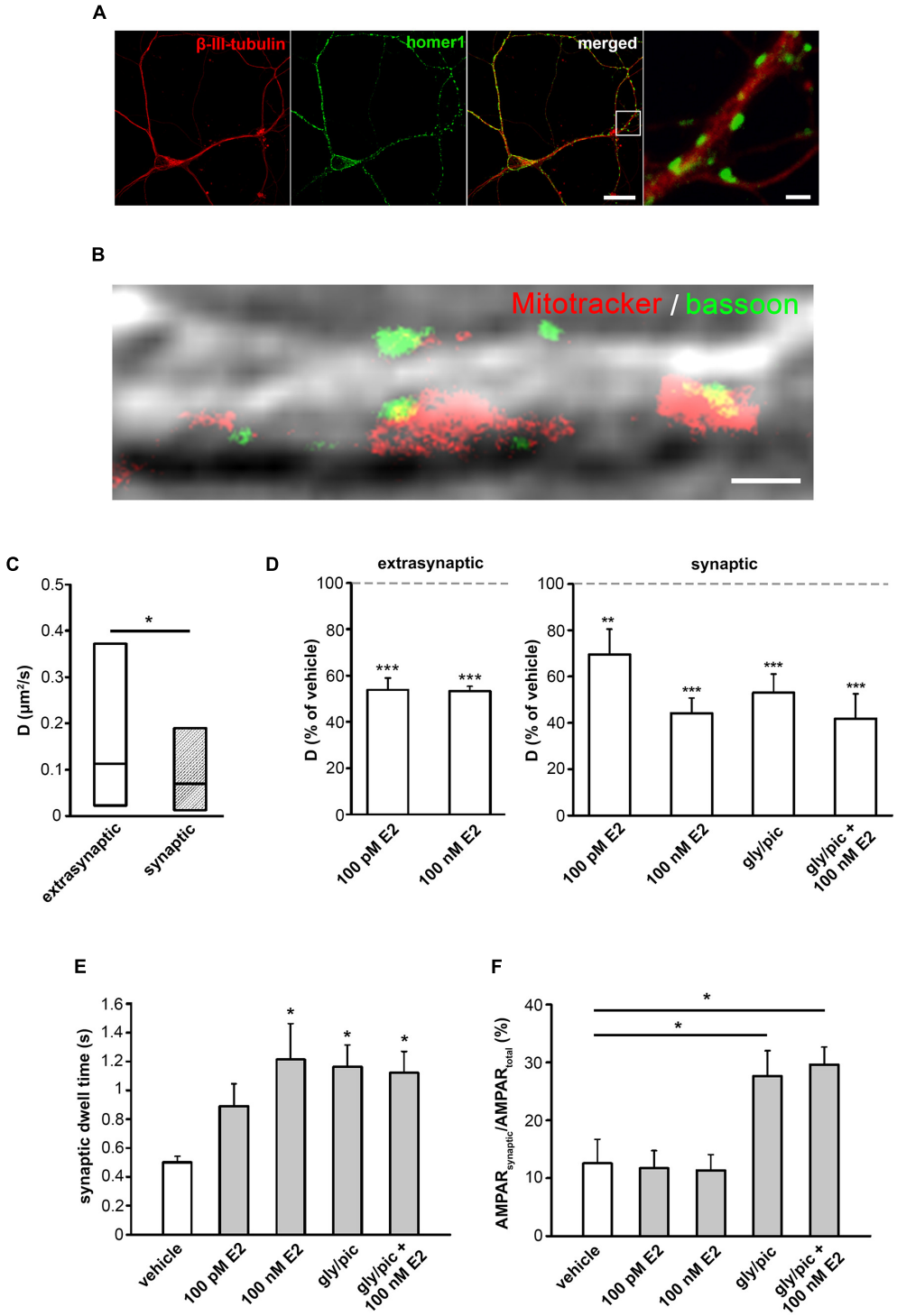

FIGURE 6 | Effect of E2 on the surface movement of GluR2-AMPA on primary hippocampal neurons. **(A)** Photomicrograph shows a primary hippocampal neuron labeled with homer-1 (synapse) and β-III tubulin (neuron). Scale bar = 10 μm, insert Scale bar = 2 μm. **(B)** Dual color STED image of a hippocampal neuron overlayed to differential interference contrast microscopy image depicts live-cell synapse labeling MitoTracker Deep Red (red) and presynaptic protein bassoon (green). Scale bar = 1 μm. **(C)** Distribution of D values of extrasynaptic and synaptic GluR2-AMPAR under control conditions (median ± IQR, n = 754 extrasynaptic trajectories and n = 104 synaptic trajectories). **(D)** Effect of E2 (100 pM and 100 nM) on D of extrasynaptic and synaptic GluR2-AMPA with or without chemical LTP (cLTP) induced by glycine/picrotoxin (gly/pic) (% of vehicle treatment as the mean ± SEM; n = 742–928 extrasynaptic trajectories and n = 104–155 synaptic trajectories). **(E,F)** Effect of vehicle, E2 (100 n, 100 pM) with or without cLTP (gly/pic) on synaptic dwell time (mean ± SEM (s); n = 104–155) **(E)** and relative surface distribution of synaptic GluR2-AMPAR content (synaptic/total GluR2-AMPA molecule trajectories) (mean ± SEM, n = 8–18 recordings) **(F)**. $^{*}p < 0.05$; $^{**}p < 0.01$; $^{***}p < 0.001$.

with presynaptic marker bassoon. Only 10% of the bassoon labeled synapses showed no colocalization with MitoTracker Deep Red labeling (**Figure 6B**).

Our single-molecule imaging experiment revealed the surface movement of ATTO 488-labeled GluR2-AMPAR on neurites in extrasynaptic (**Supplementary Movie 6**) and synaptic (**Supplementary Movie 7**) regions. D values of GluR2-AMPAR molecules were significantly lower in synapse compared to extrasynaptic regions (**Figure 6C**). Fluorescence intensity histograms and step sizes for photobleaching suggest that most of the spots represented single fluorophores and single receptors (**Supplementary Figure 4**). Our *in vivo* labeling failed to show GluR2-AMPAR molecules on soma of hippocampal neurons using highly illuminated laminated optical sheet microscopy (HILO; data not shown).

Both 100 pM and 100 nM of E2 decreased extrasynaptic and synaptic D_{AMPAR} in neurites (**Figure 6D**). Similar to E2, chemical strengthening of synapses [chemical long term potentiation (cLTP)] elicited a decrease in synaptic D_{AMPAR} (**Figure 6D**) (vehicle D_{AMPAR} mean ± SEM ($\mu m^2/s$): synaptic: 0.253 ± 0.038, extrasynaptic: 0.247 ± 0.014). Furthermore, 100 nM, but not 100 pM of E2, increased the synaptic dwell time of GluR2-AMPAR to a similar extent as cLTP (**Figure 6D**). Treatment with 100 nM of E2 did not change the cLTP-induced increase in the synaptic dwell time of GluR2-AMPAR. E2 (100 nM, 100 pM) did not affect synaptic AMPAR content (**Figure 6E**), and it did not alter cLTP-induced increase in synaptic AMPAR content (**Figure 6F**).

DISCUSSION

We found that E2 rapidly decreased the D_{AMPAR} in live dPC12 via rapid membrane-initiated GPER1 signaling in neurites but both GPER1 and ERβ was required for the effect of E2 in soma. Nevertheless, different dose was effective on soma compared to neurites. On soma 100 pM E2 while on neurites 1 nM or 100 nM E2 decreased the D_{AMPAR}. This difference may be the consequence of GPER1 internalization in soma induced by 100 nM E2. We show that D_{AMPAR} is affected by the cortical actin network in dPC12 cells. Furthermore, the effects of E2 on D_{AMPAR} in soma and neurites were mediated by actin via the ROCK-cofilin and JNK-cofilin pathways. Importantly, we confirmed our results on dPC12 showing that E2 also decreases D_{AMPAR} in live hippocampal neurons. Similarly, to cLTP induction, E2 decreases D_{AMPAR} and increases the synaptic dwell time of GluR2-AMPAR.

PC12 cells offer an extensively used model in neurobiology as they exhibit some features of mature dopaminergic neurons and in the presence of NGF they differentiate into sympathetic ganglion neurons (dPC12) morphologically and functionally (Wiatrak et al., 2020). Previous experiments demonstrated that dPC12 cells have action potential (Hu et al., 2018), and express GluR2-AMPA, mGluR1 mRNA and protein (Kane et al., 1998; Mehmood et al., 2013). Our results confirmed that dPC12 has abortive action potential similar to immature neurons with moderate amount sodium current (Belinsky et al., 2011) and expresses GluR2-AMPAR and mGluR1 in soma and neurites, providing an effective platform to examine the surface movement of glutamate receptors. Our single-molecule tracking experiments showed that glutamate receptors exhibit either Brownian or confined motions on dPC12 cells. The functional consequence of a changing the diffusion mode is receptor type dependent. For instance, tyrosine receptor kinase A has been shown to induces signaling during immobile phase (Shibata et al., 2006). However, AMPARs become confined when they are trapped inside the synapse in order to strengthen its efficiency (Ehlers et al., 2007). Although previous findings demonstrated that dPC12 exhibits synapse-like structures (Jeon et al., 2010), it does not form classical synapses. Therefore, we used cultured hippocampal neurons to study synaptic GluR2-AMPAR. Our results demonstrated that these neurons were effectively labeled with pre- and postsynaptic markers, MitoTracker Deep Red and homer-1, respectively. Experiments performed by Ehlers et al. (2007) demonstrated that *in vivo* MitoTracker labeling exhibited around 84% colocalization with the presynaptic marker bassoon. Our immunofluorescence stainings showed that MitoTracker Deep Red entirely colocalized with bassoon, although some synapses were labeled with bassoon alone in our hippocampal culture. In agreement with previous studies (Groc et al., 2008) our results demonstrated that synaptic D_{AMPAR} is lower than extrasynaptic D_{AMPAR} suggesting that GluR2-AMPAR exhibited a more confined motion in the synapses.

Compartment Specific E2 Action on the Surface Movements of GluR2-AMPAR

Besides its classical genomic action, E2 exerts rapid non-classical effects on glutamate receptors. The surface movement of glutamate receptors plays critical roles in functions, such as glutamatergic neurotransmission and synaptic plasticity. It has been described that AMPAR, the most abundant glutamate receptor in excitatory synapses, showed immobile or relatively slow diffusion in the postsynaptic density but exhibited Brownian movement outside the synapse (Borgdorff and Choquet, 2002). It was also reported that E2 decreased the surface movement of GluN2-N-methyl-D-aspartate receptors (NMDA) (Potier et al., 2016). However, the effect of E2 on surface movement of AMPAR is unknown. In this study, we examined whether E2 alters the surface movement of GluR2-AMPAR molecules, the most ample AMPAR subunit in neurons. Here, we show that E2 decreases D_{AMPAR} in a concentration-dependent manner, with distinct effects on soma and neurites in dPC12. However, E2 altered only D_{AMPAR} but not D_{mGluR1}, suggesting that the rapid modulation of glutamatergic receptor surface diffusion by E2 is type-dependent. It is worth noting that the rapidity of E2 action on D_{AMPAR} ($\leq$5 min) indicates a non-classical mechanism.

ERs, namely GPER1, ERα, and ERβ, are of great interest and have been suggested to be involved in non-classical E2 actions. Our PCR results showed the expression of GPER1 and ERβ but not ERα in dPC12. Interestingly, our experiments with ER agonists and antagonists demonstrated a compartment-specific effect on dPC12, as they have different effects on soma and neurites. In soma, the ability of E2 to reduce D_{AMPAR} requires both ERβ and GPER1 since this response was observed after the

co-application of ERβ and GPER1 agonists (DPN and G1) but not after application of DPN or G1 alone. The complementary effect of liganded ERβ and GPER1 on soma is also corroborated by the fact that GPER1 blocker G15 inhibits the effect of E2 on somatic D_{AMPAR}. In contrast, on neurites G1 reduced D_{AMPAR}, DPN was not effective, and G15 antagonized the effect of E2. In summary, both ERβ and GPER1 are required for E2 effect on soma, but on neurite E2 effect occurs through GPER1 only. Studies have revealed that cortical actin network differs in soma and neurite and its dynamics is regulated by ERβ (Zhao et al., 2017). As discussed later, we found in dPC12 that actin structure influenced the membrane movement of receptors differently on soma and neurite. We assume that on soma ERβ and GPER1 regulates receptor dynamics through cortical actin rearrangement, while on neurite GPER1 alone affects receptor movements via an unknown mechanism unrelated to cortical actin network.

The concentration dependence of E2 action differs between soma and neurites in dPC12. While 100 pM of E2 reduced D_{AMPAR} in soma, higher concentrations (1 nM or 100 nM) were required to decrease the D_{AMPAR} in neurites. One possible reason for the compartement-specific E2 action may be the differences in the distribution of GPER1 molecules on the membrane. Indeed, our STORM experiments showed that the GPER1/GluR2-AMPAR ratio was higher in soma than in neurites, indicating that neurites express less GPER1 than soma do. These observations are consistent with our finding showing a significant decrease in D_{AMPAR} in neurites after exposure to high E2 (1 nM and 100 nM).

Interestingly, high doses of E2 (1 nM and 100 nM) did not alter D_{AMPAR} in soma. Previous studies have indicated that GPER1 undergoes desensitization after the administration of the ligand at high concentrations (Brailoiu et al., 2007). Thus, it is likely that a high concentration of E2 induces GPER1 desensitization in the soma. Previous experiments demonstrated that E2 administration could induce translocation of GPER1 from the cell membrane to the cytoplasm (*33, 34*), resulting in the desensitization of the receptor (Filardo and Thomas, 2012). Our STED experiments corroborated these findings because 10 min after administration of 100 nM of E2, GPER1 immunolabeling relocated from the membrane region to the cytoplasm (Funakoshi et al., 2006), indicating a rapid internalization of GPER1 on soma. Rapid internalization indicates the desensitization of GPER1, which may explain why high doses of E2 were ineffective on the soma. The lack of GPER1 internalization on neurites may be the consequence of the low expression level of GPER1. We hypothesize that an even higher concentration of E2 would be sufficient to induce internalization due to the low level of GPER1.

Role of Cortical Actin in the Effect of E2 on the Surface Movement of GluR2-AMPARs

It has been shown earlier that the actin cytoskeleton can interact with the intracellular domains of membrane receptors, thus regulating their movement (Kusumi et al., 2014). Single-particle tracking studies of lipid-anchored molecules demonstrated reduced mobility in the axon initial segment and that the confined motion was due to actin structures (Albrecht et al., 2016). Our present findings confirm these previous observations (Hanley, 2014), as the disruption of cortical actin by latA increased D_{AMPAR} in soma. Interestingly, latA has a compartment-specific effect because it is not effective in neurites. Furthermore, we found that D_{AMPAR} and D_{mGluR1} were higher for neurites than for soma. Super-resolution imaging studies revealed that soma and neurites have different cortical actin structures (Lukinavičius et al., 2014; Han et al., 2017). Actin has a polygonal lattice structure in soma (Han et al., 2017), and its associated proteins such as adducin and spectrin form 190-nm-spaced ring-like structures around the circumference of neurites (Xu et al., 2013; Han et al., 2017). We hypothesize that the higher D values measured on neurites arise from the difference between the structural arrangement of actin in soma and neurites. This may also provide an effective basis for the compartment-specific effect of latA and surface dynamics of GluR2-AMPARs.

Recent evidence implicates that cortical actin is important in receptor crosstalk through modulation of protein dynamics (Mattila et al., 2016). Cofilin is a highly abundant constitutively active actin-binding protein that alters the properties of F-actin and is regulated by the ROCK-cofilin and JNK-cofilin pathways (Hu et al., 2018; Kim et al., 2019). Phosphorylation inactivates cofilin and facilitates actin filament assembly. E2 increases the activity of cofilin (Kramár et al., 2009a; Brandt and Rune, 2019) and stabilizes the F-actin cytoskeleton via GPER1 (Wang et al., 2019). Cofilin has been reported to mediate cortical actin dynamics that regulate AMPAR trafficking in synaptic plasticity (Gu et al., 2010). Therefore, we investigated the role of actin in the effect of E2 on D_{AMPAR}. Our results demonstrated that latA diminished the effect of E2, indicating that cortical actin plays a pivotal role in E2 action on D_{AMPAR}. Our results also demonstrated that the E2-induced decrease in D_{AMPAR} is completely blocked by the inhibition of the ROCK-cofilin or JNK-cofilin pathways in soma and neurites. We suggest that E2 binding to GPER1 activates both the ROCK-cofilin and JNK-cofilin pathways, which then change the cortical actin dynamics and decrease the surface movement of GluR2-AMPAR.

Effect of E2 on D_{AMPAR} in the Hippocampal Neurons

The pressing question related to the rapid E2 effect on AMPARs is that of explaining the physiological relevance of the observed changes.

To confirm the effect of E2 on D_{AMPAR} in another *in vitro* neuron system and examine the effect of E2 on synaptic GluR2-AMPAR, we performed single-molecule tracking experiments on a primary hippocampal neuron culture. Cultured hippocampal neurons expressing ERα, ERβ, and GPER1 (Wehrenberg et al., 2001; Prange-Kiel et al., 2003; Zhao et al., 2016) provide physiologically relevant *in vitro* model for studying E2 effect. Our results showed that E2 administration (100 pM and 100 nM) rapidly decreased the synaptic and extrasynaptic D_{AMPAR} in hippocampal neurons similar to dPC12.

Long term potentiation of excitatory synaptic transmission is a well-known form of synaptic plasticity and is considered

a cellular model for learning and memory. Although several studies have demonstrated that E2 plays an essential role in LTP and alters memory formation (Spencer et al., 2008; Fester and Rune, 2015), the precise molecular mechanism is not clear. AMPAR plays a pivotal role in synaptic alterations involved in synaptic transmission, synaptic plasticity, LTP, learning, and memory. Using single-molecule tracking experiments and AMPAR immobilization techniques, Penn et al. (2017) have shown that the surface movement of AMPARs is a key factor in the modulation of synaptic potentiation and learning (Phan et al., 2015). At the molecular level, the recruitment and slow diffusion of glutamate receptors at the postsynaptic site have been shown after LTP (Kovács et al., 2018). Indeed, our single-molecule tracking of hippocampal neurons demonstrated that cLTP decreased D_{AMPAR} in synapses and increased the synaptic dwell time and content of GluR2-AMPARs. Similar to cLTP, 100 nM of E2 decreased D_{AMPAR} and increased the dwell time of GluR2-AMPA in the synapse. Although recent morphological studies have demonstrated that E2 increased the expression of GluR2 in mushroom spines at 120 min *in vivo* (Avila et al., 2017) our results show that E2 did not affect the GluR2-AMPAR content in the synapses within 20 min. We suggest that E2 can rapidly enhance the synaptic efficacy of glutamatergic synapses by decreasing D_{AMPAR}. Interestingly, E2 did not change the effect of cLTP on D_{AMPAR}, dwell time, and synaptic content of GluR2-AMPAR. However, E2 can likely increase the efficacy of cLTP by retaining the AMPARs in the synapses.

CONCLUSION

Our study demonstrates that E2 rapidly and dose-dependently decreases the surface movement of GluR2-AMPARs via compartment-specific ER-mediated mechanisms in live neurons. Our results also suggest that cortical actin mediates liganded GPER1 action on the surface movement of GluR2-AMPARs via the ROCK-cofilin and JNK-cofilin pathways. This study provides the first evidence that E2 decreases the surface movement and increases the dwell time of GluR2-AMPARs in the synapses. These results provide a strong foundation for understanding the molecular mechanism by which E2 affects neuronal plasticity and glutamatergic neurotransmission. Finally, these observations will likely be of physiological importance for cognitive functions and of particular relevance to E2 action on memory formation.

MATERIALS AND METHODS

Cell Culture and Neuronal Differentiation

For single-molecule tracking of glutamate receptors, rat pheochromocytoma cells (PC12, Sigma-Aldrich) were differentiated into dPC12. PC12 cells were plated at a density of 2 x 10^3 cells/cm^2 on collagen IV-coated 35-mm glass-bottom dishes (MatTek Corporation, Ashland, MA, United States) in phenol red-free RPMI 1640 medium supplemented with 10% horse serum (HS), 5% fetal bovine serum (FBS), and 2 mM L-glutamine (culture RPMI, cRPMI). Twelve hours after plating, the medium was replaced with phenol red-free RPMI 1640 medium supplemented with 1% HS, 2 mM L-glutamine, and 50 ng/mL nerve growth factor (NGF-2.5S, Sigma-Aldrich, St. Louis, MO, United States). The cells were fed with dRPMI after 2 days and used for imaging after 4 days of differentiation.

For antibody specificity testing chinese hamster ovary cells (CHO) were cultured in phenol-red free F12 medium supplemented with 10% fetal bovine serum (FBS), and 2 mM L-glutamine (culture F12, cF12). A day before transfection 2 x 10^5 CHO cells were plated onto untreated coverslip.

Cultures of the hippocampal neurons were prepared from C57BL/6 mouse embryos (E17-18) to examine the surface movement of extrasynaptic and synaptic GluR2-AMPAR molecules. The brains were aseptically removed from the skull, meninges were pulled off, and both hippocampi were separated from the cortex. Dissected hippocampi were incubated in pre-warmed MEM (Thermo Fisher Scientific) containing 0.05% trypsin (Gibco) and 0.05% DNaseI (Gibco) at 37°C for 15 min. Two milliliters of FBS was added to stop the digestion, and the mixture was centrifuged for 5 min at 1200 rpm. Cells were triturated in Neurobasal (NB, Thermo Fisher Scientific) supplemented with B27 (Thermo Fisher Scientific), 5% FBS, 1% penicillin-streptomycin (Thermo Fisher Scientific). Then, 100.000 cells were plated on glass bottoms coated with poly-D-lysine (PDL)- and laminin-coated 35-mm glass-bottom dishes (Kovács et al., 2018). Neurons were cultured in an incubator at 95% relative humidity and 5% CO_2. After 3 days of seeding, one-third of the medium was replaced with pre-warmed MEM every third-day until day *in vitro* 19–21.

Validation of the Neuronal Differentiation of PC12 and Synapses on Hippocampal Neurons

To validate the neuronal differentiation of PC12 cells, immunofluorescent staining was performed with microtubule-associated protein 2 (MAP2) and β-III tubulin antibodies. Cells were fixed in 4% paraformaldehyde (PFA) for 15 min and permeabilized with 0.03% Triton X-100 for 30 min after 4 days of differentiation. The cells were then incubated overnight at 4°C with either mouse anti-MAP2 antibody (1:1000, MAB3418, Millipore) or mouse neuron-specific anti-β-III tubulin antibody (1:1000, MAB1195, RD Systems), before being incubated with biotinylated donkey anti-mouse $F(ab')_2$ (1:200, Jackson ImmunoResearch) and Alexa Fluor 647-conjugated streptavidin (1:2000, Thermo Fisher Scientific).

The electrophysiological properties of dPC12 were tested using whole-cell patch-clamp recording. Patch pipettes (1.5 mm outer diameter and 1.1 inner diameter) with a resistance of 6 MΩ were pulled from borosilicate glass capillaries with a micropipette puller (Sutter Instruments). The pipette recording solution contained (in mM) 10 KCl, 130 K-gluconate, 1.8 NaCl, 0.2 EGTA, 10 HEPES, and 2 Na-ATP, 0.2% biocytin and the pH was adjusted to 7.3 with KOH. All recordings were performed at 32°C in a chamber perfused with oxygenated artificial cerebrospinal fluid (ACSF) containing (in mM) 2.5 KCl, 10 glucose, 126 NaCl,

1.25 NaH_2PO_4, 2 $MgCl_2$, 2 $CaCl_2$, and 26 $NaHCO_3$. Whole-cell recordings were made with an Axopatch 700B amplifier (Molecular Devices) using an upright microscope (Nikon Eclipse FN1) equipped with infrared differential interference contrast optics. Cells with access resistance below 20 MΩ were used for analysis. Signals were low-pass filtered at 5 kHz and digitized at 20 kHz (Digidata 1550B, Molecular Devices). Acquisition and subsequent analysis of the data were performed using Clampex9 and Clampfit software (Axon Instruments). After measurement cells were fixed with 4% PFA for 15 min and permeabilized with 0.03% Triton X-100 for 30 min and Alexa Fluor 488 conjugated Streptavidin (1:2000) was applied for 2 h at room temperature.

Dual-label immunofluorescence was performed to detect mature synapses in hippocampal neurons (**Figure 6A**). Cells were treated as described above except that they were incubated overnight at 4°C with anti-homer1 (1:1000, 160006, Synaptic Systems) and anti-β-III tubulin (1:1000, MAB1195, RD Systems) antibodies followed by Alexa Fluor 488-conjugated anti-chicken antibody and Alexa Fluor 647-conjugated anti-mouse antibody, respectively.

All immunofluorescence images were taken on CLSM (Zeiss LSM710, 100X). A helium-neon laser with 488 and 633 nm wavelength was used to excite Alexa Fluor 488 and Alexa Fluor 647, respectively. Images were captured at 2048x2048 pixel resolution with a 2 μm optical thickness.

We applied MitoTracker Deep Red, carbocyanine-based MitoTracker dye, for synaptic labeling of live neurons. Previous experiments showed that MitoTracker effectively labels mitocondria live presynaptic terminals (Ehlers et al., 2007). To validate Mitotracker Deep Red as a synapse labeling in our experiments, hippocampal neurons were incubated with MitoTracker Deep Red (1 nM, Thermo Fisher Scientific) at 37°C for 10 min. After washing neurons were fixed as described above and incubated overnight at 4°C with anti-bassoon antibody (1:1000, ab82958, Abcam) followed by abberior STAR ORANGE conjugated anti-mouse secondary antibody (1:500, STORANGE, Abberior). 2 dimensional stimulated emission depletion (STED) images were taken on Abberior Expert Line STED system equipped with Plan Apo 100X/1.45 objective (Nikon). STAR ORANGE and MitoTracker were excited at 561 nm and 640 nm, respectively. The wavelength of the depletion laser was 775 nm. Super-resolution images were captured with 20 nm pixel size, 20 ms dwell time, and the pinhole was set to 1 A.U.

Detection of Estrogen Receptors

Expression levels of estrogen receptor α (ERα), estrogen receptor β (ERβ), and the membrane estrogen receptor, GPER1, were examined in the dPC12. Total ribonucleic acid (RNA) was extracted from dPC12 with a conventional TRIzol (Thermo Fisher Scientific)-based protocol, and complementary deoxyribonucleic acid (cDNA) was constructed using a High-Capacity RNA-to-cDNA Kit (Thermo Fisher Scientific). The following polymerase chain reaction (PCR) primers were used: ERα, 5′-CGTAGCCAGCAACATGTCAA-3′, and 5′-AATGGGCACTTCAGGAGACA-3′; ERβ, 5′-GAGGTGC TAATGGTGGGACT-3′ and 5′-CTGAGCAGATGTTCCAT GCC-3′; and GPER1, 5′-TGCACCTTCATGTCCCTCTT-3′ and 5′-AAGGACCACTGCGAAGATCA-3′.

Glutamate Receptor Labeling in Live dPC12 and Primary Hippocampal Neurons

To detect GluR2-AMPAR and mGluR1 molecules in the plasma membranes of dPC12, live-cell immunofluorescent labeling was performed. Before single-molecule imaging, dPC12 were incubated in dRPMI with ATTO 488-labeled antibodies directed against the extracellular N-terminal domain of either rat GluR2 (1:100, Alomone Labs) or rat mGluR1 (1:100, Alomone Labs) at 37°C for 6 min. Specificity of ATTO 488-labeled GluR2-AMPAR antibody has been reported previously in brain sections of GluR2 knockout mice (Egbenya et al., 2018). The specificity of the antibodies was also tested with control peptides ($GluA2_{179-193}$ peptide and $mGluR1_{501-516}$ peptide, Alomone Labs), and no immunoreactivity was observed (**Supplementary Figure 5**). In order to further test the specificity of anti-GluR2 antibody CHO cells were transfected with plasmid encoding GluR2 subunit using Lipofectamine 3000 (Sigma) according to the manufacturer's protocol. Rat GluR2 cDNA sequence was subcloned into a pCl mammalian expression vector under XhoI-NotI place. The GluR2 cDNA sequence was a gift from Jeremy Henley (Addgene plasmid #64941). The construct was verified with Sanger sequencing. 24 h after transfection cells were labeled and imaged the same manner as detailed above. **Supplementary Movie 8** shows the movements of ATTO 488-labeled GluR2 subunits in the membrane of a transfected CHO cell. The omission of GluR2 subunit transfection resulted in complete absence of ATTO 488 labeling (**Supplementary Movie 8**).

To simultaneously label live synapses and GluR2-AMPAR, cultured hippocampal neurons were incubated in MEM containing MitoTracker Deep Red (1 nM, Thermo Fisher Scientific) and ATTO 488-labeled antibodies directed against the extracellular N-terminal domain of rat GluR2 (1:100, Alomone Labs) at 37°C for 10 min. Neurons were imaged after they were carefully washed 3 times with pre-warmed MEM.

Drug Application and Cell Viability Detection

The following drugs were applied immediately before imaging the dPC12 in dRPMI: 17β-estradiol (E2, Sigma-Aldrich, 100 pM in 10^{-5}% EtOH, 1 nM and 100 nM in 10^{-3}% EtOH); G1, a selective GPER1 agonist [Tocris, 100 nM in 10^{-5}% dimethyl sulfoxide (DMSO)] (Sárvári et al., 2009); and diarylpropionitrile (DPN), a selective ERβ agonist (Tocris, 10 pM in 2 x 10^{-5}% DMSO) (Bálint et al., 2016). To block GPER1, dPC12 were incubated in dRPMI containing G15, a selective GPER1 antagonist (Tocris, 1 μM in 2x10^{-3} % DMSO) (Sárvári et al., 2009), for 10 min before E2 application and imaging. To inhibit actin polymerization, we applied latrunculin A (latA, Sigma-Aldrich, 1 μM in 0.1% DMSO) for 5 min before E2 addition and imaging. We also inhibited the actin polymerization regulator cofilin (Bamburg and Bernstein, 2010), via application of a selective Rho-associated protein kinase (ROCK) inhibitor, GSK429286 (Tocris, 1 μM

in 0.1% DMSO) for 1 h (Liu et al., 2018) or selective c-Jun N-terminal kinase (JNK) inhibitor, SP600125 (Tocris, 1 μM in 0.1% DMSO) for 1 h (Kim et al., 2019).

After latA treatment, that is, at the end of the experiments, the viability of the dPC12 was tested with a LIVE/DEAD viability/cytotoxicity kit (Thermo Fisher Scientific) according to the manufacturer's instructions. The results demonstrated that the cells retained their plasma membrane integrity until the end of the experiments.

The hippocampal neurons were treated with E2 in the same manner as detailed above, with the exception that chemical long term potentiation (cLTP) was induced by incubating the neurons in MEM containing glycine (200 μM) and picrotoxin (1 μM) for 3 min (Groc et al., 2008) at room temperature. After washing 3 times, the cells were placed back at 37°C for 20 min.

Single-Molecule Imaging of Glutamate Receptors Using Total Internal Reflection Fluorescence and Highly Illuminated Laminated Optical Sheet Microscopy

Single-molecule imaging of labeled glutamate receptors was carried out on an Olympus IX81 fiber TIRF microscope equipped with Z-drift compensation (ZDC2) stage control, a plan apochromat objective (100X, NA 1.49, Olympus), and a humidified chamber heated to 37°C and containing 5% CO_2.

The dish containing dPC12 was mounted in the humidified chamber of the TIRF microscope immediately after *in vivo* labeling. A 491 nm diode laser (Olympus) was used to excite ATTO 488, and emission was detected above the 510 nm emission wavelength range. The angle of the excitation laser beam was set to reach a 100 nm penetration depth of the evanescent wave.

Hippocampal neurons were imaged using an Olympus IX81 fiber TIRF microscope with HILO illumination (Tokunaga et al., 2008). The ATTO 488 dye was excited with the same laser as described above, and emission was detected with a 518QM32 filter. MitoTracker was excited with a 633 diode laser (Olympus), and emission was detected with a 655WB20 filter. A Hamamatsu 9100-13 electron-multiplying charge-coupled device (EMCCD) camera and Olympus Excellence Pro imaging software were used for image acquisition by TIRF and HILO microscopy.

Experiments were performed for 20 min. During the measurement period of ATTO 488-GluR2-AMPAR and ATTO 488-mGluR1, 20–30 images were recorded with 10-s sampling intervals and 33-ms acquisition times. Single-molecule tracking of ATTO 488-GluR2-AMPAR and ATTO 488-mGluR1 was performed with custom-made software written in C++ (WinATR (Kusumi Lab, Membrane Cooperativity Unit, OIST). The center of each particle was localized by two-dimensional Gaussian fitting, and the trajectory for each signal was created by a minimum step size linking algorithm that connected the localized dots in subsequent images. The trajectories were individually checked, and artifacts or tracks shorter than 15 frames were excluded from further analysis. A minimum of 400 trajectories was collected in each experiment from both the soma and neurites. To examine the effect of E2 or vehicle (EtOH), 100–150 trajectories were collected in every consecutive 5-min interval for up to 20 min (0–5, 5–10, 10–15, and 1–20 min). To identify the live synapses in hippocampal neurons, the MitoTracker Deep Red signal was detected as time-lapse stacks for 10 s. Time-lapse stacks were defined as Z-stacks, and an average intensity Z-projection was applied to increase the image quality and optimize the signal-to-noise ratio of the MitoTracker Deep Red signal.

Calculation of the Surface Movement Parameters of the Glutamate Receptors

The mean square displacement curve for each trajectory was calculated by the following equation:

$$MSD\,(m\Delta T) = \frac{1}{N-m}\sum_{i=1}^{N-m}\left((x_{i+m}-x_i)^2+\left(y_{i+m}-y_i\right)^2\right)$$

where, x_i and y_i are the coordinates of the signal's center, ΔT *is* the time interval between two consecutive frames, N *is* the total number of frames, and m represents the time delay.

The maximum likelihood estimation (Berglund, 2010) was applied to obtain the corresponding diffusion coefficient (D) value for each trajectory. Δx_k and Δy_k represent the observed displacements ($\Delta x_k = x_{k+1} - x_k$ and $\Delta y_k = y_{k+1} - y_k$) arranged in N-component column vectors, where the total number of frames is equal to $N+1$, and x_n and y_n are the coordinates of the signal center on the nth frame. Σ is the $N \times N$ covariance matrix defined by the following equation:

$$\sum_{ij} = \begin{cases} 2D\Delta t - 2(2DR\Delta t - \sigma^2), & if\ i = j \\ 2DR\Delta t - \sigma^2, & if\ i = j \pm 1 \\ 0, & \text{otherwise} \end{cases}$$

where, D is the diffusion coefficient, Δt is the frame integration time, σ is the static localization noise, and R summarizes the motion blur effect. In our case, R = 1/6 as a consequence of continuous illumination.

The likelihood was defined by the following function:

$$L\left(\Delta x, \Delta y\right) = -log\,|\Sigma| - \frac{1}{2}\left(\Delta x\right)^T \Sigma^{-1}\left(\Delta x\right) - \frac{1}{2}\left(\Delta y\right)^T \Sigma^{-1}\left(\Delta y\right)$$

D and σ, which provide the maximal likelihood, are the estimated diffusion coefficient and static localization noise, respectively. The calculation of the determinant and the inverse of the covariance matrix at each step of the optimization method can be a severe computational difficulty at high values of N. An approximation (Gray, 2006) based on the theory of circulant matrices is applicable (Berglund, 2010). The global optimization of the likelihood function based on this approximation was implemented in MATLAB. The goodness of optimization was judged by evaluating the static localization noise. An optimization was considered to be inaccurate, and the corresponding trajectory was excluded from further analysis when the estimated static localization noise was out of ±90% range of the group's mean.

To examine the synaptic movements of GluR2-AMPAR, the maximum intensity Z-projected MitoTracker labeled synaptic area was determined manually. GluR2-AMPAR molecules were identified as synaptic if the trajectory was colocalized at least on one frame with the MitoTracker signal, and extrasynaptic if there was no co-localization (Groc et al., 2006, 2007). D values were calculated as described above for both synaptic and extrasynaptic GluR2-AMPAR (Groc et al., 2008). The synaptic dwell time for each treatment was determined as the mean time spent by synaptic receptors within the synaptic (MitoTracker labeled) area. The relative surface distribution of synaptic GluR2-AMPAR content (synaptic/total GluR2-AMPAR molecule trajectories) was calculated for each recording after vehicle or E2 treatment.

Co-Localization Analysis of GluR2-AMPAR and GPER1 Using Stochastic Optical Reconstruction Microscopy

Super-resolution 3D STORM imaging was performed to examine the number of receptors and the probability of interaction between GluR2-AMPAR and GPER1 in dPC12. PC12 cells were plated onto poly-D-lysine (PDL)- and laminin-coated coverslips (Kovács et al., 2018), and differentiated into neurons as described above. The neurons were incubated in dRPMI medium containing either vehicle (EtOH) or E2 (100 pM or 100 nM) at 37°C for 10 min. Immediately after treatment, GluR2-AMPAR was applied to live PC12 cells with mouse anti-GluR2-AMPAR antibody (1:1000, MAB397, raised in mouse, Millipore) at 37°C for 20 min, followed by fixation in 4% paraformaldehyde (PFA). After a thorough wash, the cells were incubated with anti-GPER1 primary antibody (1:5000, AF5534, Novus Biological) at 4°C for 48 h. CF-568-labeled donkey anti-goat antibody (1:400, Biotium) was applied at room temperature for 2 h. Following three consecutive washes, Alexa Fluor 647-labeled anti-mouse antibody was applied at room temperature for 2 h (1:200, Jackson ImmunoResearch). The coverslips were washed, covered with imaging medium prepared from the following reagents in Dulbecco' PBS: 5% glucose, 0.1 M mercaptoethylamine, 1 mg/mL glucose oxidase and μl/mL 2.5 catalase (1500 U/mL) (Dudok et al., 2015), and transferred onto standard glass slides immediately before imaging. Using a CFI Apochromat TIRF 100X objective, corresponding confocal and super-resolution images were collected with a Nikon N-STORM/C2+ super-resolution system based on the platform of a Nikon Ti-E inverted microscope equipped with Nikon Perfect Focus System and a Nikon C2 confocal scan head. 3D STORM images were captured with an Andor iXon Ultra 897 EMCCD camera (pixel size: 160 nm/pixel) using an astigmatic imaging method which enables us to localize molecules within an axial distance of −300 to 300 nm from the center plane. STORM images were acquired by illuminating the samples with high-power lasers (561 and 647 nm). Image acquisition and processing were performed using the Nikon NIS-Elements AR software with the N-STORM module. The obtained 3D STORM localization points were filtered for the collected photon number, z-position (within an axial distance of −300 to 300 nm from the center plane), and local density using the VividSTORM software (Barna et al., 2016). Localization points were selected according to the regions of interest (ROIs) that were manually defined based on the correlated high-resolution confocal images. The clusters of selected localization points were determined using the density-based spatial clustering of applications with noise (DBSCAN) algorithm. A cluster was defined if 3 or more localization points were detected within a 100 nm radius. The center of mass representing a single molecule was calculated for each cluster. In order to examine the number of GPER1 molecules relative to GluR2-AMPAR molecules, the ratio between the number of GPER1 and GluR2-AMPAR molecules (GPER1/GluR2-AMPAR) was calculated for both the soma and neurites.

Analysis of the Subcellular Distribution of GPER1 in dPC12 Using 2D-STED Microscopy

To examine whether GPER1 is internalized after E2 administration, super-resolution 2D-STED microscopy was used. After 10 min of treatment with vehicle (10^{-3}% EtOH) or 100 nM, E2 dPC12 was fixed with 4% PFA. Then, GPER1 immunocytochemistry was performed in the same manner as detailed in the section on STORM, with the exception that Alexa Fluor 647 conjugated anti-goat secondary antibody was used (1:2000) to visualize GPER1. To determine the boundary between the membrane and cytoplasm, dPC12 were treated with a vehicle or 100 nM E2 and cell surface biotin labeling was performed prior to GPER1 immunocytochemistry. Cells were washed with PBS containing 1 mM Ca^{+} and 1 mM Mg^{+} and incubated with biotin (0.5 mg/mL in PBS, EZ-Link Sulfo-NHS-LC-Biotin, Thermo Fisher Scientific) for 10 min at room temperature followed by wash and fixation with 4% PFA for 20 min. After washing, cells were incubated with Alexa Fluor 594 conjugated streptavidin (1:2000, Thermo Fisher Scientific) for 20 min at room temperature. STED images were taken as described above. Based on the result of STED microscopy, 1 μm thick membrane area was defined from the outer edge of GPER1 signal (**Figures 4C2,D**). For image analysis of GPER1 internalization we used cells labeled with GPER1 antibody alone. The captured images were analyzed using Fiji (Schindelin et al., 2012). After background subtraction, the mean intensity value was calculated with the plot profile algorithm within a specified rectangle (ROI size: 12 μm^2) (**Figures 4C2,E**). From each cell (n = 15 total) one ROI (with 2 μm^2 membrane and 10 μm^2 cytoplasmic area) was selected, integrated density was calculated and normalized to the area (μm^2) (**Figure 4F**).

Imaging of the Cortical Actin Morphology

To validate the effect of latA, GSK429286 and SP600125 on dPC12, the morphology of the cortical actin network of dPC12, were examined after drug administration. After 10 min of treatment with 1 μM of latA, or after 60 min of treatment with 1 μM of GSK429286, 1 μM of SP600125, or vehicle (in 10^{-3}% DMSO), dPC12 were fixed in 4% PFA, permeabilized with 0.1% Triton X-100 for 30 min, and incubated with Alexa Fluor 488 phalloidin (1:200, Thermo Fisher Scientific) for 45 min at room

temperature. Imaging was performed on CLSM (Zeiss LSM710, 100X), and Alexa Fluor 488 was excited with an argon laser at a wavelength of 488 nm. Images with 2 μm optical thickness and 4096x4096 (X/Y) resolution were captured with the use of ZEN software applying the same settings (laser power, digital gain) to all images. 6 cells were selected from each treatment group (vehicle, latA, GSK, SP6001235). Three ROIs (ROI size: 4.3 μm^2) were selected from each cell and the average integrated density was calculated from raw images using FIJI software. Results are expressed in the percentage of ROI in order to obtain the integrated density values per μm^2 (in arbitrary units).

Statistics

To compare the surface movements of GluR2-AMPAR and mGluR1 in soma and neurites, D values were expressed as cumulative probability functions. In the rest of the experiments, the D values were expressed as the mean percentage of control (vehicle) + SEM in figures. GPER1/AMPAR ratios and extrasynaptic/synaptic D_{AMPAR} values were expressed as the median±25–75% (interquartile range). To compare the distributions of D values of vehicle control and treatment and extrasynaptic/synaptic D_{AMPAR} values the Kolmogorov-Smirnov test was used. The integrated GPER1/AMPAR ratios of the soma and neurites and densities of Alexa Fluor 488-phalloidin and Alexa Fluor 647-GPER1 immunolabeling were compared with the Mann-Whitney U test. Synaptic dwell time and exchange frequency of GluR2-AMPAR were compared using the Kruskal-Wallis test followed by Dunn's post hoc test. Statistical differences were considered significant at a p-value of < 0.05. All statistical analyses were performed with Statistica version 13.3 for Windows (TIBCO Software Inc., CA, United States).

DATA AVAILABILITY STATEMENT

The original contributions presented in the study are included in the article/**Supplementary Material**, further inquiries can be directed to the corresponding author.

ETHICS STATEMENT

The animal study was reviewed and approved by Animal Welfare Committee of University of Pécs, Hungary.

AUTHOR CONTRIBUTIONS

SG, KB, TK, DE, GK, BO, GM, TJ, MK, CV, and FL performed experiments. SG, KB, TK, DE, GK, BO, GM, TJ, MK, CV, FL, TF, AK, and IÁ developed the methodology. SG, TJ, GM, TF, and AK analyzed the data. IÁ and SG designed the experiments. SG, KB, and IÁ wrote the manuscript. IÁ obtained funding. All authors contributed to the article and approved the submitted version.

FUNDING

This work was supported by the Hungarian Brain Research Program (KTIA_NAP_13-2014-0001,20017-1.2.1-NKP-2017-00002), Hungarian Scientific Research Fund (OTKA; 112807), and European Union, and was co-financed by the European Social Fund under the following grants: EFOP-3.6.1.-16-2016-00004 (Comprehensive Development for Implementing Smart Specialization Strategies at the University of Pécs), EFOP 3.6.2-16-2017-00008 (The Role of Neuroinflammation in Neurodegeneration: From Molecules to Clinics), the Higher Education Institutional Excellence Program of the Ministry for Innovation and Technology in Hungary, within the framework of the (5th thematic program) of the University of Pécs, GINOP-2.3.2-15-2016-00048 (Stay Alive), GINOP-2.3.3-15-2016-00030 (Nano-Bioimaging), and ÚNKP-18-3-III (New National Excellence Program of the Ministry of Human Capacities).

ACKNOWLEDGMENTS

We thank Allan Herbison for valuable comments on this manuscript and Imre Farkas for the generous gift of DPN. The research was performed in collaboration with the Nano-Bio-Imaging core facility at the Szentágothai Research Centre of the University of Pécs. We also wish to thank to the Nikon Microscopy Center at the Institute of Experimental Medicine (IEM), Nikon Austria GmbH as well as Auro-Science Consulting Ltd for kindly providing microscopy support.

SUPPLEMENTARY MATERIAL

The Supplementary Material for this article can be found online at: https://www.frontiersin.org/articles/10.3389/fcell.2021.708715/full#supplementary-material

REFERENCES

Albrecht, D., Winterflood, C. M., Sadeghi, M., Tschager, T., Noé, F., and Ewers, H. (2016). Nanoscopic compartmentalization of membrane protein motion at the axon initial segment. *J. Cell Biol.* 215, 1–10. doi: 10.1083/jcb.201603108

Ashby, M. C., De La Rue, S. A., Ralph, G. S., Uney, J., Collingridge, G. L., and Henley, J. M. (2004). Removal of AMPA receptors (AMPARs) from synapses is preceded by transient endocytosis of extrasynaptic AMPARs. *J. Neurosci.* 24, 5172–5176. doi: 10.1523/JNEUROSCI.1042-04.2004

Avila, J. A., Alliger, A. A., Carvajal, B., Zanca, R. M., Serrano, P. A., and Luine, V. N. (2017). Estradiol rapidly increases GluA2-mushroom spines and decreases GluA2-filopodia spines in hippocampus CA1. *Hippocampus* 27, 1224–1229. doi: 10.1002/hipo.22768

Babayan, A. H., and Kramár, E. A. (2013). Rapid effects of oestrogen on synaptic plasticity: interactions with actin and its signalling proteins. *J. Neuroendocrinol.* 25, 1163–1172. doi: 10.1111/jne.12108

Bálint, F., Liposits, Z., and Farkas, I. (2016). Estrogen receptor beta and 2-arachidonoylglycerol mediate the suppressive effects of estradiol on frequency of postsynaptic currents in gonadotropin-releasing hormone neurons of

metestrous mice: an acute slice electrophysiological study. *Front. Cell Neurosci.* 10:77. doi: 10.3389/fncel.2016.00077

Bamburg, J. R., and Bernstein, B. W. (2010). Roles of ADF/cofilin in actin polymerization and beyond. *F1000 Biol. Rep.* 2:62. doi: 10.3410/B2-62

Barna, L., Dudok, B., Miczán, V., Horváth, A., László, Z. I., and Katona, I. (2016). Correlated confocal and super-resolution imaging by VividSTORM. *Nat. Protoc.* 11, 163–183. doi: 10.1038/nprot.2016.002

Belinsky, G. S., Moore, A. R., Short, S. M., Rich, M. T., and Antic, S. D. (2011). Physiological properties of neurons derived from human embryonic stem cells using a dibutyryl cyclic AMP-based protocol. *Stem Cells Dev.* 20, 1733–1746. doi: 10.1089/scd.2010.0501

Berglund, A. J. (2010). Statistics of camera-based single-particle tracking. *Phys. Rev. E Stat. Nonlin. Soft Matter Phys.* 82, 1–8. doi: 10.1103/PhysRevE.82.011917

Borgdorff, A. J., and Choquet, D. (2002). Regulation of AMPA receptor lateral movements. *Nature* 417:649.

Brailoiu, E., Dun, S. L., Brailoiu, G. C., Mizuo, K., Sklar, L. A., Oprea, T. I., et al. (2007). Distribution and characterization of estrogen receptor G protein-coupled receptor 30 in the rat central nervous system. *J. Endocrinol.* 193, 311–321. doi: 10.1677/JOE-07-0017

Brandt, N., and Rune, G. M. (2019). Sex-dependency of oestrogen-induced structural synaptic plasticity: inhibition of aromatase versus application of estradiol in rodents. *Eur. J. Neurosci.* 52, 2548–2559. doi: 10.1111/ejn.14541

Choquet, D. (2018). Linking nanoscale dynamics of AMPA receptor organization to plasticity of excitatory synapses and learning. *J. Neurosci.* 38, 9318–9329. doi: 10.1523/JNEUROSCI.2119-18.2018

Dudok, B., Barna, L., Ledri, M., Szabó, S. I., Szabadits, E., Pintér, B., et al. (2015). Cell-specific STORM super-resolution imaging reveals nanoscale organization of cannabinoid signaling. *Nat. Neurosci.* 18, 75–86. doi: 10.1038/nn.3892

Egbenya, D. L., Hussain, S., Lai, Y. C., Xia, J., Anderson, A. E., and Davanger, S. (2018). Changes in synaptic AMPA receptor concentration and composition in chronic temporal lobe epilepsy. *Mol. Cell. Neurosci.* 92, 93–103. doi: 10.1016/j.mcn.2018.07.004

Ehlers, M. D., Heine, M., Groc, L., Lee, M. C., and Choquet, D. (2007). Diffusional trapping of GluR1 AMPA receptors by input-specific synaptic activity. *Neuron* 54, 447–460. doi: 10.1016/j.neuron.2007.04.010

Fester, L., and Rune, G. M. (2015). Sexual neurosteroids and synaptic plasticity in the hippocampus. *Brain Res.* 1621, 162–169. doi: 10.1016/j.brainres.2014.10.033

Filardo, E. J., and Thomas, P. (2012). Minireview: G protein-coupled estrogen receptor-1, GPER-1: its mechanism of action and role in female reproductive cancer, renal and vascular physiology. *Endocrinology* 153, 2953–2962. doi: 10.1210/en.2012-1061

Funakoshi, T., Yanai, A., Shinoda, K., Kawano, M. M., and Mizukami, Y. (2006). G protein-coupled receptor 30 is an estrogen receptor in the plasma membrane. *Biochem. Biophys. Res. Commun.* 346, 904–910. doi: 10.1016/j.bbrc.2006.05.191

Gowrishankar, K., Ghosh, S., Saha, S., Mayor, S., and Rao, M. (2012). Active remodeling of cortical actin regulates spatiotemporal organization of cell surface molecules. *Cell* 149, 1353–1367. doi: 10.1016/j.cell.2012.05.008

Gray, R. M. (2006). Toeplitz and circulant matrices: a review. *Found. Trends Commun. Inf. Theory* 2, 155–239. doi: 10.1561/0100000006

Groc, L., and Choquet, D. (2006). AMPA and NMDA glutamate receptor trafficking: multiple roads for reaching and leaving the synapse. *Cell Tissue Res.* 326, 423–438. doi: 10.1007/s00441-006-0254-9

Groc, L., Choquet, D., and Chaouloff, F. (2008). The stress hormone corticosterone conditions AMPAR surface trafficking and synaptic potentiation. *Nat. Neurosci.* 11:868.

Groc, L., Choquet, D., Stephenson, F. A., Verrier, D., Manzoni, O. J., and Chavis, P. (2007). NMDA receptor surface trafficking and synaptic subunit composition are developmentally regulated by the extracellular matrix protein reelin. *J. Neurosci.* 27, 10165–10175. doi: 10.1523/JNEUROSCI.1772-07.2007

Groc, L., Heine, M., Cousins, S. L., Stephenson, F. A., Lounis, B., Cognet, L., et al. (2006). NMDA receptor surface mobility depends on NR2A-2B subunits. *Proc. Natl. Acad. Sci. U.S.A.* 103, 18769–18774. doi: 10.1073/pnas.0605238103

Gu, J., Lee, C. W., Fan, Y., Komlos, D., Tang, X., Sun, C., et al. (2010). ADF/Cofilin-mediated actin dynamics regulate AMPA receptor trafficking during synaptic plasticity HHS public access author manuscript. *Nat. Neurosci.* 13, 1208–1215. doi: 10.1038/nn.2634

Han, B., Zhou, R., Xia, C., and Zhuang, X. (2017). Structural organization of the actin-spectrin-based membrane skeleton in dendrites and soma of neurons. *Proc. Natl. Acad. Sci. U.S.A.* 114, E6678–E6685. doi: 10.1073/pnas.1705043114

Hanley, J. G. (2014). Actin-dependent mechanisms in AMPA receptor trafficking. *Front. Cell. Neurosci.* 8:381. doi: 10.3389/fncel.2014.00381

Hokenson, R. E., Short, A. K., Chen, Y., Pham, A. L., Adams, E. T., Bolton, J. L., et al. (2021). Unexpected role of physiological estrogen in acute stress-induced memory deficits. *J. Neurosci.* 41, 648–662. doi: 10.1523/JNEUROSCI.2146-20.2020

Hu, R., Cao, Q., Sun, Z., Chen, J., Zheng, Q., and Xiao, F. (2018). A novel method of neural differentiation of PC12 cells by using Opti-MEM as a basic induction medium. *Int. J. Mol. Med.* 41, 195–201. doi: 10.3892/ijmm.2017.3195

Isaac, J. T. R., Ashby, M. C., and McBain, C. J. (2007). The role of the GluR2 subunit in ampa receptor function and synaptic plasticity. *Neuron* 54, 859–871. doi: 10.1016/j.neuron.2007.06.001

Jeon, C. Y., Jin, J. K., Koh, Y. H., Chun, W., Choi, I. G., Kown, H. J., et al. (2010). Neurites from PC12 cells are connected to each other by synapse-like structures. *Synapse* 64, 765–772. doi: 10.1002/syn.20789

Kane, M. D., Vanden Heuvel, J. P., Isom, G. E., and Schwarz, R. D. (1998). Differential expression of group I metabotropic glutamate receptors (mGluRs) in the rat pheochromocytoma cell line PC12: Role of nerve growth factor and ras. *Neurosci. Lett.* 252, 1–4. doi: 10.1016/S0304-3940(98)00484-4

Kim, J., Schalk, J. C., Koss, W. A., Gremminger, R. L., Taxier, L. R., Gross, K. S., et al. (2019). Dorsal hippocampal actin polymerization is necessary for activation of g-protein-coupled estrogen receptor (GPER) to increase CA1 dendritic spine density and enhance memory consolidation. *J. Neurosci.* 39, 9598–9610. doi: 10.1523/JNEUROSCI.2687-18.2019

Kovács, G., Környei, Z., Tóth, K., Baranyi, M., Brunner, J., Neubrandt, M., et al. (2018). Modulation of P2X7 purinergic receptor activity by extracellular Zn2+ in cultured mouse hippocampal astroglia. *Cell Calcium* 75, 1–13. doi: 10.1016/j.ceca.2018.07.010

Kramár, E. A., Chen, L. Y., Rex, C. S., Gall, C. M., and Lynch, G. (2009b). Estrogen's place in the family of synaptic modulators. *Mol. Cell. Pharmacol.* 1, 258–262.

Kramár, E. A., Chen, L. Y., Brandon, N. J., Rex, C. S., Liu, F., Gall, C. M., et al. (2009a). Cytoskeletal changes underlie estrogen's acute effects on synaptic transmission and plasticity. *J. Neurosci.* 29, 12982–12993. doi: 10.1523/JNEUROSCI.3059-09.2009

Kramár, E. A., Lin, B., Rex, C. S., Gall, C. M., and Lynch, G. (2006). Integrin-driven actin polymerization consolidates long-term potentiation. *Proc. Natl. Acad. Sci. U.S.A.* 103, 5579–5584. doi: 10.1073/pnas.0601354103

Kusumi, A., Tsunoyama, T. A., Hirosawa, K. M., Kasai, R. S., and Fujiwara, T. K. (2014). Tracking single molecules at work in living cells. *Nat. Chem. Biol.* 10:524.

Kwakowsky, A., Koszegi, Z., Cheong, R. Y., and Abrahám, I. M. (2013). Neuroprotective effects of non-classical estrogen-like signaling activators: from mechanism to potential implications. *CNS Neurol. Disord. Drug Targets* 12, 1219–1225.

Ledoux, V. A., Smejkalova, T., May, R. M., Cooke, B. M., and Woolley, C. S. (2009). Estradiol facilitates the release of neuropeptide Y to suppress hippocampus-dependent seizures. *J. Neurosci.* 29, 1457–1468. doi: 10.1523/JNEUROSCI.4688-08.2009

Lee, S. H., Jin, C., Cai, E., Ge, P., Ishitsuka, Y., Teng, K. W., et al. (2017). Super-resolution imaging of synaptic and extra-synaptic AMPA receptors with Different-Sized fluorescent probes. *Elife* 6:e27744. doi: 10.7554/eLife.27744

Liu, S., Wang, X., Pan, L., Wu, W., Yang, D., Qin, M., et al. (2018). Endogenous hydrogen sulfide regulates histone demethylase JMJD3-mediated inflammatory response in LPS-stimulated macrophages and in a mouse model of LPS-induced septic shock. *Biochem. Pharmacol.* 149, 153–162. doi: 10.1016/j.bcp.2017.10.010

Lu, Y., Sareddy, G. R., Wang, J., Wang, R., Li, Y., Dong, Y., et al. (2019). Neuron-derived estrogen regulates synaptic plasticity and memory. *J. Neurosci.* 39, 2792–2809. doi: 10.1523/JNEUROSCI.1970-18.2019

Lukinavičius, G., Reymond, L., D'Este, E., Masharina, A., Göttfert, F., Ta, H., et al. (2014). Fluorogenic probes for live-cell imaging of the cytoskeleton. *Nat. Methods* 11, 731–733. doi: 10.1038/nmeth.2972

Marbouti, L., Zahmatkesh, M., Riahi, E., and Sadr, S. S. (2020a). Inhibition of brain 17β-estradiol synthesis by letrozole induces cognitive decline in male

and female rats. *Neurobiol. Learn. Mem.* 175:107300. doi: 10.1016/J.NLM.2020.107300

Marbouti, L., Zahmatkesh, M., Riahi, E., and Shafiee Sabet, M. (2020b). GnRH protective effects against amyloid β-induced cognitive decline: A potential role of the 17β-estradiol. *Mol. Cell. Endocrinol.* 518:110985. doi: 10.1016/J.MCE.2020.110985

Mattila, P. K., Batista, F. D., and Treanor, B. (2016). Dynamics of the actin cytoskeleton mediates receptor cross talk: an emerging concept in tuning receptor signaling. *J. Cell Biol.* 212, 267–280. doi: 10.1083/jcb.201504137

McEwen, B. (2002). Estrogen actions throughout the brain. *Recent Prog. Horm. Res.* 57, 357–384. doi: 10.1210/rp.57.1.357

Mehmood, T., Schneider, A., Pannetier, S., and Hanauer, A. (2013). Rsk2 knockdown in PC12 cells results in Sp1 dependent increased expression of the Gria2 gene, encoding the AMPA receptor subunit GluR2. *Int. J. Mol. Sci.* 14, 3358–3375. doi: 10.3390/ijms14023358

Micevych, P. E., and Mermelstein, P. G. (2008). Membrane estrogen receptors acting through metabotropic glutamate receptors: an emerging mechanism of estrogen action in brain. *Mol. Neurobiol.* 38, 66–77. doi: 10.1007/s12035-008-8034-z

Murakami, G., Hojo, Y., Kato, A., Komatsuzaki, Y., Horie, S., Soma, M., et al. (2018). Rapid nongenomic modulation by neurosteroids of dendritic spines in the hippocampus: androgen, oestrogen and corticosteroid. *J. Neuroendocrinol.* 30, e12561. doi: 10.1111/JNE.12561

Oberlander, J. G., and Woolley, C. S. (2016). 17β-estradiol acutely potentiates glutamatergic synaptic transmission in the hippocampus through distinct mechanisms in males and females. *J. Neurosci.* 36, 2677–2690. doi: 10.1523/JNEUROSCI.4437-15.2016

Penn, A. C., Zhang, C. L., Georges, F., Royer, L., Breillat, C., Hosy, E., et al. (2017). Hippocampal LTP and contextual learning require surface diffusion of AMPA receptors. *Nature* 549, 384–388. doi: 10.1038/nature23658

Phan, A., Suschkov, S., Molinaro, L., Reynolds, K., Lymer, J. M., Bailey, C. D. C., et al. (2015). Rapid increases in immature synapses parallel estrogen-induced hippocampal learning enhancements. *Proc. Natl. Acad. Sci. U.S.A.* 112, 16018–16023. doi: 10.1073/pnas.1522150112

Potier, M., Georges, F., Brayda-Bruno, L., Ladépêche, L., Lamothe, V., Al Abed, A. S., et al. (2016). Temporal memory and its enhancement by estradiol requires surface dynamics of hippocampal CA1 N-Methyl-D-aspartate receptors. *Biol. Psychiatry* 79, 735–745. doi: 10.1016/j.biopsych.2015.07.017

Prange-Kiel, J., Wehrenberg, U., Jarry, H., and Rune, G. M. (2003). Para/autocrine regulation of estrogen receptors in hippocampal neurons. *Hippocampus* 13, 226–234. doi: 10.1002/hipo.10075

Rudolph, L. M., Cornil, C. A., Mittelman-Smith, M. A., Rainville, J. R., Remage-Healey, L., Sinchak, K., et al. (2016). Actions of steroids: new neurotransmitters. *J. Neurosci.* 36, 11449–11458. doi: 10.1523/JNEUROSCI.2473-16.2016

Sárvári, M., Szego, E. M., Barabás, K., Jávor, A., Tóth, S., Kovács, Z., et al. (2009). Genistein induces phosphorylation of cAMP response element-binding protein in neonatal hypothalamus in vivo. *J. Neuroendocrinol.* 21, 1024–1028. doi: 10.1111/j.1365-2826.2009.01925.x

Schevzov, G., Curthoys, N. M., Gunning, P. W., and Fath, T. (2012). *Functional Diversity of Actin Cytoskeleton in Neurons and its Regulation by Tropomyosin*, 1st Edn. Amsterdam: Elsevier Inc, doi: 10.1016/B978-0-12-394309-5.00002-X

Schindelin, J., Arganda-Carreras, I., Frise, E., Kaynig, V., Longair, M., Pietzsch, T., et al. (2012). Fiji: an open-source platform for biological-image analysis. *Nat. Methods* 9, 676–682. doi: 10.1038/nmeth.2019

Shibata, S. C., Hibino, K., Mashimo, T., Yanagida, T., and Sako, Y. (2006). Formation of signal transduction complexes during immobile phase of NGFR movements. *Biochem. Biophys. Res. Commun.* 342, 316–322.

Spencer, J. L., Waters, E. M., Romeo, R. D., Wood, G. E., Milner, T. A., and McEwen, B. S. (2008). Uncovering the mechanisms of estrogen effects on hippocampal function. *Front. Neuroendocrinol.* 29:219–237. doi: 10.1016/j.yfrne.2007.08.006

Teyler, T. J., Vardaris, R. M., Lewis, D., and Rawitch, A. B. (1980). Gonadal steroids: effects on excitability of hippocampal pyramidal cells. *Science* 209, 1017–1018. doi: 10.1126/science.7190730

Tokunaga, M., Imamoto, N., and Sakata-Sogawa, K. (2008). Highly inclined thin illumination enables clear single-molecule imaging in cells. *Nat. Methods* 5, 159–161. doi: 10.1038/nmeth1171

Vierk, R., Brandt, N., and Rune, G. M. (2014). Hippocampal estradiol synthesis and its significance for hippocampal synaptic stability in male and female animals. *Neuroscience* 274, 24–32. doi: 10.1016/J.NEUROSCIENCE.2014.05.003

Wang, Z., Sun, L., Liang, S., Liu, Z., Zhao, Z. Y., Yang, J., et al. (2019). GPER stabilizes F-actin cytoskeleton and activates TAZ via PLCβ-PKC and Rho/ROCK-LIMK-Cofilin pathway. *Biochem. Biophys. Res. Commun.* 516, 976–982. doi: 10.1016/j.bbrc.2019.06.132

Wehrenberg, U., Prange-Kiel, J., and Rune, G. M. (2001). Steroidogenic factor-1 expression in marmoset and rat hippocampus: co-localization with StAR and aromatase. *J. Neurochem.* 76, 1879–1886. doi: 10.1046/j.1471-4159.2001.00207.x

Wiatrak, B., Kubis-Kubiak, A., Piwowar, A., and Barg, E. (2020). PC12 cell line: cell types, coating of culture vessels, differentiation and other culture conditions. *Cells* 9:958. doi: 10.3390/cells9040958

Wong, M., and Moss, R. L. (1992). Long-term and short-term electrophysiological effects of estrogen on the synaptic properties of hippocampal CA1 neurons. *J. Neurosci.* 12, 3217–3225. doi: 10.1523/JNEUROSCI.12-08-03217.1992

Xu, K., Zhong, G., and Zhuang, X. (2013). Actin, spectrin, and associated proteins form a periodic cytoskeletal structure in axons. *Science* 339, 452–456. doi: 10.1126/science.1232251

Zhao, T. Z., Shi, F., Hu, J., He, S. M., Ding, Q., and Ma, L. T. (2016). GPER1 mediates estrogen-induced neuroprotection against oxygen-glucose deprivation in the primary hippocampal neurons. *Neuroscience* 328, 117–126. doi: 10.1016/j.neuroscience.2016.04.026

Zhao, Y., He, L., Zhang, Y., Zhao, J., Liu, Z., Xing, F., et al. (2017). Estrogen receptor alpha and beta regulate actin polymerization and spatial memory through an SRC-1/mTORC2-dependent pathway in the hippocampus of female mice. *J. Steroid Biochem. Mol. Biol.* 174, 96–113. doi: 10.1016/J.JSBMB.2017.08.003

Conflict of Interest: The authors declare that the research was conducted in the absence of any commercial or financial relationships that could be construed as a potential conflict of interest.

Publisher's Note: All claims expressed in this article are solely those of the authors and do not necessarily represent those of their affiliated organizations, or those of the publisher, the editors and the reviewers. Any product that may be evaluated in this article, or claim that may be made by its manufacturer, is not guaranteed or endorsed by the publisher.

Hormones and Behavior xxx (xxxx) xxx–xxx

Contents lists available at ScienceDirect

Hormones and Behavior

journal homepage: www.elsevier.com/locate/yhbeh

Review article

Rapid non-classical effects of steroids on the membrane receptor dynamics and downstream signaling in neurons

Klaudia Barabás, Soma Godó, Ferenc Lengyel, Dávid Ernszt, József Pál, István M. Ábrahám*

MTA NAP-B Molecular Neuroendocrinology Research Group, Institute of Physiology, Medical School, Centre for Neuroscience, Szentágothai Research Institute, University of Pécs, Pécs, Hungary

A B S T R A C T

Although rapid effects of steroid hormones on membrane receptors and intracellular signaling molecules have been extensively studied in neurons, we are only beginning to understand the molecular mechanisms behind these non-classical steroid actions. Single molecule tracking (SMT) studies on live cells demonstrated that surface trafficking of membrane receptors determines their ligand binding properties and downstream signaling events. Recent findings suggest that one of the underlying mechanisms of non-classical steroid actions is the alteration of receptor movements on the membrane surface. In order to highlight this novel aspect of steroid effects, we first address the types of receptor movements in the plasma membrane and the role of cortical actin dynamics in receptor movement. We then discuss how single molecules and the surface movements of receptors can be detected in live cells. Next, we review the fundamental processes, which determine the effect of steroids on the plasma membrane: steroid movement through the lipid bilayer and the role of steroid membrane receptors. Using glutamate and neurotrophin receptors (NTRs) as examples, we demonstrate the features of receptor dynamics in the membrane. In addition, we survey the available data of rapid steroid actions on membrane receptor trafficking: we discuss how glucocorticoids act on the surface diffusion of glutamate receptor molecules and how estradiol acts on NTRs and gamma-aminobutyric acid type A receptors ($GABA_ARs$) and their related signaling events as well as on cortical actin. Finally, we address the physiological relevance of rapid steroid action on membrane receptors dynamics.

1. Introduction

Steroids, such as the gonadal steroid 17β-estradiol (E2) and the stress hormone, corticosterone (CORT) are potent molecules with a wide range of biological actions from fertility to neuroprotection and stress response to neurodegeneration, respectively (Ábrahám et al., 2009; Kwakowsky et al., 2013a; McEwen, 2002; Szegő et al., 2011). Besides their classical action, E2 and CORT rapidly alter the functions of membrane receptors and the activity of second messenger molecules and transcription factors in neurons. This action of steroids can be defined as a non-classical effect, because this downstream signaling process acts indirectly on gene transcription via the activation of second messenger pathways. Since intracellular signaling is initiated at the membrane, it is critical to understand the molecular mechanism of non-classical steroid action on neuronal membrane receptors. The effect of steroids such as E2 results in either local effects in the membrane like modulating the function of ion channels, or altering intracellular signaling events such as cyclic adenosine monophosphate (cAMP), protein kinase A (PKA), extracellular regulated kinase 1/2 (ERK1/2), and transcription factors such as cAMP response element binding protein (CREB) (Cheong et al., 2012; Kwakowsky et al., 2014; Micevych and Dominguez, 2009).

Using super-resolution imaging, it became possible to quantify the dynamic and kinetic parameters of single-molecules in live cells. Single molecule imaging techniques revealed the features of membrane receptor dynamics and their related downstream signaling. The first observation of individual molecules in living cells was performed for Ras, the key downstream signaling molecule of receptor-type tyrosine kinases with a single-molecule fluorescence resonance energy transfer method (Murakoshi et al., 2004). Since then, major progress has been made towards clarifying the role of individual molecules in complex biological processes. However, the molecular mechanisms of steroid hormone effects based on single molecule imaging technique are just beginning to unfold. The advance in this line of research was the identification of CORT action on glutamate receptor molecules (Groc et al., 2008). Single molecule imaging techniques showed that CORT modulates synaptic plasticity by changing the surface dynamics of glutamate receptors.

* Corresponding author.
E-mail address: istvan.abraham@aok.pte.hu (I.M. Ábrahám).

https://doi.org/10.1016/j.yhbeh.2018.05.008
Received 28 February 2018; Received in revised form 8 May 2018; Accepted 9 May 2018

In this review, we summarize the essential aspects of single molecule imaging technology and critical features of membrane receptor dynamics in live neurons. We also highlight the recently acquired evidence of rapid steroid effects in the neuronal plasma membrane at the single molecule level.

2. Receptor dynamics in plasma-membrane of neurons: lateral diffusion

The activation of the signaling pathways is determined by the activation of the receptors, which in turn can be precisely described by the changes of their lateral diffusion in the plasma membrane. Accordingly, measuring the diffusion parameters of the steroid membrane receptors can provide a better understanding of the non-classical steroid effects in plasma-membrane.

Single molecule tracking (SMT) is a powerful technology that enables us to observe receptor movements at the single molecule level in live neurons. Studies using SMT revealed changes in the lateral movement of receptors in the plasma membrane that are essential to their function (Fujiwara et al., 2002). The lateral diffusion of membrane receptors is restricted by cell components and structures such as actin filaments. In this section, we summarize the types of receptor movements in the plasma membrane and the role of cortical actin filaments in receptor diffusion. In addition, we discuss the key features of SMT technology to highlight the technological background of these experiments.

2.1. The surface movement of receptors and actin-based membrane skeleton the: "hop diffusion" model

According to the Singer-Nicolson fluid mosaic model, the phospholipids, membrane-associated proteins and cholesterol are moving all over the plasma membrane with Brownian diffusion. However, using SMT combined with ultra-fast CMOS cameras, four basic types of molecule diffusion were identified: simple Brownian, stationary, directed and confined (restricted) diffusion (Kusumi et al., 1993). Molecules with Brownian motion show free diffusion in the membrane region. Stationary diffusion is a type of diffusion when molecules move over a very limited area, almost with no apparent movement. Directed diffusion refers to Brownian motion superimposed on a directional movement. In confined diffusion, molecules move with Brownian motion in a limited area, referred to as a "confinement zone" (Fig. 1). Confinement zones can be considered as membrane compartments. The size of the compartments depends on the cell type and the molecule examined and it is 40 to 500 nm in diameter as determined by single particle tracking (SPT) experiments (Fujiwara et al., 2002; Renner et al., 2009; Simson et al., 1998). Tracking molecules for a longer period of time revealed that they can move from one membrane compartment to another, though these inter-compartment jumps are infrequent. The type of confined diffusion, when free diffusion in restricted spaces alternates with jumps ("hops") from one confined area to another is called "hop diffusion" (Piskorz and Ochab-Marcinek, 2014) (Fig. 1).

All eukaryotic cells have a microfilamental meshwork right adjacent to the plasma membrane, with actin as the main constituent (cortical actin network). This cortical actin network is regulated, stabilized and tethered to other components of the cytoskeleton and to the cell membrane by several adaptor proteins (Köster and Mayor, 2016). Its submembrane localization, mesh-like structure and the ability to bind to the cell membrane make cortical actin a tempting candidate as the barrier limiting membrane confinement zones. Indeed, the distance between the cortical actin network and the inner surface of the membrane is estimated to be ≤ 3.5 nm (Shirai et al., 2017), so it might limit the movement of transmembrane molecules protruding the cytosol. The role of cortical actin as a determinant of membrane compartmentalization was suggested by several observations in non-neural (Andrade et al., 2015; Fujiwara et al., 2002; Koppel et al., 1980; Ritchie et al., 2003; Sadegh et al., 2017) and neural (Chamma et al., 2013) cells. Transmembrane proteins and the cortical actin limit the surface movements of membrane molecules. This theory is described in the model of fences and pickets by Kusumi and colleagues (Ritchie et al., 2003). This theory states that the cell membrane is divided to confinement zones, inside which membrane proteins move with Brownian motion and which are limited by pickets of transmembrane proteins. These pickets are anchored to the cortical actin meshwork, creating a network-like picket fence system. Either because of the imperfect insulation between transmembrane protein pickets or the dynamic nature of the cortical actin meshwork, membrane proteins have a chance to escape through the picket-fence to a neighboring confinement zone, giving rise to the phenomenon of "hop diffusion" (Suzuki et al., 2005) (Fig. 1). Importantly, the membrane of dendritic spines in neurons behaves as a membrane compartment: receptor molecules are enriched in these membrane regions and their diffusion is often restricted to the

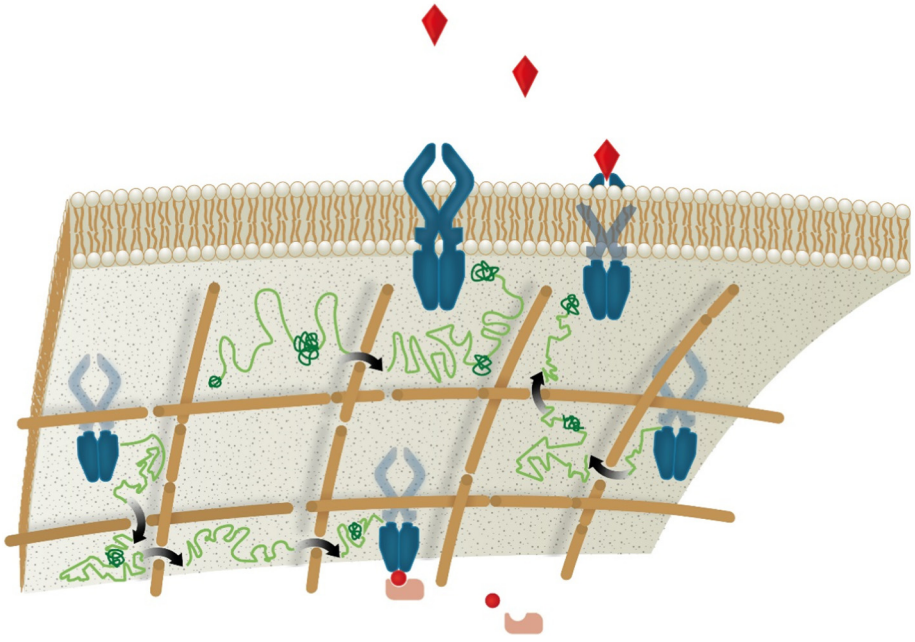

Fig. 1. Surface movements of membrane receptors and hop diffusion. Membrane receptors (blue shape) move in limited area and cross the actin barriers (brown rods) with hop diffusion (black arrows) during Brownian movement (light green line). Immobility (dark green line) occurs upon ligand binding (red rhombus) and intracellular signaling complex formation (red sphere). (For interpretation of the references to color in this figure legend, the reader is referred to the web version of this article.)

neck of the spines. This restriction, at least in part, depends on the actin cytoskeleton (Wang et al., 2016). Axons also have a characteristic cytoskeletal system under the plasma membrane. This system is composed of actin rings repeating every 190 nm, bridged by spectrin tetramers, and sodium channel localization follows this pattern (Xu et al., 2013). Further, diffusion of membrane molecules seems to be restricted by this actin-spectrin network (Albrecht et al., 2016).

2.2. Labeling, measuring and analysis of single molecule receptor dynamics in live neurons

In order to better understand the concept of SMT experiments and lateral diffusion of molecules we survey the technological background that is required for SMT including sample labeling, molecular imaging and analysis methods. Sample preparation and labeling are the most critical steps in SMT experiments. Due to technical challenges, SMT experiments are usually conducted on primary cell cultures or cell lines, but recent work using brain slices have demonstrated that the results obtained from those relatively simple models can be extrapolated to more complex systems such as adult neuronal network (Biermann et al., 2014).

In SMT, fluorescent labeling is the most widely used technique to visualize single molecules. The fluorescent probes can be classified into three categories, such as nanocrystal particles, fluorescent proteins (FP) and organic dyes (OD). Nanocrystal particles such as quantum dots (QD) have strong photostability and superior brightness, but their relatively large size and photoblinking properties can interfere with SMT experiments. QDs can be easily conjugated to antibodies that recognize the extracellular domain of the membrane receptor protein molecule (Movie). Since labeling is performed at the genomic level, FPs such as green florescent protein (GFP) has the highest labeling specificity. Although FPs are smaller than QDs, they are bulky enough to modify the structure and function of the labeled protein. The drawbacks of FPs are also the weak intensity and fast photobleaching. In contrast, ODs are smaller than FPs (~1 kD compared to ~25 kD) and they have stronger photostability and better photoemission features. However, they must be conjugated to an antibody to bind to a specific protein and thus their labeling specificity is lower than that of FPs (Kremers et al., 2011; Kwakowsky et al., 2013a, b).

The crucial part of the SMT technology is the optical resolution that is in the same range as the size of the molecule of interest (around 10 nm). Given the diffraction limit, the x/y resolution of conventional light microscopy is around 250 nm, which is not suitable for SMT. SMT studies became possible when the super resolution technologies were developed to bypass the diffraction limit to increase the resolution to few-tens of nanometer range.

Super resolution microscopy techniques such as total internal reflection fluorescence microscopy (TIRFM) (Axelrod, 2001) and highly inclined laminated optical sheet microscopy (HILOM) (Tokunaga et al., 2008) are the most commonly used imaging techniques in SMT studies. In TIRFM, the laser beam reaches a solid/liquid interface (e.g. coverslip/cell interface) with an angle of incidence which is higher than the so-called critical angle (θ_c). Under these conditions, the light totally reflects rather than propagates through the specimen. The reflected light generates an electromagnetic field, so-called “evanescent field”, in the vicinity of the solid/liquid interface which excites the fluorophores. As the width of the evanescent field is smaller than 100 nm, only fluorophores near the cell surface will be excited (Axelrod, 2001). As deeper structures are not excited, the background is lower and localization can be as precise as 50 nm. Though it allows higher precision in molecule localization, the low thickness of the excited volume has a drawback: it decreases the field of view along the z-axis. This limitation is resolved by HILOM, where single molecules of the intracellular space can be investigated. HILOM uses a similar optical arrangement as TIRFM, but the incident angle of the laser beam is smaller than the critical angle. This illumination results in a thin light beam running almost parallel to the coverslip. This light beam penetrates into the cell and excites intracellular fluorophores allowing single molecule detection inside the cell (Tokunaga et al., 2008).

Data analysis is a crucial and time consuming part of SMT. The tracking analysis includes estimating the position of the molecules, compiling trajectories and determining the physical parameters of molecular movements. It is beyond the scope of this review to explain the analysis in detail. Briefly, all of the molecule detection methods are based on the point spread function, where the center of the signal is calculated with a Gaussian fit (Rogers et al., 2007). The majority of trajectory assembling algorithms use the nearest neighbor method, where a spot is linked to another spot of the next frame if their distance is below a given threshold level (Hansen et al., 2017; Rogers et al., 2007; Sergé et al., 2008). From the assembled trajectories, the mobility parameters of the molecules can be calculated. The two commonly used basic parameters are the mean square displacement (MSD) and the diffusion coefficient. The MSD shows the average distance that a molecule covers during a given time interval. The diffusion coefficient numerically describes the molecule's susceptibility to move. The diffusion coefficient as well as the type of mobility can be determined by using the MSD versus time lag curve. The type of mobility can be determined from the plots of MSD as a function of time.

3. Steroid and steroid receptor diffusion at neuronal membrane

Rapid steroid effects on receptor molecule dynamics in the membrane require the understanding of the steroid diffusion through the plasma-membrane and the lateral diffusion of steroid receptors in the plasma membrane.

3.1. Movement of steroids through the lipid bilayer: conceptual problems and new players in membrane action

The current consensus is that lipophilic steroids pass freely through the lipid bilayer of the plasma membrane into the cytoplasm and bind to intracellular steroid receptors. However, there are potential pitfalls of this theory. Since steroids are strongly lipophilic, they cannot merge into the cytosol via the hydrophobic extracellular space or leave the cytosol through the lipid bilayer without hindrance. Alléra and Wildt (1992) clearly demonstrated that a plasma membrane-inserted carrier helps the glucocorticoids such as CORT to pass through the lipid bilayer. The research group of Caldwell used time lapse confocal laser scanning microscopy to demonstrate the entry of fluorescently labeled E2 (E2Glow) into Chinese hamster ovary (CHO) cells (Caldwell et al., 2016). They found that E2 was concentrated only around the edges of the cell for 10s suggesting a rapid E2 accumulation in the membrane. After 30s, E2 appeared in the cytoplasm as well as around the cell. Administration of an antibody produced against the sex hormone-binding globulin (SHBG) delayed the E2 penetration across the plasma-membrane of CHO cells proposing that the presence of SHBG is essential for E2 uptake. Caldwell and colleagues hypothesized that steroids cannot freely pass through the plasma membrane but carrier proteins such as steroid-binding globulins assist in their internalization and they are also responsible for carrying steroids within the cell (Caldwell et al., 2016). Further experiments are required to examine the possible role of carrier proteins in movement of steroids across the plasma membrane in neurons.

3.2. Steroid membrane receptors and lateral diffusion

Several findings indicate that membrane-associated receptors can provide a potential platform for direct membrane actions of steroids (Simpkins et al., 2012; Treen et al., 2016; Qiu et al., 2008). However, limited data is available on the membrane dynamics of steroid receptors. Using real-time TIRFM measurements, Kisler and colleagues examined the lateral diffusion of estrogen receptor alpha in N-38

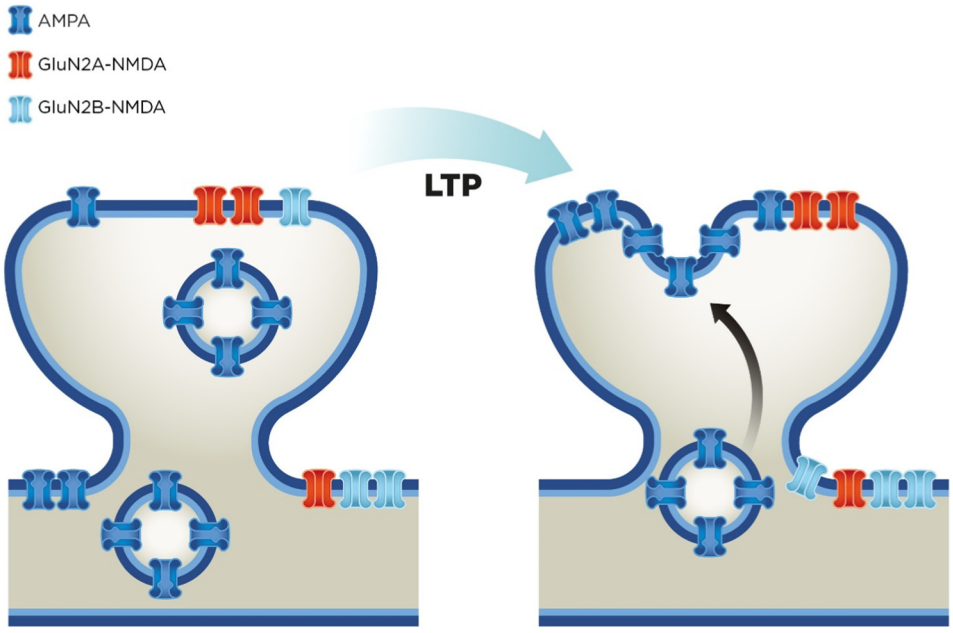

Fig. 2. Schematic overview of the glutamate receptor redistribution during LTP. AMPARs are recruited into the synaptic cleft from the extrasynaptic vesicles, while GluN2B-NMDARs leave the synaptic membrane with lateral diffusion, thus changing the GluN2A/B ratio.

neuronal cells using a membrane impermeable fluorescently labeled ER ligand, E6BSA-FITC and GFP-labeled ERα. They found two main types of E6BSA-FITC dots based on their movement parameters and changes in their fluorescent intensity. “Type 1 dot” moved laterally adjacent to the plasma membrane with directed motion and dimming fluorescence intensity before disappearing. “Type 2 dot” or stationary puncta appeared quickly and brightened up markedly before rapidly vanishing. “Type 1 dot” correspond to endocytotic vesicle trafficking, while “Type 2 dot” represent exocytotic events (Kisler et al., 2013).

Besides the study of Kisler and colleagues, literature suggests that the membrane dynamics of steroid receptors are important regulators of neuronal functions. Various rapid effects of E2 are exerted by activating G-proteins. However, it remains controversial whether membrane-localized estrogen receptors bind G-proteins directly or regulate G-protein signaling via lateral movements and interaction with surface membrane receptors. Previous findings support the latter hypothesis. Membrane bound ERα and ERβ can interact with different metabotropic glutamate receptors (mGluRs) in a cell-type specific manner in the brain and within the same neuron as well. The interaction between membrane estrogen receptors and mGluRs is governed by caveolin proteins. ERα activates mGluR1 when it is associated with caveolin-1, while ERα and ERβ trigger mGluR2/3 signaling in the presence of caveolin-3. It raises the question if caveolins are involved in regulating ER membrane dynamics as well (Boulware et al., 2007; Meitzen and Mermelstein, 2011).

Rapid non-classical actions of CORT are elicited by stimulating or inhibiting receptor related intracellular signaling, ion channels and neurotransmitters via membrane localized mineralocorticoid receptors (MRs) or GRs. One of the ways CORT induces its rapid effects in neurons is by modulating glutamatergic transmission. For instance the enhancement of glutamatergic transmission is preceded by pre- and postsynaptically positioned membrane MRs. Presynaptic MRs stimulate glutamate release through the activation of ERK pathway, while postsynaptic membrane MRs increase membrane diffusion of α-amino-3-hydroxy-5-methyl-4-isoxazolepropionic acid (AMPA) receptors (Groeneweg et al., 2011).

4. Rapid action of steroids on the surface diffusion of receptors and downstream signaling processes

CORT elevation induced by acute stress increases the surface *N*-methyl-D-aspartate (NMDA) and AMPA receptor level in the pyramidal neurons of prefrontal cortex through genomic mechanisms, via the stimulation of GRs. Besides, glucocorticoids alter the levels of glutamate receptors and in response to stress CORT rapidly modulate glutamatergic transmission via altering the membrane dynamics of AMPA and NMDA receptors (Mikasova et al., 2017).

So far there has been only one study published examining how E2 can change the surface movement of receptors: it describes the E2 effect on $GABA_AR$ membrane dynamics. However, several experiments have established that E2 interacts with membrane receptors such as NTRs, which then alters downstream signaling.

4.1. Surface movement of glutamate receptors

N-methyl-D-aspartate receptors (NMDARs) are heterotetramers, composed of two ionotropic glutamate receptor subunit 1 (GluN1) and two ionotropic glutamate receptor subunit 2 A-D (GluN2A-D). Choquet and his colleagues used SMT to determine the mobility and distribution of QD labeled GluN2A- and GluN2B-NMDARs on the surface of hippocampal neurons. GluN2A-NMDARs are in the postsynaptic densities (PSD), whereas GluN2B-NMDARs are more frequent in the perisynaptic domain (Groc et al., 2006). GluN2A exhibits mostly restricted or immobile movement type both in synaptic and extrasynaptic areas, while GluN2B-NMDARs show a more complex movement profile containing both mobile and immobile trajectories (Groc et al., 2006; van Zundert et al., 2004). SMT and electrophysiological experiments showed that during long term potentiation (LTP)-induced rapid remodeling, Glun2B-NMDARs leave the synaptic membrane and accumulate in the perisynaptic area, while the stable Glun2A-NMDARs remain in the synapse (Dupuis et al., 2014; Ladépêche et al., 2014) (Fig. 2). The differences in the diffusion dynamics of the two NMDAR subtypes are mainly the result of the interactions with the components of the postsynaptic density protein 95 (PSD-95). This scaffolding protein anchors the Glun2A-NMDAR to the center of the synapse, whereas synapse associated protein 102 forms a complex with Glun2B-NMDAR and

translocates it to the perisynaptic membrane (Bard et al., 2010; Sans et al., 2000; Townsend et al., 2003; Yoshii et al., 2003).

The number of AMPARs in a synapse correlates with spine size and synaptic strength (Chater and Goda, 2014). In the latest comprehensive studies, trafficking of AMPARs was examined in hippocampal cell cultures by SMT. It was found that > 90% of the AMPARs diffuse in PSD and < 10% is extrasynaptic (Lee et al., 2017). SMT experiments revealed that half of the synaptic AMPA receptors are immobile, while the other half are relatively slow (diffusion coefficient < 0.1 $\mu m^2/s$) and display confined movement (Tardin et al., 2003). The immobile receptors are most likely bound to scaffold proteins such as PSD-95 (Opazo et al., 2012), *N*-ethylmaleimide sensitive fusion protein (Nishimune et al., 1998; Noel et al., 1999) and synapse-associated protein-97 (Leonard et al., 1998). In contrast, most AMPA receptors display Brownian movements outside the synapse (Borgdorff and Choquet, 2002). Upon ligand binding, AMPARs activate downstream signaling pathways resulting in phosphorylation of the receptor. Phosphorylation increases the binding affinity of the receptor to adaptor proteins whose role is to couple the AMPARs to the clathrin-dependent endocytic machinery (Glebov et al., 2015). After internalization, AMPARs enter different endosomal sorting pathways: early endosomes and recycling endosomes for reinsertion into the membrane, or late endosomes and lysosomes for degradation (Ashby et al., 2004). Importantly, most of the synapses in the mature central nervous system (CNS) are wrapped by a dense extracellular matrix (ECM), which hinders the lateral diffusion of AMPARs. Enzymatic removal of the ECM increases the diffusion coefficient of extrasynaptic AMPARs and the rate of exchange between synaptic and extrasynaptic receptor pools (Frischknecht et al., 2009).

In summary, we conclude that the movement of both NMDA and AMPA receptors become more confined or immobile after entering the synapse and scaffolding proteins such as PSD-95 are major regulators of the trafficking of both glutamate receptors by anchoring them to the postsynaptic membrane. However, the lateral diffusion of AMPARs into the synapse is more prominent than that of NMDARs during LTP.

4.2. Effect of glucocorticoids on lateral diffusion of glutamate receptors

As discussed in the previous section, synaptic plasticity involves modification of surface dynamics and the number of NMDA and AMPA receptors. Live cell SMT and QD labeling revealed that the subunits of NMDARs responded differently in the presence of CORT. The vast majority of GluN1, the constant subunit of NMDAR, and the GluN2B subunit became immobile in the synapses of hippocampal neuronal culture, while mobility of the GluN2A subunit did not change after CORT exposure. Aldosterone, a potent MR agonist, elicited the same effect on membrane dynamics of the GluN2B subunit as CORT. RU28362, a glucocorticoid receptor (GR) agonist had no effect either on the number of GluN2B subunits in the membrane or on their mobility, suggesting that this mechanism is coordinated by the MR related pathway (Mikasova et al., 2017).

The influence of CORT on synaptic receptor remodeling also includes an effect on AMPARs. QD conjugated antibodies produced against different subunits of AMPAR (GluR1 and GluR2) and SMT were used to examine this effect on live primary mouse hippocampal neurons. 100 nM CORT administration rapidly increased the diffusion coefficient of both GluR1- and GluR2-AMPAR molecules. The same effect was mimicked by aldosterone, but inhibited by RU28362 (Groc et al., 2008). To observe the long-term effect of CORT, GluR1- and GluR2-AMPAR were immunostained after 150 min of brief CORT exposure. In the presence of CORT GluR2-AMPARs remained longer in the synaptic area. Experiments with GR agonist (RU28362) and GR antagonist (RU38486) presented that GR mediates long-term effects of CORT on the surface diffusion of AMPARs (Groc et al., 2008; Sarabdjitsingh et al., 2014; Zhang et al., 2013).

4.3. Surface movement of neurotrophin receptors

The activation of NTRs (Tropomyosin receptor kinase A-C receptors: TrkAR, TrkBR, TrkCR) is determined by several factors: activated signaling pathways, the localization of receptors, composition of lipid rafts, presence of the available ligands and the interactions between NTRs (Barford et al., 2017; Ioannou and Fahnestock, 2017; Spencer et al., 2017; Zhang et al., 2000). TrkRs diffuse laterally in the cell membrane (Movie) and upon ligand binding, they dimerize, undergo autophosphorylation and promote cell survival (Marchetti et al., 2015).

The outcome of the neurotrophin-induced functional responses also depends on the receptor dynamics in the membrane. Using SMT, trajectories of TrkA receptors in living PC12 cells revealed two distinct transient modes of movement, characterized as mobile and immobile phases (Shibata et al., 2006). Immobilization of the receptor has been shown to correspond to the start of signal transduction (Tani et al., 2005). Membrane recruitment of downstream intracellular signaling proteins such as mitogen activated protein kinase (MAPK) occurs when the TrkA receptor is in the immobile phase (Shibata et al., 2006). In another study, SMT was performed on TrkA-deficient PC12 cells transfected with acyl carrier protein (ACP)-tagged TrkA receptor and labeled with QDs. SMT experiments with ACP tagged-TrkA receptors show a remarkably heterogeneous diffusive behavior with diffusion coefficients ranging from $-10^{-5}\,\mu m^2/s$ to 0.5 $\mu m^2/s$. These ACP-TrkA receptors presented Brownian, confined and directed motion with the majority of the receptors displaying confined diffusion both in somatic and neuritic compartments (Callegari et al., 2012). The same research group, using the same ACP-TrkA construct in SH-SY5Y neuroblastoma cells, investigated how receptor-membrane dynamics can be altered in response to different ligands. They found that all examined ligands increased immobilization by redistributing the slow and fast diffusing trajectories of the TrkA receptors. Ligand-induced immobilization was related to the formation of dimers and oligomers of TrkA receptors serving as signaling platforms. This study also showed that the lateral mobility of TrkA receptors is ligand dependent and each ligand promotes different trajectory patterns of TrkA receptor molecules at the cell membrane triggering specific biological outcomes (Marchetti et al., 2013). Although the interaction of TrkA receptor with its co-receptor $p75^{NTR}$ and their dimerization are crucial steps in the activation of TrkA receptors (Huang and Reichardt, 2003), the single molecule dynamics of the interaction/dimerization is not known.

4.4. Rapid action of E2 on NTRs and downstream signaling

As opposed to CORT much less is known about how E2 influences membrane dynamics. There is only indication that E2 might influence the membrane dynamics of NTRs. E2 and NTRs bidirectionally interact with each other in the reproductive organs and in the CNS as well. E2 acts on the neurotrophin signaling system by modulating the expression levels of neurotrophins and their receptors: E2 modifies the expression of BDNF and its low affinity receptor, $p75^{NTR}$ in the uterus (Wessels et al., 2015), controls the plasticity of sympathetic nerves by altering the levels of TrkA and $p75^{NTR}$ in uterine-projecting sympathetic neurons (Richeri et al., 2005). It works other way around too, neurotrophins can also modify the effect of E2: TrkA receptor activation stimulates E2 secretion directly and indirectly by increasing the expression of follicle-stimulating hormone receptors in the human ovary (Salas et al., 2006). E2 increases BDNF levels through action on nuclear receptors to increase dendritic spine density in the prefrontal cortex and hippocampus (Luine and Frankfurt, 2013) or in the developing cerebellum in a nuclear estrogen receptor dependent manner to promote Purkinje dendritic growth, spinogenesis, and synaptogenesis (Haraguchi et al., 2012). Besides that E2 alters the levels of neurotrophins directly it can converge on the same signaling pathways as neurotrophins.

It has been shown that both E2 and BDNF induce spine plasticity via

rapid membrane effects through the CREB pathway (Luine and Frankfurt, 2013). Several experimental evidence indicates that the gonadal hormone, estradiol has a robust neuroprotective effect on BFC neurons (Baldereschi et al., 1998; Horvath et al., 2002). Previous experiments in our laboratory showed that a single dose of the gonadal sex steroid, the 17β-estradiol (E2) significantly reduced the $A\beta_{1-42}$-induced fiber loss in BFCN neurons (Kwakowsky et al., 2016). Previous results in our laboratory also demonstrated that E2 acts upon the MAPK intracellular signaling pathway via ERα to alter downstream signaling in BFC neurons (Szego, 2006). As TrkA also modulates the MAPK signaling pathway (Nguyen et al., 2009; Song and Yoo, 2011), the effect of Aβ and 17β-estradiol might converge on the TrkA/$p75^{NTR}$ system and their downstream signaling pathways. The research group of Toran-Allerand provided a new concept for the interaction of E2 and Trk receptors. In their study they showed that E2 elicits rapid (5–15 min) and sustained (2 h) tyrosine phosphorylation of ERK1/2 as a consequence of E2-induced activation of B-Raf in the developing cerebral cortex (Singh et al., 1999). ERK, B-Raf and ER being part of a multimeric complex serve as an intracellular platform for E2 to regulate ERK and at the same time for neurotrophins to influence ER function. Consequently, plasma membrane located ERs and NTRs share downstream signaling effectors; therefore they can interact with each other and act on the same signaling pathway, giving rise to their functional interplay.

4.5. Rapid action of E2 on $GABA_A$ receptors

$GABA_A$Rs are chloride ion selective ligand gated ion channels, which play an important role in inhibitory neurotransmission. While it is well established that E2 is an effective regulator of excitatory neurotransmission, its role in modulating inhibitory transmission is less clear. Recently published data using SPT showed that E2 influences the dynamics of $GABA_A$Rs at inhibitory synapses in cultured cortical neurons. Acute E2 treatment decreases the confinement of $GABA_A$Rs without effecting the diffusion coefficients and reduces their dwell time in the synaptic compartment of cortical neurons, while increases the diffusion coefficient of the $GABA_A$Rs at the extrasynaptic sites (Mukherjee et al., 2017).

5. The physiological consequence of rapid steroid action on membrane receptors dynamics and downstream signaling process

Rapid non-classical actions of steroids on membrane receptor dynamics and their related signaling events are involved in physiologically important processes. Accordingly, we summarize the role of CORT and E2 in synaptic plasticity and the effect of E2 on remodeling of dendritic spines.

5.1. The role of rapid steroid effects effect on glutamate receptor and $GABA_AR$ dynamics in synaptic plasticity

AMPARs and NMDARs play pivotal role in the molecular processes of the synaptic plasticity and the formation of LTP, the model of neuronal plasticity and behavior learning. The critical event during LTP is the rearrangement of glutamate receptors in the synapse (Fig. 2). By these changes, the synapse becomes more effective, favouring behavioral adaptations and memory formation (Mikasova et al., 2017).

Both CORT treatment and LTP cause alteration in the subunit ratio of NMDARs in hippocampal neurons that serves as a signal for changes in synaptic plasticity. AMPAR rearrangement also contributes to synaptic plasticity changes. LTP significantly elevates the surface content of AMPARs in the postsynaptic membrane, while CORT pretreatment synergistically acts on LTP further increasing the number of AMPARs molecules in the synapse (Groc et al., 2008) suggesting that CORT affects rapid redistribution of glutamate receptors thus controls synaptic plasticity and learning.

Since CORT levels show an ultradian rhythm it has been confirmed by electrophysiological studies that consecutive application of CORT regulates glutamate transmission differently, it would be worthwhile examining the membrane dynamics of glutamate receptors in a physiologically more relevant experimental model in which CORT is applied with naturally occurring 1 h intervals (Sarabdjitsingh et al., 2016, 2014).

Persistent changes in GABAergic neurotransmission also contributes to synaptic plasticity. This is partly due to a continuous exchange between the synaptic and extrasynaptic pool of $GABA_A$Rs, which is enabled by lateral diffusion in the plasma membrane. Accumulation and translocation of $GABA_A$Rs to the synapse alter their membrane dynamics. The strengthening of GABAergic inhibitory synapses requires the confinement of $GABA_A$Rs in the synaptic compartment. E2 has been shown to decrease the confinement of $GABA_A$Rs leading to weakening of the GABAergic inhibition (Lorenz-Guertin and Jacob, 2018; Mukherjee et al., 2017).

5.2. E2-induced changes on dendritic spines: effect on cortical actin and related signaling molecules

Several experiments demonstrate that E2 affects actin metabolism, actin dependent morphological changes and related cellular processes. Giretti and colleagues have shown that E2 stimulates motility of breast cancer cells via actin remodeling (Giretti et al., 2008). They found that short term E2 treatment results in activation of moesin, a protein tethering actin to the cell membrane. Moesin is activated via the ERα-Rho-associated kinase (ROCK)-moesin pathway, which is indispensable for the effect of E2 on breast cancer cell motility. ROCK also activates LIM kinase, which in turn phosphorylates (inactivates) cofilin, an actin severing protein that is important for normal actin remodeling (Arber et al., 1998; Babayan and Kramár, 2013). The development of dendritic spines and the increase number of postsynaptic AMPAR molecules are dependent on the rearrangement of actin cytoskeleton (Krucker et al., 2000). The intimate relationship between actin metabolism and LTP is reflected by treatments disrupting LTP, such as adenosine or low-frequency stimulation, to block or reverse actin remodeling (Kramár et al., 2006). LTP begins with the opening of NMDA-type glutamate receptors, followed by CAMKII and AMPA receptor activation. Simultaneously, entry of calcium through NMDA receptors initiates two signaling pathways: the RhoA-ROCK and the RAC-PAK pathways (Rex et al., 2009). In turn, ROCK inactivates cofilin and PAK activates cortactin, a protein facilitating actin polymerization. Together, these two pathways strongly facilitate actin network remodeling.

The above results indicate that E2 and LTP share the RhoA-ROCK-cofilin pathway to induce actin remodeling. Based on their single-cell electrophysiology experiments, Kramár and colleagues suggest that as E2 and LTP use the same pathways for spine maturation; E2 elicits a weak LTP when applied on its own, and facilitates LTP when applied together with LTP-inducing synaptic or electrical stimulation. Considering the fact that E2 is produced in the hippocampus locally (Tuscher et al., 2016), E2 might be a potent physiological neuromodulator during LTP and a critical factor for actin remodeling in dendritic spines. Though this function of E2 is supported by the above, indirect findings, further studies are needed to clarify the precise role of E2 in LTP-induced changes in the structure of cortical actin and membrane diffusion of receptor molecules.

6. Discussion

The present review attempts to highlight the non-classical features of E2 and CORT action in the neuronal membrane with special attention to receptor dynamics and related signaling molecules.

We point out that SMT technology provides researchers an excellent tool to directly observe surface diffusion of single receptor molecules in living cells with high spatiotemporal resolution, and they are limited only by the fluorescent probes. One of the most advanced super-

resolution technique is the background-free stimulated emission depletion fluorescence microscope with 1 nm resolution (Balzarotti et al., 2017). Thus, SMT is becoming an extremely useful method for neuroendocrinology research opening new avenues for understanding the molecular mechanism of rapid non-classical hormonal actions.

Dimerization of G-protein coupled or tyrosine kinase receptors plays critical role in their function. SMT is probably the best method for determining receptor dimerizations since it directly follows the molecular dynamics of each molecule. Using dual-color SMT, it was possible to follow dimerization and immobilization of TrkA receptor molecules as well as membrane recruitment of intracellular signaling proteins such as Raf (Shibata et al., 2006). However, experiments observing real time effects of steroids on dimerization of membrane receptor molecules are still warranted.

The plasma membrane is partitioned into compartments by the cortical actin-based membrane skeleton. Cortical actin network plays an active role in surface diffusion of membrane receptors. Transmembrane receptor proteins exhibit confined diffusion within a compartment and “hop” movement between the compartments. Experiments demonstrated that E2 alters the remodeling of the cortical actin (Carnesecchi et al., 2015; Kusumi et al., 2014; Zhao et al., 2017). Using super-resolution imaging techniques, further studies are required to visualize the action of E2 on cortical actin.

SMT is an excellent method for studying interactions between potential drug candidates and target receptors in live cells. Activators of non-genomic estrogen like signaling (ANGELS) hold great potential for novel estrogen replacement therapy and therapeutic intervention for preventing age related neurodegenerative diseases and protection against brain insults (Kwakowsky et al., 2013a). Classical membrane localized estrogen receptors are known to mediate neuroprotective actions of estrogen. SMT experiments in live cells may help clarify the effect of ANGELS compounds on membrane estrogen receptors.

Steroid action on single membrane receptor molecule dynamics is a new frontier in neuroendocrine research. Future investigations must continue to understand underlying mechanism of non-classical steroid actions using novel super-resolution imaging techniques. These experiments might unravel novel and exciting molecular mechanisms behind steroid hormone effects, providing a platform for designing new drugs.

Supplementary data to this article can be found online at https://doi.org/10.1016/j.yhbeh.2018.05.008.

Acknowledgements

We thank Dr. Rachel Cheong for her valuable comments on the manuscript. We thank Daniil Popatov for assistance in single molecule imaging of TrkA receptors. This work was supported by Hungarian Brain Research Program (KTIA_NAP_13-2014-0001, 20017-1.2.1-NKP-2017-00002), OTKA (112807), EFOP-3.6.1.-16-2016-00004, Comprehensive Development for Implementing Smart Specialization Strategies at the University of Pécs, EFOP-3.6.2-16-2017-00008. The role of neuro-inflammation in neurodegeneration: from molecules to clinics.

References

Ábrahám, I.M., Kőszegi, Z., Tolod-Kemp, E., Szegő, É.M., 2009. Action of estrogen on survival of basal forebrain cholinergic neurons: promoting amelioration. Psychoneuroendocrinology 34, S104–S112.

Albrecht, D., Winterflood, C.M., Sadeghi, M., Tschager, T., Noé, F., Ewers, H., 2016. Nanoscopic compartmentalization of membrane protein motion at the axon initial segment. J. Cell Biol. 215, 1–10.

Alléra, A., Wildt, L., 1992. Glucocorticoid-recognizing and -effector sites in rat liver plasma membrane. Kinetics of corticosterone uptake by isolated membrane vesicles—II. Comparative influx and efflux. J. Steroid Biochem. Mol. Biol. 42, 757–771.

Andrade, D.M., Clausen, M.P., Keller, J., Mueller, V., Wu, C., Bear, J.E., Hell, S.W., Lagerholm, B.C., Eggeling, C., 2015. Cortical actin networks induce spatio-temporal confinement of phospholipids in the plasma membrane - a minimally invasive investigation by STED-FCS. Sci. Rep. 5, 1–12.

Arber, S., Barbayannis, F.A., Hanser, H., Schneider, C., Stanyon, C.A., Bernard, O., Caroni, P., 1998. Regulation of actin dynamics through phosphorylation of cofilin by LIM-kinase. Nature 393, 805–809.

Ashby, M.C., De La Rue, S.A., Ralph, G.S., Uney, J., Collingridge, G.L., Henley, J.M., 2004. Removal of AMPA receptors (AMPARs) from synapses is preceded by transient endocytosis of extrasynaptic AMPARs. J. Neurosci. 24, 5172–5176.

Axelrod, D., 2001. Total internal reflection fluorescence microscopy in cell biology. Traffic 2, 764–774.

Babayan, A.H., Kramár, E.A., 2013. Rapid effects of oestrogen on synaptic plasticity: interactions with actin and its signaling proteins. J. Neuroendocrinol. 25, 1163–1172.

Baldereschi, M., Di Carlo, A., Lepore, V., Bracco, L., Maggi, S., Grigoletto, F., Scarlato, G., Amaducci, L., 1998. Estrogen-replacement therapy and Alzheimer's disease in the Italian longitudinal study on aging. Neurology 50, 996–1002.

Balzarotti, F., Eilers, Y., Gwosch, K.C., Gynnå, A.H., Westphal, V., Stefani, F.D., Elf, J., Hell, S.W., 2017. Nanometer resolution imaging and tracking of fluorescent molecules with minimal photon fluxes. Science 355, 606–612.

Bard, L., Sainlos, M., Bouchet, D., Cousins, S., Mikasova, L., Breillat, C., Stephenson, F.A., Imperiali, B., Choquet, D., Groc, L., 2010. Dynamic and specific interaction between synaptic NR2-NMDA receptor and PDZ proteins. Proc. Natl. Acad. Sci. U. S. A. 107, 19561–19566.

Barford, K., Deppmann, C., Winckler, B., 2017. The Neurotrophin receptor signaling endosome: where trafficking meets signaling. Dev. Neurobiol. 77, 405–418.

Biermann, B., Sokoll, S., Klueva, J., Missler, M., Wiegert, J.S., Sibarita, J.-B., Heine, M., 2014. Imaging of molecular surface dynamics in brain slices using single-particle tracking. Nat. Commun. 5, 3024.

Borgdorff, A.J., Choquet, D., 2002. Regulation of AMPA receptor lateral movements. Nature 417, 649–653.

Boulware, M.I., Kordasiewicz, H., Mermelstein, P.G., 2007. Caveolin Proteins Are Essential for Distinct Effects of Membrane Estrogen Receptors in Neurons. J. Neurosci. 27, 9941–9950.

Caldwell, J.D., Gebhart, V.M., Jirikowski, G.F., 2016. Estradiol's interesting life at the cell's plasma membrane. Steroids 111, 4–11.

Callegari, A., Luin, S., Marchetti, L., Duci, A., Cattaneo, A., Beltram, F., 2012. Single particle tracking of acyl carrier protein (ACP)-tagged TrkA receptors in PC12nnr5 cells. J. Neurosci. Methods 204, 82–86.

Carnesecchi, J., Malbouyres, M., de Mets, R., Balland, M., Beauchef, G., Vié, K., Chamot, C., Lionnet, C., Ruggiero, F., Vanacker, J.-M., 2015. Estrogens induce rapid cytoskeleton re-organization in human dermal fibroblasts via the non-classical receptor GPR30. PLoS One 10, e0120672.

Chamma, I., Heubl, M., Chevy, Q., Renner, M., Moutkine, I., Eugene, E., Poncer, J.C., Levi, S., 2013. Activity-dependent regulation of the K/Cl transporter KCC2 membrane diffusion, clustering, and function in hippocampal neurons. J. Neurosci. 33, 15488–15503.

Chater, T.E., Goda, Y., 2014. The role of AMPA receptors in postsynaptic mechanisms of synaptic plasticity. Front. Cell. Neurosci. 8, 1–14.

Cheong, R.Y., Kwakowsky, A., Barad, Z., Porteous, R., Herbison, A.E., Ábrahám, I.M., 2012. Estradiol acts directly and indirectly on multiple signaling pathways to phosphorylate cAMP-response element binding protein in GnRH neurons. Endocrinology 153, 3792–3803.

Dupuis, J.P., Ladépêche, L., Seth, H., Bard, L., Varela, J., Mikasova, L., Bouchet, D., Rogemond, V., Honnorat, J., Hanse, E., Groc, L., 2014. Surface dynamics of GluN2B-NMDA receptors controls plasticity of maturing glutamate synapses. EMBO J. 33, 842–861.

Frischknecht, R., Heine, M., Perrais, D., Seidenbecher, C.I., Choquet, D., Gundelfinger, E.D., 2009. Brain extracellular matrix affects AMPA receptor lateral mobility and short-term synaptic plasticity. Nat. Neurosci. 12, 897–904.

Fujiwara, T., Ritchie, K., Murakoshi, H., Jacobson, K., Kusumi, A., 2002. Phospholipids undergo hop diffusion in compartmentalized cell membrane. J. Cell Biol. 157, 1071–1081.

Giretti, M.S., Fu, X.-D., De Rosa, G., Sarotto, I., Baldacci, C., Garibaldi, S., Mannella, P., Biglia, N., Sismondi, P., Genazzani, A.R., Simoncini, T., 2008. Extra-nuclear signalling of estrogen receptor to breast cancer cytoskeletal remodelling, migration and invasion. PLoS One 3, e2238.

Glebov, O.O., Tigaret, C.M., Mellor, J.R., Henley, J.M., 2015. Clathrin-independent trafficking of AMPA receptors. J. Neurosci. 35, 4830–4836.

Groc, L., Heine, M., Cousins, S.L., Stephenson, F.A., Lounis, B., Cognet, L., Choquet, D., 2006. NMDA receptor surface mobility depends on NR2A-2B subunits. Proc. Natl. Acad. Sci. 103, 18769–18774.

Groc, L., Choquet, D., Chaouloff, F., 2008. The stress hormone corticosterone conditions AMPAR surface trafficking and synaptic potentiation. Nat. Neurosci. 11, 868–870.

Groeneweg, F.L., Karst, H., de Kloet, E.R., Joëls, M., 2011. Rapid non-genomic effects of corticosteroids and their role in the central stress response. J. Endocrinol. 209, 153–167.

Hansen, A.S., Woringer, M., Grimm, J.B., Lavis, L.D., Tjian, R., Darzacq, X., 2017. Spot-On: Robust Model-based Analysis of Single-particle Tracking Experiments. bioRxiv 171983.

Haraguchi, S., Hara, S., Ubuka, T., Mita, M., Tsutsui, K., 2012. Possible role of pineal allopregnanolone in Purkinje cell survival. Proc. Natl. Acad. Sci. U. S. A. 109, 21110–21115.

Horvath, K.M., Hårtig, W., Van der Veen, R., Keijser, J.N., Mulder, J., Ziegert, M., Van der Zee, E.A., Harkany, T., Luiten, P.G.M., 2002. 17β-estradiol enhances cortical cholinergic innervation and preserves synaptic density following excitotoxic lesions to the rat nucleus basalis magnocellularis. Neuroscience 110, 489–504.

Huang, E.J., Reichardt, L.F., 2003. Trk receptors: roles in neuronal signal transduction.

Annu. Rev. Biochem. 72, 609–642.
Ioannou, M.S., Fahnestock, M., 2017. ProNGF, but not NGF, switches from neurotrophic to apoptotic activity in response to reductions in TrKA receptor levels. Int. J. Mol. Sci. 18, 599.
Kisler, K., Chow, R.H., Dominguez, R., 2013. Fluorescently-labeled estradiol internalization and membrane trafficking in live N-38 neuronal cells visualized with total internal reflection fluorescence microscopy. J. Steroids Horm. Sci.(Suppl. 12). http://dx.doi.org/10.4172/2157-7536.S12-002.
Koppel, D.E., Sheetz, M.P., Schindler, M., 1980. Lateral diffusion in biological membranes. A normal-mode analysis of diffusion on a spherical surface. Biophys. J. 30, 187–192.
Köster, D.V., Mayor, S., 2016. Cortical actin and the plasma membrane: inextricably intertwined. Curr. Opin. Cell Biol. 38, 81–89.
Kramár, E.A., Lin, B., Rex, C.S., Gall, C.M., Lynch, G., 2006. Integrin-driven actin polymerization consolidates long-term potentiation. Proc. Natl. Acad. Sci. U. S. A. 103, 5579–5584.
Kremers, G.-J., Gilbert, S.G., Cranfill, P.J., Davidson, M.W., Piston, D.W., 2011. Fluorescent proteins at a glance. J. Cell Sci. 124, 157–160.
Krucker, T., Siggins, G.R., Halpain, S., 2000. Dynamic actin filaments are required for stable long-term potentiation (LTP) in area CA1 of the hippocampus. Proc. Natl. Acad. Sci. U. S. A. 97, 6856–6861.
Kusumi, A., Sako, Y., Yamamoto, M., 1993. Confined lateral diffusion of membrane-receptors as studied by single-particle tracking (nanovid microscopy) - effects of calcium-induced differentiation in cultured epithelial-cells. Biophys. J. 65, 2021–2040.
Kusumi, A., Tsunoyama, T.A., Hirosawa, K.M., Kasai, R.S., Fujiwara, T.K., 2014. Tracking single molecules at work in living cells. Nat. Chem. Biol. 10, 524–532.
Kwakowsky, A., Koszegi, Z., Cheong, R.Y., Ábrahám, I.M., 2013a. Neuroprotective effects of non-classical estrogen-like signaling activators: from mechanism to potential implications. CNS Neurol. Disord. Drug Targets 12, 1219–1225.
Kwakowsky, A., Potapov, D., Ábrahám, I.M., 2013b. Tracking of single receptor molecule mobility in neuronal membranes: a quick theoretical and practical guide. J. Neuroendocrinol. 25, 1231–1237.
Kwakowsky, A., Cheong, R.Y., Herbison, A.E., Ábrahám, I.M., 2014. Non-classical effects of estradiol on cAMP responsive element binding protein phosphorylation in gonadotropin-releasing hormone neurons: mechanisms and role. Front Neuroendocrinol 35, 31–41.
Kwakowsky, A., Potapov, K., Kim, S., Peppercorn, K., Tate, W.P., Ábrahám, I.M., 2016. Treatment of beta amyloid 1–42 (Aβ1–42)-induced basal forebrain cholinergic damage by a non-classical estrogen signaling activator in vivo. Sci. Rep. 6, 21101.
Ladépêche, L., Dupuis, J.P., Groc, L., 2014. Surface trafficking of NMDA receptors: gathering from a partner to another. Semin. Cell Dev. Biol. 27, 3–13.
Lee, S.H., Jin, C., Cai, E., Ge, P., Ishitsuka, Y., Teng, K.W., de Thomaz, A.A., Nall, D., Baday, M., Jeyifous, O., Demonte, D., Dundas, C.M., Park, S., Delgado, J.Y., Green, W.N., Selvin, P.R., 2017. Correction: super-resolution imaging of synaptic and extrasynaptic AMPA receptors with different-sized fluorescent probes. elife 6, e33413.
Leonard, A.S., Davare, M.A., Horne, M.C., Garner, C.C., Hell, J.W., 1998. SAP97 is associated with the alpha-amino-3-hydroxy-5-methylisoxazole-4-propionic acid receptor GluR1 subunit. J. Biol. Chem. 273, 19518–19524.
Lorenz-Guertin, J.M., Jacob, T.C., 2018. GABA type a receptor trafficking and the architecture of synaptic inhibition. Dev. Neurobiol. 78, 238–270.
Luine, V., Frankfurt, M., 2013. Interactions between estradiol, BDNF and dendritic spines in promoting memory. Neuroscience 239, 34–45.
Marchetti, L., Callegari, A., Luin, S., Signore, G., Viegi, A., Beltram, F., Cattaneo, A., 2013. Ligand signature in the membrane dynamics of single TrkA receptor molecules. J. Cell Sci. 126, 4445–4456.
Marchetti, L., Luin, S., Bonsignore, F., de Nadai, T., Beltram, F., Cattaneo, A., 2015. Ligand-induced dynamics of neurotrophin receptors investigated by single-molecule imaging approaches. Int. J. Mol. Sci. 16, 1949–1979.
McEwen, B., 2002. Estrogen actions throughout the brain. Recent Prog. Horm. Res. 57, 357–384.
Meitzen, J., Mermelstein, P.G., 2011. Estrogen receptors stimulate brain region specific metabotropic glutamate receptors to rapidly initiate signal transduction pathways. J. Chem. Neuroanat. 42, 236–241.
Micevych, P., Dominguez, R., 2009. Membrane estradiol signaling in the brain. Front. Neuroendocrinol. 30, 315–327.
Mikasova, L., Xiong, H., Kerkhofs, A., Bouchet, D., Krugers, H.J., Groc, L., 2017. Stress hormone rapidly tunes synaptic NMDA receptor through membrane dynamics and mineralocorticoid signalling. Sci. Rep. 7, 1–12.
Mukherjee, J., Cardarelli, R.A., Cantaut-Belarif, Y., Deeb, T.Z., Srivastava, D.P., Tyagarajan, S.K., Pangalos, M.N., Triller, A., Maguire, J., Brandon, N.J., Moss, S.J., 2017. Estradiol modulates the efficacy of synaptic inhibition by decreasing the dwell time of GABA $_A$ receptors at inhibitory synapses. Proc. Natl. Acad. Sci. 114, 11763–11768.
Murakoshi, H., Iino, R., Kobayashi, T., Fujiwara, T., Ohshima, C., Yoshimura, A., Kusumi, A., 2004. Single-molecule imaging analysis of Ras activation in living cells. Proc. Natl. Acad. Sci. U. S. A. 101, 7317–7322.
Nguyen, N., Lee, S.B., Lee, Y.S., Lee, K.H., Ahn, J.Y., 2009. Neuroprotection by NGF and BDNF against neurotoxin-exerted apoptotic death in neural stem cells are mediated through TRK receptors, activating PI3-kinase and MAPK pathways. Neurochem. Res. 34, 942–951.
Nishimune, A., Isaac, J.T.R., Molnar, E., Noel, J., Nash, S.R., Tagaya, M., Collingridge, G.L., Nakanishi, S., Henley, J.M., 1998. NSF binding to GluR2 regulates synaptic transmission. Neuron 21, 87–97.
Noel, J., Ralph, G.S., Pickard, L., Williams, J., Molnar, E., Uney, J.B., Collingridge, G.L., Henley, J.M., 1999. Surface expression of AMPA receptors in hippocampal neurons is regulated by an NSF-dependent mechanism [in process citation]. Neuron 23, 365–376.
Opazo, P., Sainlos, M., Choquet, D., 2012. Regulation of AMPA receptor surface diffusion by PSD-95 slots. Curr. Opin. Neurobiol. 22, 453–460.
Piskorz, T.K., Ochab-Marcinek, A., 2014. A universal model of restricted diffusion for fluorescence correlation spectroscopy. J. Phys. Chem. B 118, 4906–4912.
Qiu, J., Rønnekleiv, O.K., Kelly, M.J., 2008. Modulation of Hypothalamic Neuronal Activity through a Novel G-Protein Coupled Estrogen Membrane Receptor. Steroids 73, 985–991.
Renner, M.L., Cognet, L., Lounis, B., Triller, A., Choquet, D., 2009. The excitatory postsynaptic density is a size exclusion diffusion environment. Neuropharmacology 56, 30–36.
Rex, C.S., Chen, L.Y., Sharma, A., Liu, J., Babayan, A.H., Gall, C.M., Lynch, G., 2009. Different Rho GTPase–dependent signaling pathways initiate sequential steps in the consolidation of long-term potentiation. J. Cell Biol. 186, 85–97.
Richeri, A., Bianchimano, P., Mármol, N.M., Viettro, L., Cowen, T., Brauer, M.M., 2005. Plasticity in rat uterine sympathetic nerves: the role of TrkA and p75 nerve growth factor receptors. J. Anat. 207, 125–134.
Ritchie, K., Iino, R., Fujiwara, T., Murase, K., Kusumi, A., 2003. The fence and picket structure of the plasma membrane of live cells as revealed by single molecule techniques (review). Mol. Membr. Biol. 20, 13–18.
Rogers, S.S., Waigh, T.A., Zhao, X., Lu, J.R., 2007. Precise particle tracking against a complicated background: polynomial fitting with Gaussian weight. Phys. Biol. 4, 220–227.
Sadegh, S., Higgins, J.L., Mannion, P.C., Tamkun, M.M., Krapf, D., 2017. Plasma membrane is compartmentalized by a self-similar cortical actin meshwork. Phys. Rev. X 7, 1–11.
Salas, C., Julio-Pieper, M., Valladares, M., Pommer, R., Vega, M., Mastronardi, C., Kerr, B., Ojeda, S.R., Lara, H.E., Romero, C., 2006. Nerve growth factor-dependent activation of trkA receptors in the human ovary results in synthesis of follicle-stimulating hormone receptors and estrogen secretion. J. Clin. Endocrinol. Metab. 91, 2396–2403.
Sans, N., Petralia, R.S., Wang, Y.-X., Blahos, J., Hell, J.W., Wenthold, R.J., 2000. A developmental change in NMDA receptor-associated proteins at hippocampal synapses. J. Neurosci. 20, 1260–1271.
Sarabdjitsingh, R.A., Jezequel, J., Pasricha, N., Mikasova, L., Kerkhofs, A., Karst, H., Groc, L., Joëls, M., 2014. Ultradian corticosterone pulses balance glutamatergic transmission and synaptic plasticity. Proc. Natl. Acad. Sci. 111, 14265–14270.
Sarabdjitsingh, R.A., Pasricha, N., Smeets, J.A.S., Kerkhofs, A., Mikasova, L., Karst, H., Groc, L., Joëls, M., 2016. Hippocampal fast glutamatergic transmission is transiently regulated by corticosterone pulsatility. PLoS One 11, e0145858.
Sergé, A., Bertaux, N., Rigneault, H., Marguet, D., 2008. Dynamic multiple-target tracing to probe spatiotemporal cartography of cell membranes. Nat. Methods 5, 687–694.
Shibata, S.C., Hibino, K., Mashimo, T., Yanagida, T., Sako, Y., 2006. Formation of signal transduction complexes during immobile phase of NGFR movements. Biochem. Biophys. Res. Commun. 342, 316–322.
Shirai, Y.M., Tsunoyama, T.A., Hiramoto-Yamaki, N., Hirosawa, K.M., Shibata, A.C.E., Kondo, K., Tsurumune, A., Ishidate, F., Kusumi, A., Fujiwara, T.K., 2017. Cortical actin nodes: their dynamics and recruitment of podosomal proteins as revealed by super-resolution and single-molecule microscopy. PLoS One 12, e0188778.
Simpkins, J.W., Singh, M., Brock, C., Etgen, A.M., 2012. Neuroprotection and estrogen receptors. Neuroendocrinology 96, 119–130.
Simson, R., Yang, B., Moore, S.E., Doherty, P., Walsh, F.S., Jacobson, K.A., 1998. Structural mosaicism on the submicron scale in the plasma membrane. Biophys. J. 74, 297–308.
Singh, M., Sétáló, G., Guan, X., Warren, M., Toran-Allerand, C.D., 1999. Estrogen-induced activation of mitogen-activated protein kinase in cerebral cortical explants: convergence of estrogen and neurotrophin signaling pathways. J. Neurosci. 19, 1179–1188.
Song, E.J., Yoo, Y.S., 2011. Nerve growth factor-induced neurite outgrowth is potentiated by stabilization of TrkA receptors. BMB Rep. 44, 182–186.
Spencer, A., Yu, L., Guili, V., Reynaud, F., Ding, Y., Ma, J., Jullien, J., Koubi, D., Gauthier, E., Cluet, D., Falk, J., Castellani, V., Yuan, C., Rudkin, B.B., 2017. Nerve growth factor signaling from membrane microdomains to the nucleus: differential regulation by caveolins. Int. J. Mol. Sci. 18, 693.
Suzuki, K., Ritchie, K., Kajikawa, E., Fujiwara, T., Kusumi, A., 2005. Rapid hop diffusion of a G-protein-coupled receptor in the plasma membrane as revealed by single-molecule techniques. Biophys. J. 88, 3659–3680.
Szego, E.M., 2006. Estrogen induces estrogen receptor -dependent cAMP response element-binding protein phosphorylation via mitogen activated protein kinase pathway in basal forebrain cholinergic neurons in vivo. J. Neurosci. 26, 4104–4110.
Szegő, É.M., Csorba, A., Janáky, T., Kékesi, K.A., Ábrahám, I.M., Mórotz, G.M., Penke, B., Palkovits, M., Murvai, Ü., Kellermayer, M.S.Z., Kardos, J., Juhász, G.D., 2011. Effects of estrogen on beta-amyloid-induced cholinergic cell death in the nucleus basalis magnocellularis. Neuroendocrinology 93, 90–105.
Tani, T., Miyamoto, Y., Fujimori, K.E., Taguchi, T., Yanagida, T., Sako, Y., Harada, Y., 2005. Trafficking of a ligand-receptor complex on the growth cones as an essential step for the uptake of nerve growth factor at the distal end of the axon: a single-molecule analysis. J. Neurosci. 25, 2181–2191.
Tardin, C., Cognet, L., Bats, C., Lounis, B., Choquet, D., 2003. Direct imaging of lateral movements of AMPA receptors inside synapses. EMBO J. 22, 4656–4665.
Tokunaga, M., Imamoto, N., Sakata-Sogawa, K., 2008. Highly inclined thin illumination enables clear single-molecule imaging in cells. Nat. Methods 5, 159–161.
Townsend, M., Yoshii, A., Mishina, M., Constantine-Paton, M., 2003. Developmental loss of miniature *N*-methyl-D-aspartate receptor currents in NR2A knockout mice. Proc. Natl. Acad. Sci. U. S. A. 100, 1340–1345.
Treen, A.K., Luo, V., Chalmers, J.A., Dalvi, P.S., Tran, D., Ye, W., Kim, G.L., Friedman, Z.,

Belsham, D.D., 2016. Divergent regulation of ER and kiss genes by 17β-estradiol in hypothalamic ARC versus AVPV models. Mol. Endocrinol. 30, 217–233.

Tuscher, J.J., Szinte, J.S., Starrett, J.R., Krentzel, A.A., Fortress, A.M., Remage-Healey, L., Frick, K.M., 2016. Inhibition of local estrogen synthesis in the hippocampus impairs hippocampal memory consolidation in ovariectomized female mice. Horm. Behav. 83, 60–67.

van Zundert, B., Yoshii, A., Constantine-Paton, M., 2004. Receptor compartmentalization and trafficking at glutamate synapses: a developmental proposal. Trends Neurosci. 27, 428–437.

Wang, L., Dumoulin, A., Renner, M., Triller, A., Specht, C.G., 2016. The role of synaptopodin in membrane protein diffusion in the dendritic spine neck. PLoS One 11, e0148310.

Wessels, J.M., Leyland, N.A., Agarwal, S.K., Foster, W.G., 2015. Estrogen induced changes in uterine brain-derived neurotrophic factor and its receptors. Hum. Reprod. 30, 925–936.

Xu, K., Zhong, G., Zhuang, X., 2013. Actin, spectrin, and associated proteins form a periodic cytoskeletal structure in axons. Science 339, 452–456.

Yoshii, A., Sheng, M.H., Constantine-Paton, M., 2003. Eye opening induces a rapid dendritic localization of PSD-95 in central visual neurons. Proc. Natl. Acad. Sci. U. S. A. 100, 1334–1339.

Zhang, Y.-Z., Moheban, D.B., Conway, B.R., Bhattacharyya, A., Segal, R.A., 2000. Cell surface Trk receptors mediate NGF-induced survival while internalized receptors regulate NGF-induced differentiation. J. Neurosci. 20, 5671–5678.

Zhang, H., Etherington, L.-A., Hafner, A.-S., Belelli, D., Coussen, F., Delagrange, P., Chaouloff, F., Spedding, M., Lambert, J.J., Choquet, D., Groc, L., 2013. Regulation of AMPA receptor surface trafficking and synaptic plasticity by a cognitive enhancer and antidepressant molecule. Mol. Psychiatry 18, 471–484.

Zhao, Y., He, L., Zhang, Y., Zhao, J., Liu, Z., Xing, F., Liu, M., Feng, Z., Li, W., Zhang, J., 2017. Estrogen receptor alpha and beta regulate actin polymerization and spatial memory through an SRC-1/mTORC2-dependent pathway in the hippocampus of female mice. J. Steroid Biochem. Mol. Biol. 174, 96–113.